A parameter sensitivity study for a Soft Yoke Mooring System (SYMS)

Developing a design tool

O.D. (Oscar) van den Heuvel

Delft University of Technology

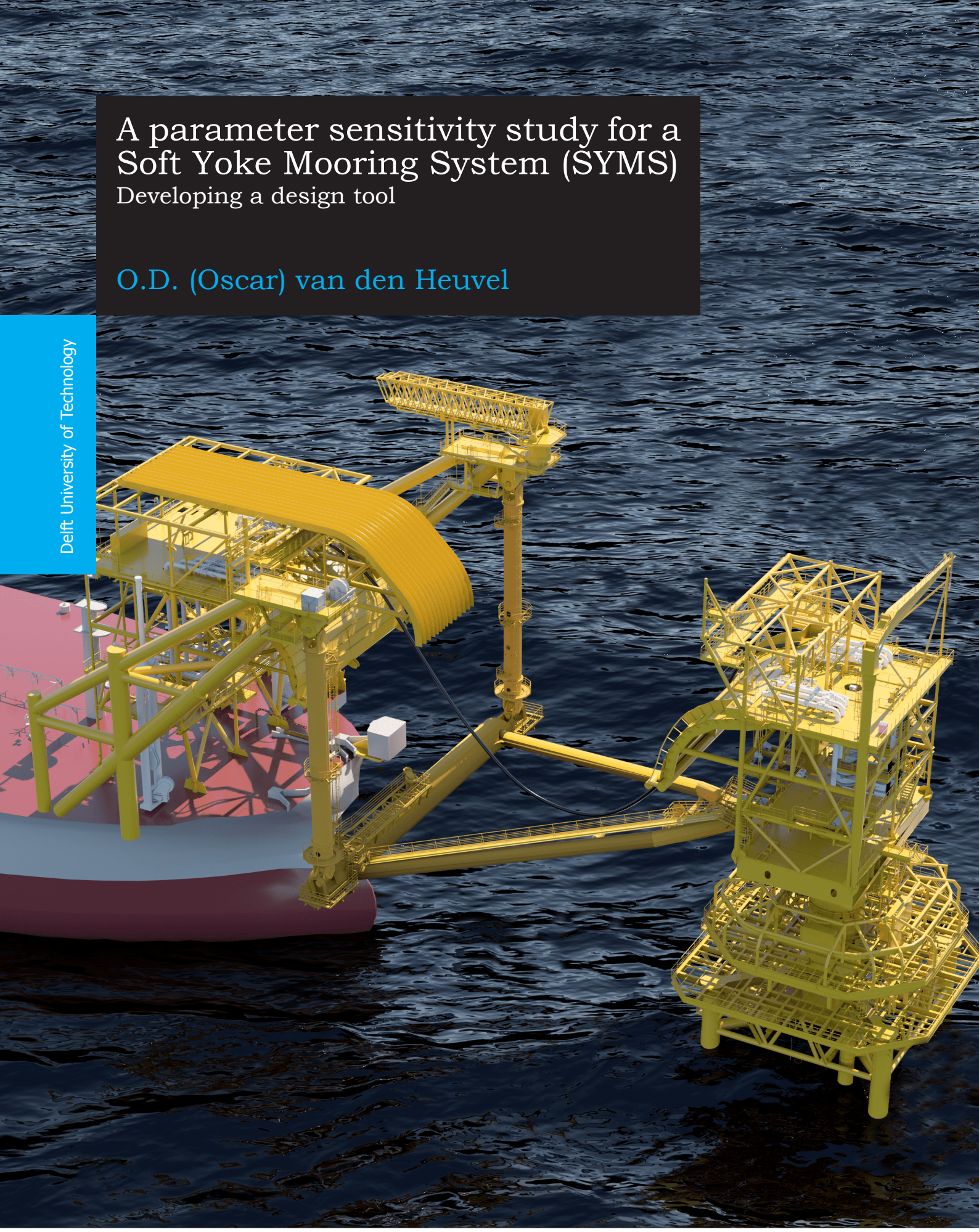

TU Delft Delft University of Technology

Challenge the future

A parameter sensitivity study for a Soft Yoke Mooring System (SYMS)

Developing a design tool

by

O.D. (Oscar) van den Heuvel

in partial fulfillment of the requirements for the degree of

Master of Science
in Offshore & Dredging Engineering

at the Delft University of Technology,
to be defended on Thursday February 27, 2020 at 1:00 PM.

Chairman:	Prof. dr. A. Metrikine	TU Delft
Thesis committee:	Dr. ir. C. Keijdener	TU Delft
	Ir. A. Tsetas	TU Delft
	Ir. S. van der Werff	Bluewater
	Ir. R. Leeuwenburgh	Bluewater

This thesis is confidential and cannot be made public

TU Delft

bluewater

Abstract

Floating production units require to be permanently moored offshore. For shallow water field developments, typical designs include soft yoke mooring systems which is a single point mooring technology. Produced fluid is transported via a geostatic tower along the transfer hoses to the production unit. Single point mooring systems will weathervane into the offshore environment (wind, waves and current) and can often be considered as surge dominant induced by low frequency wave drift forces. Due to low damping at these low frequencies, an oscillation close to the natural surge frequency appears causing dominant mooring loads. By connecting the floating structure to the tower with various rigid steel frame components, including multiple hinges, unconstrained motions are preserved. This results in dynamically complex systems requiring advanced numerical methods for time domain simulations, in order to deliver the mooring design loads. By selecting mass and dimensions of the soft yoke mooring system, the stiffness of the mooring system can be adapted to influence the response of the floater.

Currently, mass and dimensions of new soft yoke mooring designs are established using proven mooring solutions by conducting small adjustments of mooring components in time consuming dynamic simulation software. Improvement in efficiency of the design process is accomplished by developing a computational efficient design tool, to be used before dynamic modelling, to provide the designer with an optimized set of mooring design parameters in a given environment. The developed design tool contains an integrated single degree of freedom model including given vessel properties and extreme collinear offshore environment, in order to produce estimates of the maximum surge response based on the given mooring characteristics. Eventually, by adapting the mooring stiffness accordingly, the design tool is able to provide an optimum set of mooring design parameters which minimizes the maximum mooring load.

The mooring characteristics are implemented using a linear and non-linear approach. A validation of surge response results has been performed for three collinear extreme offshore environments including wind, waves and current using state-of-the art dynamic modelling software OrcaFlex. Results showed that the linear model can capture the sensitivity of the surge response related to mooring design parameter variation. It was demonstrated with the Runge-Kutta method that the achieved accuracy with the proposed non-linear model will be similar or even worse than using the linear model without the relevant computational costs. Therefore, the linear model was implemented in the design tool and accomplishes surge response calculations of 10,000 sets of mooring design parameters within a few minutes.

Results showed that the consequence of the linear mooring force and single degree of freedom assumptions in the design tool leads to an underestimation of the surge response in an extreme collinear environment. Despite the surge dominance, especially heave and pitch motions induce high mooring loads at maximum surge offset. Analyses of two moderate collinear environments in OrcaFlex revealed less underestimation and even overestimation of the surge response by the design tool, which indicates the high dynamic complexity of soft yoke mooring systems. However, the surge response validation procedure using OrcaFlex affirmed that the design tool provides the correct set of mooring design parameters resulting in a minimum mooring load within 2~10% accuracy for all three environments. By implementing the proposed set in OrcaFlex and obtaining the design loads, a 25% decrease in absolute maximum mooring load is demonstrated when compared to the benchmark mooring design parameters. This indicates the increased efficiency of the design process by using the developed design tool.

An additional graphical user interface is programmed where the designer can import their own vessel properties, environmental conditions and can vary desired mooring design parameters. Conclusively, a design tool has been developed for preliminary estimations of the set of mooring design parameters that have been shown to minimize the mooring loads and to limit the number of time domain analyses in future projects.

Preface

In front of you is the report describing my master's thesis conducted at Bluewater Energy Services to obtain the title Master of Science in Offshore & Dredging Engineering. After my BSc. degree in Mechanical Engineering, I realized that my interest shifted to large civil structures. Since I always had a passion for water and was fascinated by ships, I started with the master 'Offshore & Dredging Engineering' in the faculty of CiTG at Delft University of Technology. The practical applicability of the courses given was high. By having close relationships with the most successful Dutch offshore companies, this master bridged the gap between student and working environment. This turned my interest in the offshore sector into a passion.

I would like to thank Bluewater Energy Services for making it possible to work as a graduate intern on a very interesting, up-to-date project. Special thanks goes out to *Ir. S. van der Werff* and *Ir. R. Leeuwenburgh* for the great support throughout the project. They provided me with value feedback, by sharing their experience to keep me on the right track. In addition, my gratitude goes out to the colleagues of the Mooring & Subsea department for their assistance when I had questions or doubts.

I also would like to thank *Prof. dr. A. Metrikine* as well as my daily supervisors *Dr. ir. C. Keijdener* and *Ir. A. Tsetas* for their help during the multiple valuable progress meetings. Especially my daily supervisors where always available for discussion and relevant support was given to make the right decisions during the project.

Finally, special honor goes out to my parents, family, girlfriend and friends for their loyalty and support during my life as a student. Without their optimism and encouragement, this was all not possible.

O.D. (Oscar) van den Heuvel
Delft, February 2020

Contents

1

Introduction

1.1. Background information

When using Floating Production Storage and Offloading (FPSO) units for offshore field developments in deep and shallow waters, the proposed mooring system for the FPSO must be designed to stay approximately for 20 years on site. Therefore, the mooring system has to be capable to withstand all environmental loads during its operational time. Depending on location of the field and FPSO capabilities, a specific mooring system is designed. One type typically operated in shallow waters, classified under the Single Point Mooring (SPM) systems, is the so-called Soft Yoke Mooring System (SYMS). This is one of many mooring systems Bluewater Energy Services (BES) designs for specific field developments. The system consists of a rigid steel frame with multiple components and hinges, connecting the FPSO to a tower structure. Risers are leaving the water surface via the base of the tower, attached to a swivel which provides movement of flexible jumpers around the geostatic part of the tower. The flexible jumpers provide the fluid path from the tower to the topside of the FPSO. These type of systems requires a dedicated vessel with modified hull to support the rigid steel frame. This frame typically consists of the Mooring Support Structure (MSS) on the fore-deck of the FPSO, connecting two pendulums, a ballast box and a triangular shaped yoke arm to the tower. The different steel components and hinges are shown in Figure 1.1.

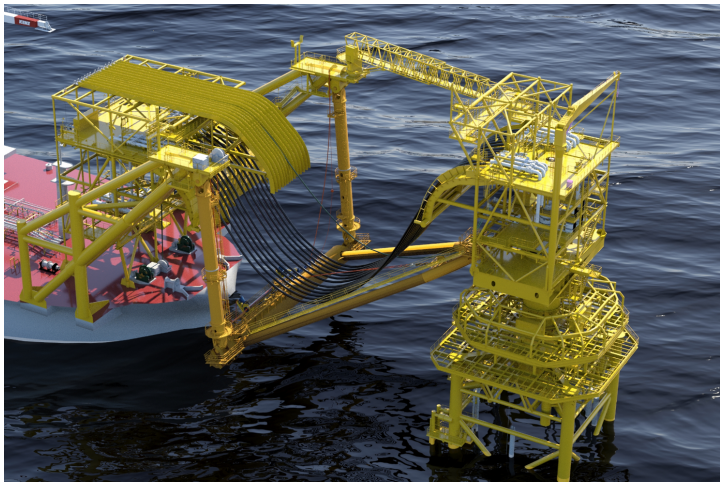

Figure 1.1: The SYMS (Bluewater Energy Services, 2018)

The two separate pendulums are connected to the MSS on the upper end, and to the ballast box on the lower end. The ballast box is connected at two points to the yoke structure. The yoke arm is a triangular shaped structure connecting the FPSO to a single point joint located on the tower. Via the turntable located on the tower, the yoke arm, an thus the whole system is able to passively move

around the tower. Using multi-dimensional joints, the system allows the FPSO to move in six Degrees of Freedom (DoF). As the vessel rotates itself with its bow into the dominant environment, resulting in a surge dominant system, it automatically minimizes the loads on the foundation of the tower. When the FPSO is excited due to environmental loads, the mooring system acts as a restoring force as the ballast box is lifted up from its equilibrium position. Therefore, due to the presence of the mooring system, the FPSO excites away from the tower when the restoring mooring force is smaller than the environmental forces and comes back to the tower when the restoring mooring force is larger.
These systems are typically applied in shallow waters up to 40 m water depth with relatively mild environmental conditions. Like with many other systems, boundary conditions are stretched to (or even over) current design limits. The demand for these systems in more harsh environments can even result in a requirement to be able to disconnect this system prior to a severe storm. Therefore, BES is able to fulfill this requirement by designing a disconnectable mooring system better known as the Disconnectable Tower Yoke Mooring System (DTYMS). Such a system was proposed for the Miztón field located in the Gulf of Mexico (GoM). A Front End Engineering Design (FEED), including model tests, were done based on proven technical solutions applied in previously built systems by BES. Results from this study contribute to the benchmark system used throughout the project. To remain front runner for complicated mooring solutions, it is of great value to keep improving the configuration. Understanding the behaviour of the connected SYMS in extreme environmental conditions could contribute to this goal. Therefore, the main focus of this project is on the SYMS, rather than the DTYMS. In this way, criteria for disconnection of a DTYMS can be set in the future.

1.2. Problem definition

It can be imagined that a SYMS, including its many rigid components and DoF, results in a dynamically complex system. As discussed above, the design process for such systems often consist of small adjustments to proven mooring solutions in the past. Since location dependent environmental conditions apply, this is an huge assumption and does not necessarily produce the most efficient mooring system. To find governing sea states that results in the maximum design loads, a fully coupled time domain analyses have to be executed. In these analyses, a hydrodynamic database dependent on shape of the FPSO and water depth can be included. Together with the systems mechanical properties, constraints and location dependent environmental data, time domain modelling software models the dynamic behaviour of the system quite realistically. Nonetheless, time-domain analyses are often computationally heavy. Hence, when evaluating multiple load cases in multiple environmental directions, mooring system dimensions and weights have to be chosen wisely. By making small adjustments in mooring design parameters, the response of the vessel is likely to be changed. This sensitivity of the vessels dynamic response related to variation of the mooring system dimensions and weights is quite unknown and lacks in the current design process. In addition, the time domain simulations have to be ran again after each adjustment in order to find the new maximum design loads. Accordingly, it is a huge advantage that design parameters are chosen, where it is known that vessels response will result in low desired mooring loads before starting time domain analyses.

1.3. Project goal

As described in Section 1.2, dynamic time domain models are developed between the motion coupling of FPSO and SYMS to estimate maximum mooring design loads in a given environment. These models can predict the dynamic behaviour of the system in unidirectional waves, current and wind, being validated by either model tests or real time monitoring during operation. Since BES uses Orcina's fully coupled numerical simulation software OrcaFlex[1], that is proven to be reliable in mooring design, it is in this project not of great relevance to redevelop such a program. Therefore, the importance of this project is to gain insight in the sensitivity of the vessels dynamic response related to mooring design parameter variation. In this way, reliable mooring system dimensions and weights can be proposed before time domain modelling to limit the required amount of computational heavy time domain simulations significantly. To achieve this, the project goal is formulated as follows:

To develop an efficient design tool, to be used before dynamic modelling, which is able to assess the sensitivity of the surge response related to variation of mooring design parameters and provide the designer with an optimum set of mooring design parameters in a given environment.

1.4. Preliminary research

This section consists of two parts, a document study on typical design methodology of a SYMS for the Miztón field according to BES documents and available literature. Since BES documents are confidential, citations to BES documents are referred to as [Bluewater Energy Services] throughout the report. The second part includes a short overview of literature on modelling of a SYMS and included validations.

1.4.1. Design methodology of SYMS

BES was asked to design a SYMS for the Miztón field located in the Gulf of Mexico. Typical FEED for these systems consists of three parts: a static, quasi-static and time domain analyses. These analyses were done for the Stena Surprise FPSO provided by the client. Relevant vessel properties can be found in Appendix C and Table C.1.
The design of the SYMS is based on proven solutions applied in previously build systems [Bluewater Energy Services]. During the design cycle, variations on the dimensions of the benchmark projects can be applied if needed. The side and top views of the SYMS with its main components can be found in Appendix B. The benchmark dimension of the mooring system designed for the Miztón project are given in Table B.1

Static analysis

It is known that single point moored systems are surge dominant systems. Therefore, the first step in the static analysis is to give the vessel a predefined surge excursion, measured from the equilibrium position shown in Figure B.1. Using the position, weights and angles between the rigid components the mooring force can be calculated. By doing this for a desired excursion range towards and away from the tower, a load-excursion curve can be created. Due to the geometry of the mooring system, these load-excursion curves are non-linear. The gradient of the load-excursion curve at each point represents the stiffness of the mooring system. Depending on the dimensions and masses of the different components of the mooring system, the shape, and thus the stiffness of the mooring system changes. The force of main interest is the horizontal mooring force which results in the highest moment at the foundation of the tower.
When the FPSO is in operation, it can be imagined that the relative vertical height between the connection point of the pendulum to the MSS and the connection point between the yoke and the tower (HC) will decrease. Therefore, the mooring characteristics are changing when the wells are producing. This has to be kept in mind when designing the SYMS. By using the load-excursion curves, an indication of mooring forces at a specific excursion can be estimated resulting from an in-plane motion only. The next step is to include the FPSO properties and environmental conditions to provide first estimates of the excursion and the related mooring force.

Quasi-static analysis

The static analysis delivers first raw estimates of the expected mooring force at a given excursion. However, no environmental forces and vessel dependent hydrodynamic coefficients that induce these excursions are included in this analysis. Therefore, it is preferred that before doing dynamic simulations a first principles approach is applied. Since large single point moored structures have low surge natural frequencies and low surge damping, it is expected that the Low Frequent (LF) surge response has a governing contribution to the mooring load and offset[2]. Especially in shallow waters, the contribution of the LF surge motions increase with respect to deeper waters[3]. These low frequent motions are induced by the low frequency second order wave drift forces[4]. To calculate the LF surge response, hydrodynamic coefficients of the FPSO are required. These hydrodynamic coefficients include added mass and potential damping. They can be obtained by using linear and second order diffraction and radiation theory using a 3D panel method[5]. In addition, diffraction and radiation theory is used to calculate the Response Amplitude Operator (RAO) of both the first order wave force and wave induced motions and the Quadratic Transfer Function (QTF) of the second order wave force for every wave frequency and direction. In combination with the mooring characteristic obtained from the static analysis and location specific environmental conditions, the vessels surge response can be estimated. At BES, the software package Hydrostar is used to estimate these coefficients and transfer functions. Note that the added mass, potential damping and transfer functions are dependent on the draft of the FPSO. Therefore, a mesh for both ballast and fully loaded condition is created and used in the diffraction analysis. A typical mesh for two loading conditions is shown in Figure 1.2.

More information and derivations of the hydrodynamic coefficients, wave drift force QTF and motion RAO can be found in Appendix A.

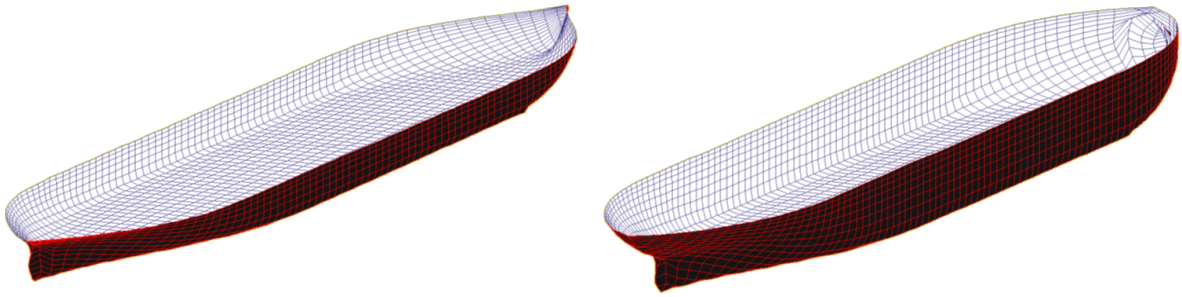

Figure 1.2: 3D mesh for ballast (right) and fully loaded (left) FPSO (Bluewater Energy Services)

Dynamic analysis

The quasi-static analysis includes preliminary estimates of the vessels surge response only. To include other motions, constraints in the mooring system and realistic environments, time domain simulations or model tests have to be carried out in order to estimate the design loads in the mooring system[6]. The time domain simulations include the multi-hinge connections of the SYMS, so that instead of hydrodynamic also the mechanical performance of the system can be analysed. This is done, since only hydrodynamics cannot describe the complete behaviour of the coupled system resulting from environmental loads[7]. Depending on the metocean data required, governing environmental load cases are defined which are implemented in Orcina's fully coupled numerical simulation software OrcaFlex. This is state-of-the-art software suitable for mooring design.
In OrcaFlex, the FPSO and mooring system are implemented using various elements. The FPSO is modeled as a floating body including a hydrodynamic database that is determined by diffraction and radiation software Hydrostar. The SYMS is modelled as different elements consisting of objects and lines, which can be connected rigidly or by constraints. These constraints are depending of the DoF of the different hinge joints. An example of the coupled system with sign convention in OrcaFlex is shown in Figure 1.3.

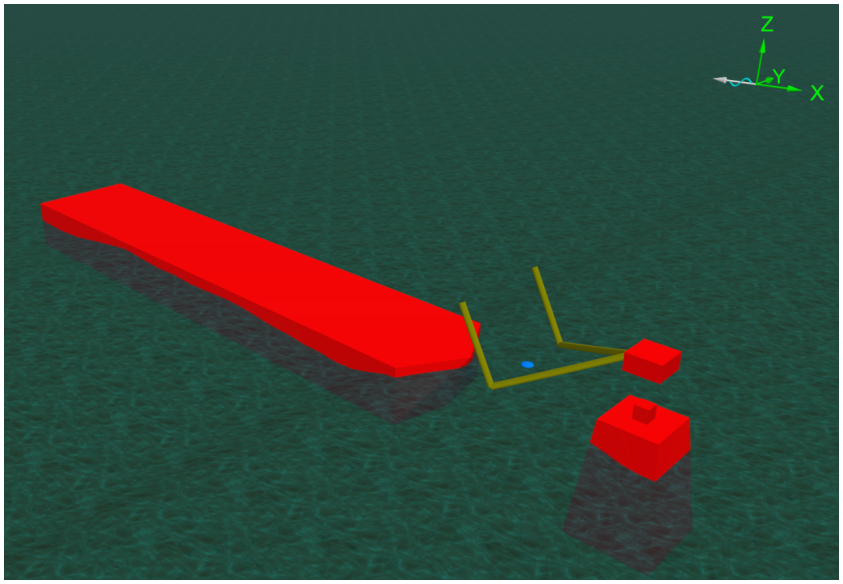

Figure 1.3: OrcaFlex model

Waves, wind and currents can be added based on user input. Wave and wind spectra are created using the metocean data available. Wave spectra are build by OrcaFlex using the significant wave height H_s, peak period T_p and the peak enhancement factor γ. Wind spectra are formed by inserting 1-hour mean

wind speed at an elevation of 10 m above Mean Sea Level (MSL). Generally, current profiles are taken constant over water depth. During a screening analysis, the critical load cases are identified resulting from different environmental conditions. Variations in significant wave height H_s and peak period T_p are performed. It shows that a general increase of both the significant wave height and peak period lead to an increase of the horizontal load on the tower.
Results of the surge excursion for different values of H_s is shown in Figure 1.4. As expected, the LF when compared to the Wave Frequent (WF) part of the surge motion is the largest contributor to the total surge motion. In addition, the surge excursion shows a significant increase when $H_s > 4$ m.

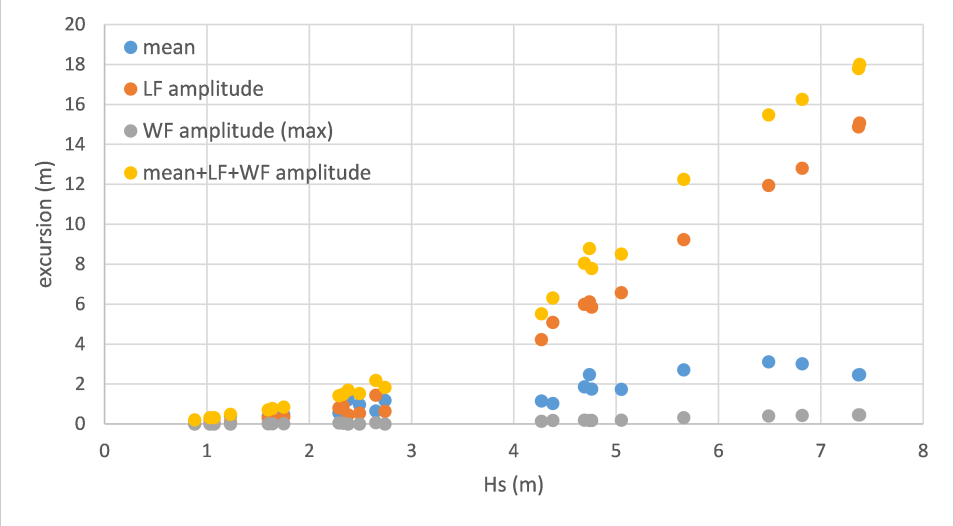

Figure 1.4: Relation between H_s and surge amplitudes (Bluewater Energy Services)

The main disadvantage of time-domain analyses is the computational time. Each time domain analysis simulates the system for a storm duration of 3.5 hours, in which the first 30 minutes of the simulation are used for swell-up. In this period, the FPSO can reach its mean equilibrium offset and heading. The swell-up period is excluded in the results. To check multiple environmental load cases and different variations of mooring systems, time domain simulations in OrcaFlex are very time consuming. Depending on the number of degrees of freedom, constraints, rigid components and computer efficiency, the simulation time will increase significantly. A suitable single run on an 8-core desktop PC giving realistic and accurate results of the vessels response and mooring load, will take approximately 1.5 hours.

1.4.2. Modelling of SYMS

This section focuses on modelling of coupled FPSO and SYMS. A handful of literature is available that describe quasi-static and dynamic modelling of the SYMS. The response of a coupled FPSO and SYMS can be executed in single degree, three-degree and six-degree of freedom models. All types including suitable methods are described below.
First of all, Pinkster *et al.* shows that for a single degree of freedom system with linear restoring properties, it is possible to estimate low frequency surge motions in the frequency domain related to the statistical variance. This can be done using estimates of the surge damping, the natural surge period and the duration of the simulation. For offshore applications, simulation time is often taken as 3 hours. It is known that the mooring characteristic does not have linear restoring properties. Therefore, this is a major assumption made in this single degree of freedom analysis. To include the non-linearity of the mooring system, frequency domain calculations are no longer possible. This also means that computational time will increase significantly. Runge-Kutta methods can be applied to calculate the surge response of the vessel per simulated time step. A significant decrease in computational time can be achieved by applying the harmonic balance principle[8]. This method assumes a periodic response containing limited frequency components. Since it is known that surge response will be close at the natural surge frequency, this may be a suitable and computational efficient method while including the non-linearity of the mooring system[9]. The application of harmonic balance for estimation of maximum mooring loads in offshore engineering is not found in literature yet. Both Runge-Kutta and

harmonic balance methods can be extended to multiple degree of freedom systems.
Li *et al.* starts with the solving the wave frequency motion and low frequency motion equations for surge, heave and pitch motions after defining the Equation of Motion (EoM) of the SYMS for surge, heave and pitch motions only. After that, the results are compared with model test that were carried out. The numerical results are approved by the experimental results. Fan *et al.* compares the calculated static and dynamic horizontal mooring force for a three-degree of freedom system with surge, heave and pitch only. By using real-time monitoring data obtained offshore it is shown that the horizontal mooring force can be described by the angle, angular velocity and angular acceleration of each part of the mooring structure only. Wu *et al.* adds the design of a fully coupled monitoring system that is able to combine measured environmental conditions with the position of the FPSO to calculate the restoring force of the SYMS. Both studies show a good agreement when comparing dynamic calculations with the monitoring data.
Lyu *et al.* develops a multibody dynamics model of a SYMS in six-degree of freedom by adding constraints and friction torque in all hinges. The model is able to calculate internal forces in the hinges and positions of all the components in the mooring system. Eventually, the numerical results are compared to real-time measured data developed by Wu *et al.* Again, it shows proper agreement with the measured dynamic behaviour of hinge joints and single bodies of the SYMS in an offshore environment.
The described studies for three-degree and six-degree of freedom systems above made use of the Kane dynamic method in order to obtain the EoM of the SYMS. An overview of the detailed steps to be taken in modelling with Kane's method is described by Hussain and Azlan.

1.4.3. Conclusion

Using the available literature, the governing motion response is likely to be the surge motion. Time domain modelling agrees with this, by confirming that the low-frequency surge motion response resulting from wave drift forces has the largest contribution to the total surge excursion and mooring load. Since time domain modelling is very time consuming, a sensitivity study of the dynamic response of the coupled system related to the variation in design parameters lacks. Until now, only screening analysis of T_p and H_s variations are done. A valuable addition to this is to find out which mooring design parameters results in the lowest mooring load.

1.5. Methodology

Section 1.3 states that it is not desired to recreate OrcaFlex by developing an extensive model. Therefore, in this project, a single degree of freedom system is adopted. By developing a linear and non-linear model, the most suitable and efficient model to propose a reliable set of mooring design parameters is embraced. To validate the surge response of both the linear and non-linear model, OrcaFlex is used. Accordingly, two major models have to be developed:

- The MATLAB design tool were the sensitivity of surge response related to design parameter change is showed and optimum design parameters are proposed. After validation of the surge response results in OrcaFlex, this will be a linear or non-linear single degree of freedom model.
- An OrcaFlex model including FPSO, SYMS and tower together with user defined environmental load cases (wind, waves and current). The model calculates the 3 hour dynamic response including mooring forces, multiple excursions and angles.

A schematic overview of the methodology is shown in Figure 1.5, including the design tool and OrcaFlex model. As can be seen, part of the design tool also consist of a static analysis. The three different steps in developing the design tool are described below:

1. The static analysis is to familiarize with the system, by creating load-excursion curves and check how these curves are influenced by variation of mooring design parameter. Related to these shape differences, the stiffness of the mooring system changes. The collection of different mooring characteristics can be used in the quasi-static model.

2. The quasi-static model uses the mooring characteristics obtained from the static analysis and adds environmental data and FPSO properties to calculate the surge motion and related mooring force. After that, optimization functions can be added to propose a set of efficient design parameters.

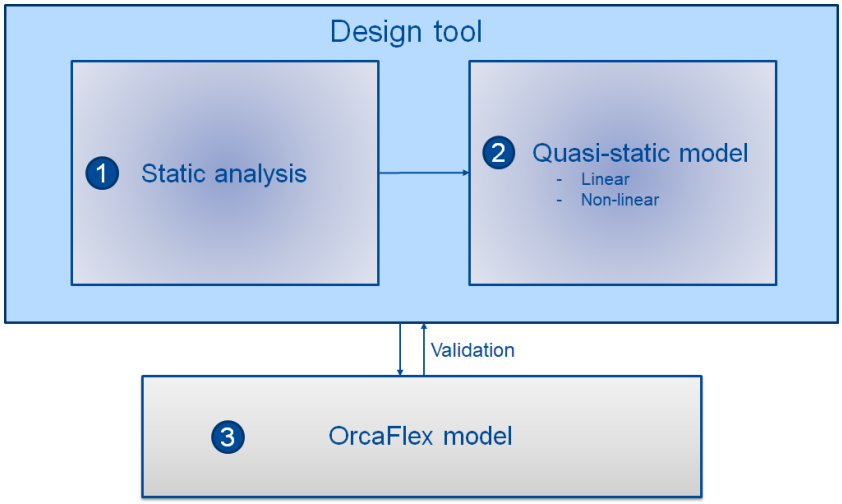

Figure 1.5: Methodology

3. The OrcaFlex model is used to validate output given by the design tool. The calculated surge response, including excursions and mooring forces, are validated together with the optimized set of mooring design parameters.

Note that goal of the design tool is not to obtain exact results when compared with OrcaFlex. After first validation in OrcaFlex, adjustments can be made to improve the design tool step by step.
To complete these models, the scope and assumptions have to be defined. These are described below.

1.5.1. Scope

The goal is to understand the sensitivities of surge response of the system related to certain design parameters. The design parameters that are going to be included in the analysis are the rigid components only. In addition, the environment analysed is based on the extreme wave height of H_S = 7.38 m in Figure 1.4. More information on the analysed extreme environment can be found in Appendix C.2. The vessel used in this project is the Stena Surprise FPSO that was provided for the Miztón project. The scope is summarized below:

- Pendulum length
- Yoke arm length
- Ballast weight
- Hang-off height for ballast (BL) and fully loaded (FL) vessel draft
- Analyse system with Stena Surprise FPSO
- Analyse collinear environment including wind, waves and current only

1.5.2. Assumptions

In the models to be developed, multiple assumptions have to be made. These assumption will be implemented in the design tool created in MATLAB. Since the moored FPSO will rotates itself into the environment, the analysed direction of waves, wind and current will be opposite to the bow (180°). The made assumptions will be:

- Analyse single degree of freedom system in head waves
- Assume dominant low frequent largely oscillating motions close to the natural surge frequency
- Estimate mooring force using the static load-excursion curve
- The OrcaFlex model is capable of describing reality and shall be used for validation purposes

1.6. Objectives

As discussed in the previous sections, the goal for this project is to develop a design tool that can assess the sensitivity of the surge response related to mooring design parameter variation. In addition, the design tool should propose optimum design parameters by minimizing the mooring load during operation. To reach this goal, several objectives are defined below. Objectives are separated in different stages, namely static analysis, the development of the design tool including Graphical User Interface (GUI) and design tool validation.

A static analysis of the SYMS only, excluding vessel properties and environmental loads, to:

- Familiarization with the system by creating load-excursion curves for predefined vessel surge excursion with benchmark mooring design parameters
- Identify the influence of mooring design parameter variation to the shape of the load-excursion curve
- Define range of mooring design parameters wherein optimization of the mooring force should be executed

The development of the design tool, by including the environmental conditions and FPSO properties to calculate extreme surge excursions and related mooring forces:

- Using the shape of the load-excursion curves to estimate the stiffness of the mooring system in a linear and non-linear way
- Define the sensitivity to the surge response following mooring design parameter variations in a given environment
- Obtain a set of efficient mooring design parameters that will minimize the mooring load in a given environment
- Understand the major assumptions made and how they may influence obtained results.

The development of a GUI in MATLAB App Designer for visualization purposes and convenience:

- Create interactivity by using sliding bars to adjust mooring design parameters that influence the shape of the load-excursion curve and calculated surge response
- Implementing the ability for users to include their own hydrodynamic data and collinear environmental load cases

Validation of the design tool by using an assembled six-degree of freedom OrcaFlex model:

- Implement the same hydrodynamic and environmental data as in the design tool
- Validate the calculated maximum surge excursions and mooring forces in the design tool
- Confirm the proposed optimum set of mooring design parameters by the design tool

1.7. Outline

This thesis includes six chapters. Chapter 2 reports the static analysis, with the goal of familiarization of the concept and by obtaining limits for mooring design parameters to be optimized. Chapter 3 describes how the mooring characteristics, FPSO properties and environmental conditions including assumptions are used to develop a linear and non-linear model. Chapter 4 outlines the results and validation of both linear and non-linear model whereafter the most appropriate model is selected. Chapter 5 reports the influence to the surge response calculations resulting from the assumptions made in the design tool. Finally, the conclusion and recommendations are given in Chapter 6.

2

Static analysis

2.1. Introduction

In this chapter, the first step in developing the design tool is made by executing a static analysis of the SYMS. The purpose of the static analysis is to get familiar with the SYMS concept by creating load-excursion curves in different components of the system. These load-excursion curves are able to describe the behaviour of the mooring system, since the gradient of the curve gives stiffness information. Here it is investigated how the shape of the load-excursion curves changes by varying mooring design parameters. According to Section 1.5.1, the analysed mooring design parameters are the pendulum length, yoke arm length, hang-off height and ballast weight. By varying each parameter separately while keeping others constant, the sensitivity of the parameter variation to the shape of the curve can be identified. By trail and error, the range of parameters for optimization of the force can be defined and implemented in the design tool. Throughout the project, the benchmark mooring design parameters are used. These mooring design parameters are based on existing projects around the world. With these parameters, realistic variations and comparisons of different mooring design parameters can be formed. The benchmark mooring design parameters are given in Table 2.1. It is assumed that the dimensions of the MSS and tower can be adjusted so that the defined mooring design parameters are physically practicable.
First, the coordinate system used to calculate the forces in the mooring system as a result of the surge excursion are defined in Section 2.2. Section 2.3 describes the static calculations to obtain the relevant mooring forces. Eventually, the sensitivity of the force related to the variation of mooring design parameters whereafter the limits can be defined are described in Section 2.4 and 2.5 respectively. In the end, the chapter summary is given in Section 2.6.

Parameters	Description	Value
L_C	Pendulum length	28.3 [m]
L_A	Yoke arm length	40.2 [m]
BW	Ballast weight	1800 [te]
HC (BL)	Relative hang-off height ballast	15.80 [m]
HC (FL)	Relative hang-off height fully loaded	8.78 [m]

Table 2.1: Benchmark mooring design parameters

2.2. Coordinate system

The coordinate system used for the static analysis, is an earth fixed reference frame located at the hang-off point between the yoke arm and tower. Positive x-axis is defined when the motion of the FPSO is towards the tower and positive z-axis is defined upwards as shown in Figure 2.1. The MSS is located at the bow of the FPSO connecting the upper end of the two pendulums. The ballast box connects the lower end of the pendulums to the yoke arm. The yoke arm connects the mooring system via a turntable to the tower. The hang-off height is defined as the relative vertical distance between

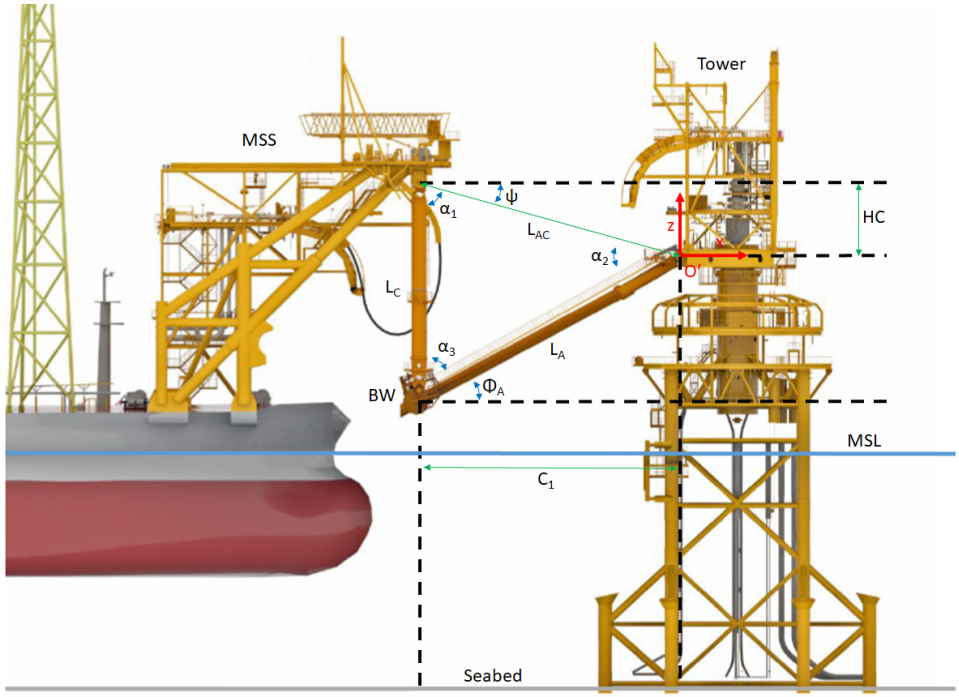

Figure 2.1: The SYMS in equilibrium position

the hang-off points of the MSS and tower. In this analysis, the Centre of Gravity (CoG) of the ballast box has no horizontal offset with respect to the MSS hang-off point, when the FPSO is in equilibrium position. In Figure 2.1 the MSL and seabed are depicted in the blue and grey line respectively. All the relevant angles and lengths that must be calculated to estimate the forces in the mooring system are described in the next section.

2.3. Mooring force calculations

The Free Body Diagram (FBD) resulting from a negative surge excursion is given in Figure 2.2. The axial forces F_C and F_A are defined as positive for tension and negative for compression for the pendulum and yoke arm respectively. The horizontal force F_{Ax} is defined positive for a pull force and negative for a push force at the tower.

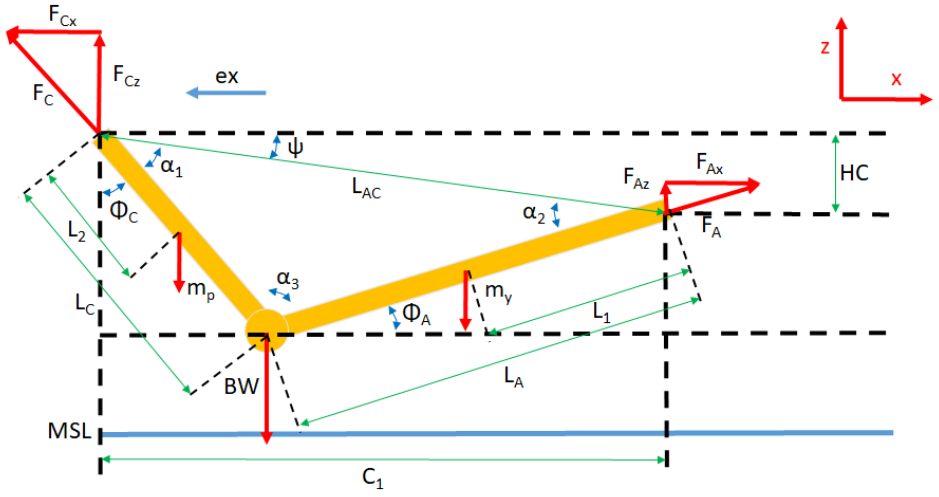

Figure 2.2: FBD for negative surge excursion

From Figure 2.2, it can be seen that horizontal distance between both hang-off points C_1 can be estimated using the excursion, yoke length, hang-off height and pendulum length. When both horizontal an shortest distance L_{12} between both hang-off points are known, all the angles can be calculated. With these angles, all forces of interest at the MSS and tower can be determined. The parameters and angles required are calculated as follows:

$$\begin{aligned} C_1 &= \sqrt{L_A^2 - (HC - L_C)^2} - ex & L_{AC} &= \sqrt{C_1^2 + HC^2} & \psi &= \tan^{-1}\left(\frac{HC}{C_1}\right) \\ \alpha_1 &= \cos^{-1}\left(\frac{L_C^2 + L_{AC}^2 - L_A^2}{2L_C L_{AC}}\right) & \alpha_2 &= \cos^{-1}\left(\frac{L_{AC}^2 + L_A^2 - L_C^2}{2L_A L_{AC}}\right) & & \\ \phi_A &= \alpha_2 - \psi & \phi_C &= \frac{\pi}{2} - \psi - \alpha_1 & & \end{aligned} \tag{2.1}$$

By including both the mass of the pendulum m_p and yoke arm m_y and applying the equilibrium relationship, the sum of horizontal and vertical forces can be written as:

$$\begin{cases} F_{Ax} &= F_{Cx} \\ F_{Az} + F_{Cz} &= (m_y + BW + m_p)g \end{cases} \tag{2.2}$$

When calculating the moment equilibrium around the CoG of the ballast weight for both the left and right side, the following equilibrium states are reached:

$$\begin{cases} F_{Az} L_A \cos\Phi_A &= F_{Ax} L_A \sin\Phi_A + m_y (L_A - L_1)\cos\Phi_A \\ F_{Cz} L_C \sin\Phi_C &= F_{Cx} \cos\Phi_C + m_p (L_C - L_2)\sin\Phi_C \end{cases} \tag{2.3}$$

By applying Equations 2.2 and 2.3, the projected horizontal force at the tower can be obtained. Using the angles between the pendulum Φ_C and yoke arm Φ_A, all the axial and projected vertical forces can be determined as well:

$$\begin{aligned} F_{Ax} &= \frac{\frac{L_2}{L_C} m_p + BW + \frac{L_1}{L_A} m_y}{\cot\Phi_C + \tan\Phi_A} g & &= F_{Cx} \\ F_A &= \frac{F_{Ax}}{\cos\Phi_A} & F_C &= \frac{F_{Cx}}{\sin\Phi_C} \\ F_{Az} &= F_A \sin\phi_A & F_{Cz} &= F_C \cos\phi_C \end{aligned} \tag{2.4}$$

All the forces can now be calculated using the mooring system dimensions. By assuming an excursion range from 20 meters away from and towards the tower, the mooring forces at every excursion can be estimated. The load-excursion curves for ballast and fully loaded condition of the FPSO with benchmark mooring properties are depicted in Figure 2.3. Note that the FPSO in ballast condition has a higher relative vertical hang-off height HC. When in operation, HC decreases till the FPSO reaches the fully loaded condition. Hence, the mooring characteristic will vary till the blue line reaches the red line. It can be seen that the horizontal mooring force and axial yoke arm force in Figure 2.3a and 2.3c respectively are almost identical. This is caused by the small yoke arm angle Φ_A at maximum excursions. Therefore, the vertical mooring force at the tower is relatively small.
In this project, the horizontal mooring force is in the same direction as the environmental forces. Accordingly, the horizontal mooring force provides the restoring force to keep the FPSO from drifting away. Hence, the horizontal mooring force is often referred to as restoring mooring force. The project goal is to minimize this restoring mooring force. Note that surging away from the tower results in a pull force, while surging towards the tower results in a push force at the connection point of the yoke arm and tower. In the next section, the limits of the mooring design parameters are defined wherein optimization of the restoring mooring force has to be executed.

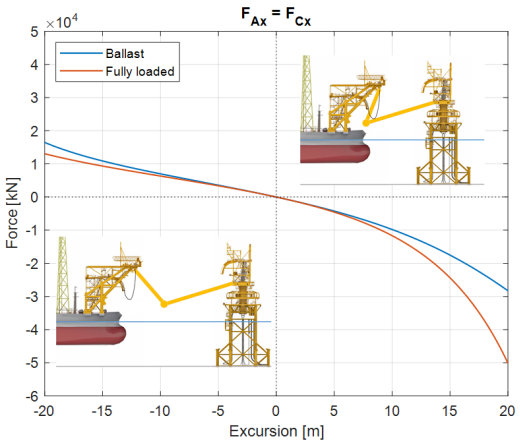

(a) Horizontal tower and MSS force

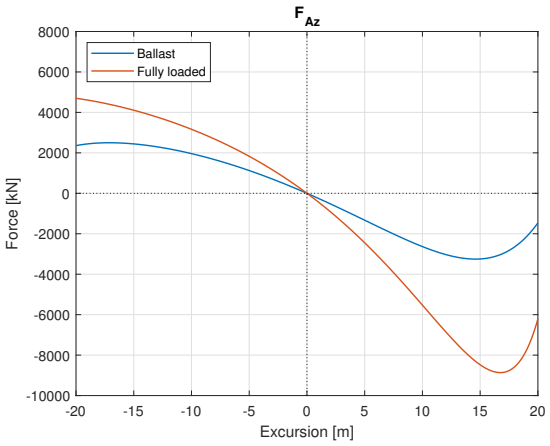

(b) Vertical tower force

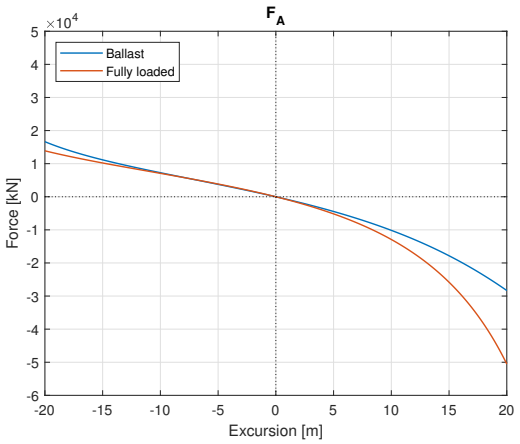

(c) Axial yoke arm force

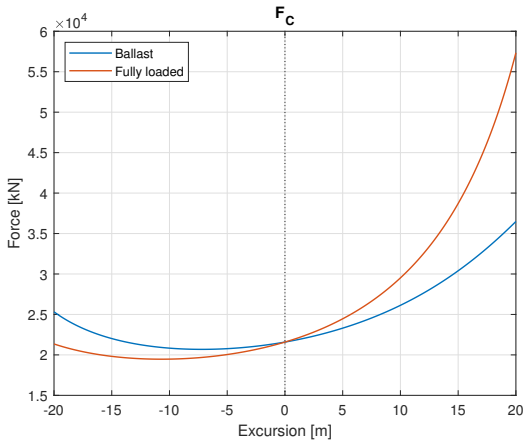

(d) Axial pendulum force

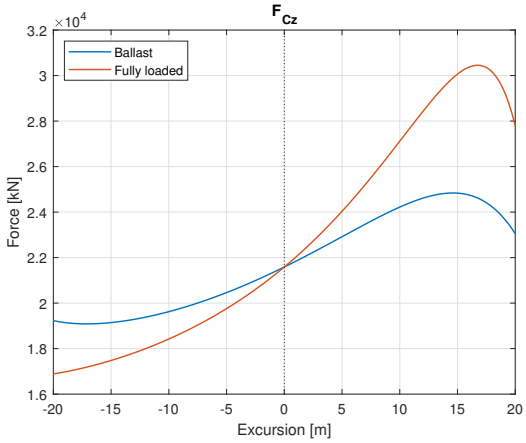

(e) Vertical MSS force

Figure 2.3: Static load-excursion curves related to surge excursion

2.4. Sensitivity to parameter variation

As mentioned in Section 2.3, the limits of mooring design parameters used to calculate the restoring mooring force F_{Ax} has to be defined. First, it has to be investigated how the shape of the load-excursion curve changes by varying mooring design parameters. The load excursion curve is divided in three parts so that the sensitivity to that part of the curve can be defined. The load-excursion curve can be divided

in the pull (negative excursion), linear (around zero) and push (positive excursion) part.
The benchmark mooring design properties given in Table 2.1 are used to vary the parameters to realistic values. Varying each mooring design parameter at once and keeping others constant results in the load-excursion curves shown in Figure 2.4.

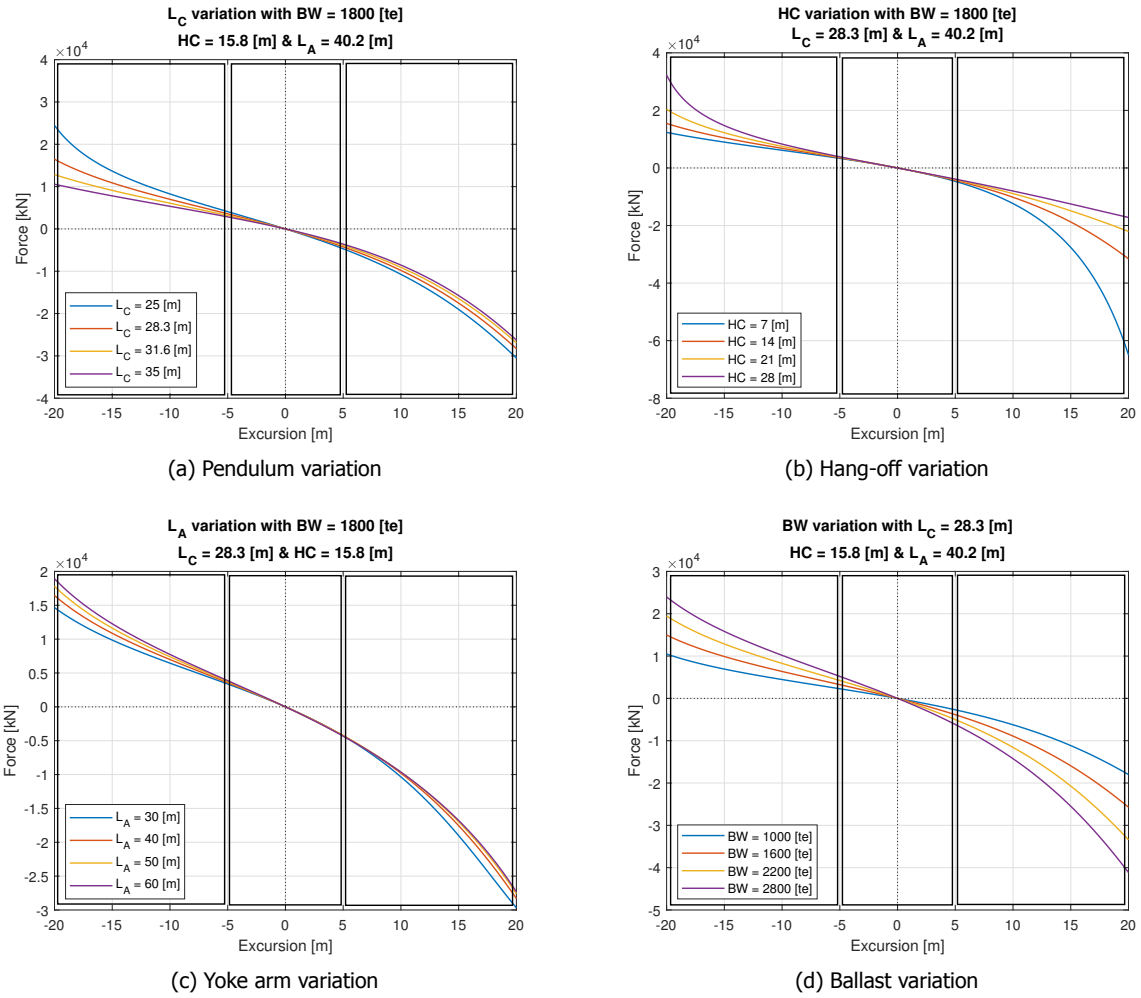

(a) Pendulum variation

(b) Hang-off variation

(c) Yoke arm variation

(d) Ballast variation

Figure 2.4: Load-excursion sensitivities

The sensitivity of every part of the load-excursion curve in Figure 2.4, by varying each mooring design parameter separately, is described below. The sensitivities are described when the parameter is increased. Note that when a decrease in parameter is required, the opposite applies.

2.4.1. Pendulum length

For the part of the pull force holds:

- Increasing the pendulum length results in a decrease of the gradient by moving the asymptote back to a larger excursion

For the linear part of the curve holds:

- Increasing the pendulum length results in a decrease of the gradient. In general, the mooring system becomes less stiff

For the part of the push force holds:

- Increasing the pendulum length does not influence the gradient and does not move the asymptote

2.4.2. Hang-off height

For the part of the pull force holds:

- Increasing the hang-off height results in an increase of the gradient by moving the asymptote closer to a smaller excursion

For the linear part of the curve holds:

- Increasing the hang-off height has insignificant influence to the linear part of the load-excursion curve. The stiffness of the mooring system at the linear part can be considered equal.

For the part of the push force holds:

- Increasing the hang-off height results in a decrease of the gradient by moving the asymptote back to a larger excursion

2.4.3. Yoke arm length

For the part of the pull force holds:

- Increasing the yoke arm length results in an insignificant increase of the gradient by moving the asymptote closer to a smaller excursion

For the linear part of the curve holds:

- Increasing the yoke arm length has insignificant influence to the linear part of the load-excursion curve. The stiffness of the mooring system at the linear part can be considered equal.

For the part of the push force holds:

- Increasing the yoke arm length does not influence the gradient and does not move the asymptote

2.4.4. Ballast weight

Increasing the ballast weight results in an increase of the gradient at every part of the curve. The asymptote is not moved by a variation in ballast weight. When increasing the ballast weight, the total mooring system can be considered more stiff.

According to Section 2.4.3, the variation of yoke arm length has insignificant influence to the shape of the load-excursion curve. Therefore, the yoke arm length variation is neglected in further analyses. Using the information given in this section, the limits of the mooring design parameters can be estimated by finding the combination of parameters resulting in asymptotes.

2.5. Mooring design parameter limits

By trail and error, the asymptotes of the mooring system can be found. For example, when the vertical hang-off height becomes larger than the pendulum length, the ballast box is located above the hang-off point at the tower. This results in an extreme increase of the restoring mooring force where it reaches an asymptote at a certain excursion. Hence, in defining the limits of optimization parameters, the hang-off height should be smaller than the pendulum length. It is known that the ballast weight does not move the asymptote. Therefore, it does not matter what the limits of the ballast weight values are. Since the benchmark value of BW is equal to 1800 tons, it is chosen to define the limits at $\pm$ 800 tons. The parameters that are able to move the asymptote are the hang-off height and pendulum length. By combining both parameters and plotting them over the excursion range, 3D surfaces can be developed. These plots are used to indicate asymptotes for different combinations of the hang-off height and pendulum length. After multiple iterations, the defined values for HC and L_C are shown in Figure 2.5. Note that each plane corresponds to a single hang-off height value, varying from 7 to 24 m. The red arrow represents the increase of the hang-off height parameter.
As described in Section 2.4.1, the variation in pendulum length for maximum positive excursions can be considered insignificant to the force. This is confirmed by the figure. On the other hand, for negative excursions, the decrease of pendulum length results in a large increase of the horizontal mooring force. Especially in combination with large hang-off heights. The optimum mooring design parameters can

be found somewhere inside the depicted plane. In combination with a suitable ballast weight, the desired mooring system can be designed. The defined limits used for optimization during the project are given in Table 2.2 for ballast and fully loaded condition of the FPSO. The difference for ballast and fully loaded draft results in separate hang-off height limits. Table 2.1 shows that this draft difference is approximately seven meters.
The next step is to include environmental conditions and FPSO properties in order to use the shape of the mooring characteristic in the estimation of the surge response. This is described in Chapter 3 by including the mooring characteristic in a linear and non-linear way.

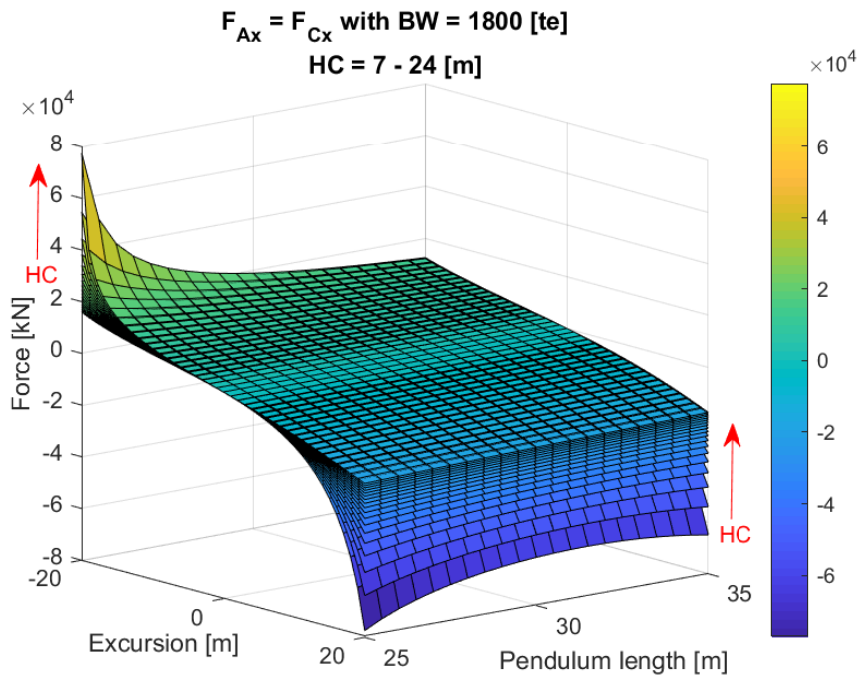

Figure 2.5: Planes of boundary values for the system

Mooring design parameter	Symbol	Unit	Ballast	Fully loaded
Pendulum length	L_C	[m]	25 - 35	
Hang-off height	HC	[m]	14 - 24	7 - 17
Ballast weight	BW	[te]	1000 - 2600	

Table 2.2: Defined limits of mooring design parameters

2.6. Chapter summary

This chapter describes the static analysis of the mooring system in the xz-plane. The first step in the development of the design tool is made by creating load-excursion curves for the surge motion only. By varying mooring design parameters, the shape of the curves are modified. By dividing the load-excursion curve in three parts, the shape variation resulting from increasing mooring design parameters are identified. It was shown that the yoke arm length has insignificant influence to the shape of the load-excursion curve. Therefore, in further analyses, the length of the yoke arm is kept constant at the benchmark value of 40.2 m. The results of the shape sensitivity analysis of the load-excursion curve are summarized in Table 2.3.
By trial and error, the limits of the mooring design parameters are defined. Within these limits, the mooring system is to be optimized by minimizing the maximum horizontal restoring mooring force. The limits are given in Table 2.2. The mooring characteristics described in this chapter are going to be used in Chapter 3. Here it is described how the surge response is calculated by including the FPSO properties and environmental conditions.

Direction	Change of shape	As a result of
Away from tower (-)	Move asymptote back	Increase pendulum length Decrease hang-off height
Linear part (±)	Increase gradient	Decrease pendulum length Increase ballast weight
Towards tower (+)	Move asymptote back	Increase hang-off height

Table 2.3: Influence of the increase/decrease of mooring design parameters to the shape of the load-excursion curve

3

Model description

3.1. Introduction

In Chapter 2, the influence of individual design parameter variation to the shape of the non-linear mooring force are identified statically. By defining a large amount of mooring design parameter sets, using chosen limits, unique load-excursion curves can be constructed. Chapter 2 also states that the gradient of these curves represents the stiffness of the mooring system. The stiffness of the mooring system can be implemented in the design tool in a linear or non-linear way. Both ways will use the mooring characteristics, environmental conditions and FPSO properties as input in order to calculate the maximum surge excursion and restoring mooring force.
As described in Section 1.4, every FPSO has unique wave frequency dependent added mass and potential damping values that are influenced by the shape of the hull. By using a mesh of the FPSO, these hydrodynamic coefficients can be estimated using diffraction and radiation software Hydrostar. Hydrostar also determines the frequency and directional dependent first order and second order transfer functions. These transfer functions includes the force and motion RAO and wave drift force QTF. The force transfer functions can be calculated by direct pressure integration on the hull of the ship. Using these force transfer functions, software packages like OrcaFlex can convert a representation of a wave spectrum in the frequency domain into a time signal in the time domain, without doing direct pressure integration on the hull of the ship. Since the hydrodynamic coefficients and transfer functions are frequency and draft dependent, Hydrostar needs to calculate them for both ballast and fully loaded draft before they can be used in this project. The calculation procedures for the wave drift force QTF, motion RAO, added mass and potential damping are described in Appendix A. The chosen linear and non-linear model to be developed in this project are described in Section 3.1.1 and 3.1.2 respectively.

3.1.1. Linear model

As stated in Section 1.4, the low frequent surge motions induced by second order wave drift forces can be considered dominant to the total surge motions and related mooring force. As described in Appendix A.3, the second order wave drift forces consists of a mean, low frequent and high frequent (wave frequent) part where the low frequent part induces these low frequent motions. Since single point moored structures have low natural surge frequencies and low surge damping, it is expected that the surge motion will be close to the natural surge frequency[2]. Pinkster *et al.* shows that for a system with linear restoring properties, it is possible to estimate low frequency surge motions related to their statistical variance. It is assumed here, that the wave elevations are normally distributed and that the resulting surge excursions are Rayleigh distributed. By doing spectral analysis in the frequency domain, the variance and standard deviation of the surge response can be estimated. By using the standard deviation as Rayleigh parameter, the Most Probable Maximum (MPM) surge excursion can be calculated. Eventually, the related mooring force using the load-excursion curve can be evaluated. The main advantage of this method is that the MPM surge excursion can be calculated extremely fast. In this project, the linear model will be referred to as 'Rayleigh model'.

3.1.2. Non-linear model

As shown in Chapter 2, the restoring mooring force is non-linear with respect to the excursion. This means that the Rayleigh model makes a major assumption by linearizing the mooring force. However, when implementing a non-linear mooring stiffness in the model, it is not possible to do frequency domain calculations anymore. Therefore, with a non-linear model time domain calculations are required to calculate the surge response of the moored system. Pinkster has shown that the surge motion for single point mooring systems in head waves contains small wave frequent motions, but are dominated by low resonant motions with large amplitude as shown in Figure 3.1.

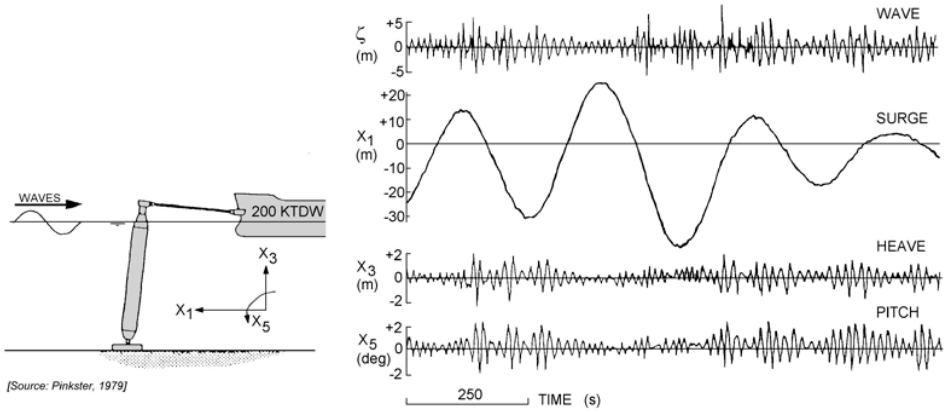

Figure 3.1: Low frequent surge motion in head waves (Pinkster, 1979)

With this information, it can be assumed that the solution (surge response) of the non-linear system can be approximated by a small number of sinusoids with a frequency close to the natural surge frequency of the moored vessel. Normally, a combination of sinusoids is referred to as a Fourier series. By assuming a periodic solution of the non-linear equation of motion in the form of a truncated Fourier series, the principle of harmonic balance is able to approximate the solution of the system[8]. By including more terms to the Fourier series, it is expected that the approximation will converge to the exact solution when the order is increased towards infinity. However, a reasonable approximation of the maximum surge excursion could already be achieved when one or a few sinusoids are considered. Since the surge response with a large number of mooring design parameter sets have to be checked, it is expected that using harmonic balance will be less time consuming when compared to numerical integration methods.
Since the non-linear system has to be analysed in the time domain, harmonic balance requires a time signal of the environmental force in order to approximate the surge response of the system. OrcaFlex is used to convert a representation of a wave spectrum to a time signal. With the calculated surge response, in the same way as for the Rayleigh model, the related restoring mooring force can be evaluated using the load-excursion curve. In this project, the non-linear model will be referred to as the 'Harmonic Balance Method'.

A schematic overview of how both the Rayleigh model and Harmonic Balance Method estimate the surge response is given in Figure 3.2. To accomplish this, the linear and non-linear equations of motions are required and described in Section 3.2 separately. Both Rayleigh model and Harmonic Balance Method, including steps and assumptions, are described in more detail in Section 3.3 and 3.4. Afterwards, the optimization procedure by minimizing the mooring force is described in Section 3.5. Eventually, the chapter summary is given in Section 3.6.

3.2. Equations of motion

This section describes the linear and non-linear coupled equations of motion including vessel properties, mooring characteristics and environmental components. Since the surge motion is dominant for the assumed head environment, a single degree of freedom system is described. Furthermore, this section demonstrates how the linear system can be converted from time domain to frequency domain.

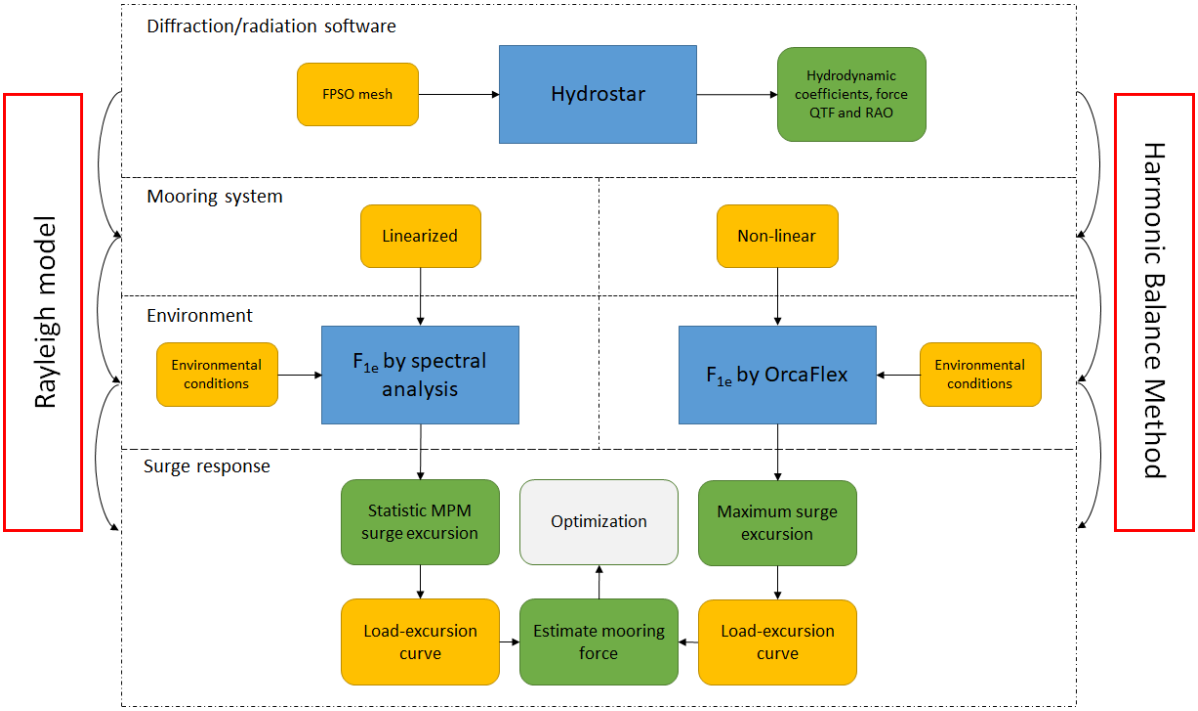

Figure 3.2: Overview of the Rayleigh model and Harmonic Balance Method

3.2.1. Vessel

Without the mooring system, consider the vessel as a free floating body with mass M_v and acting forces $F_v(t)$ on the vessel shown in Figure 3.3. Imagine a collinear environment, including wind waves and current approaching the vessel from 180°. The equation of motion for a 6 DoF system is given by Newton's second law of motion:

$$\mathbf{M}_v \ddot{\vec{x}}_v(t) = \sum \vec{F}_v(t) \tag{3.1}$$

Where for $\mathbf{M}_v$ is the 6 × 6 mass matrix, $\ddot{\vec{x}}_v(t)$ the 6 × 1 acceleration vector and $\vec{F}_v(t)$ the 6 × 1 force vector acting on the vessel. Here, indices 1,2,...6 corresponding to the motions in surge, sway, heave, roll, pitch and yaw respectively. The mass matrix $\mathbf{M}_v$ and vectors $\ddot{\vec{x}}_v(t)$ and $\vec{F}_v(t)$ given in Equation 3.1 are given below[14]:

$$\mathbf{M}_v = \begin{bmatrix} m & 0 & 0 & 0 & m \cdot z & -m \cdot y \\ 0 & m & 0 & -m \cdot z & 0 & m \cdot x \\ 0 & 0 & m & 0 & -m \cdot x & 0 \\ 0 & -m \cdot z & m \cdot y & I_{44} & -I_{45} & -I_{46} \\ m \cdot z & 0 & -m \cdot x & -I_{54} & I_{55} & -I_{56} \\ -m \cdot y & m \cdot x & 0 & -I_{64} & -I_{65} & I_{66} \end{bmatrix} \tag{3.2}$$

$$\ddot{\vec{x}}_v(t) = \begin{bmatrix} \ddot{x}_1(t) \\ \ddot{x}_2(t) \\ \ddot{x}_3(t) \\ \ddot{x}_4(t) \\ \ddot{x}_5(t) \\ \ddot{x}_6(t) \end{bmatrix} \qquad \vec{F}_v(t) = \begin{bmatrix} F_{1v}(t) \\ F_{2v}(t) \\ F_{3v}(t) \\ F_{4v}(t) \\ F_{5v}(t) \\ F_{6v}(t) \end{bmatrix} \tag{3.3}$$

Where m is the mass of the vessel and x, y and z are the coordinates of the CoG of the vessel with respect to the body fixed reference frame. I_{ij} is the mass moment of inertia of the vessel where the index pair identifies the mass moment of inertia contribution in direction i due to the motion of the vessel in direction j (i,j = 1,2...6). Let us consider a vessel symmetric around x = y = 0, where the

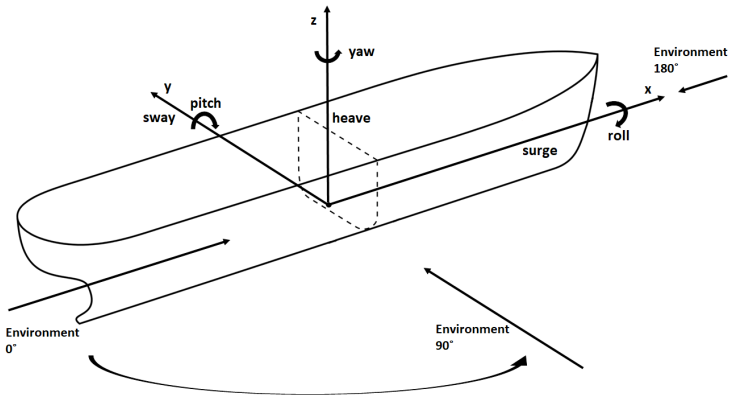

Figure 3.3: Motion axis sign convention

body fixed reference frame equals the CoG position. Using the symmetry properties, the mass matrix $\mathbf{M}_v$ can be reduced to a diagonal matrix:

$$\mathbf{M}_v = \begin{bmatrix} m & 0 & 0 & 0 & 0 & 0 \\ 0 & m & 0 & 0 & 0 & 0 \\ 0 & 0 & m & 0 & 0 & 0 \\ 0 & 0 & 0 & I_{44} & 0 & 0 \\ 0 & 0 & 0 & 0 & I_{55} & 0 \\ 0 & 0 & 0 & 0 & 0 & I_{66} \end{bmatrix} \tag{3.4}$$

Reducing the system to surge (i = 1) motion only, Equations 3.2 and 3.3 become:

$$M_v(t) = m \qquad \ddot{x}_v(t) = \ddot{x}_1(t) \qquad F_v(t) = F_{1v}(t) \tag{3.5}$$

The total forces acting on the vessel $F_v(t)$ consists of a summation of environmental $F_e(t)$ and hydromechanic reaction forces $F_h(t)$. The environmental forces consists of wave, wind and current and the hydromechanic reaction forces consists of a static and dynamic part. The total environmental force in surge direction can now be written as:

$$F_{1v}(t) = F_{1wave}(t) + F_{1wind}(t) + F_{1current}(t) + F_{1h,stat}(t) + F_{1h,dyn}(t) \tag{3.6}$$

$F_{1h,stat}$ results from the hydrostatic reaction force $\mathbf{C}_v\vec{x}_v(t)$ induced by the change of buoyancy. This change of buoyancy is caused by a displacement in heave, roll and pitch motion only. Therefore, the term $F_{1h,stat}$ in our case is equal to zero. The dynamic reaction force consist of the added mass matrix in phase with the acceleration $\mathbf{A}_v\ddot{\vec{x}}_v(t)$ and the potential damping matrix in phase with the velocity $\mathbf{B}_v\dot{\vec{x}}_v(t)$.
The added mass of the vessel in surge direction a_{11} can be considered as inertia that is is added to the vessel, since it deflects a certain volume of fluid when it moves through it. The potential surge damping b_{11} can be considered as energy loss due to wave radiation when the vessel is moving through it. Now, the total force on the vessel in surge direction can be written as:

$$F_{1v}(t) = F_{1wave}(t) + F_{1wind}(t) + F_{1current}(t) - a_{11}\ddot{x}_1(t) - b_{11}\dot{x}_1(t) \tag{3.7}$$

Substitution of Equation 3.7 in Equation 3.1 gives us the vessels surge EoM:

$$(m + a_{11})\ddot{x}_1(t) + b_{11}\dot{x}_1(t) = F_{1wave}(t) + F_{1wind}(t) + F_{1current}(t) \tag{3.8}$$

3.2.2. Mooring force

The restoring mooring force, as shown in Chapter 2, is non-linear. However, it is possible to linearize the mooring force, resulting in two different equations.

Linear system

Consider the mooring system as a linear spring with stiffness c_m and neglecting possible damping, the EoM of the mooring system with displacement x_m can be given by:

$$F_m(t) = c_m x_m(t) \tag{3.9}$$

By linearizing the mooring force derived in Section 2.3, the EoM of the mooring system in surge direction F_{1m} can be written as:

$$F_{1m}(t) = c_{1m} x_1(t) \tag{3.10}$$

Non-linear system

Now, consider a mooring system with non-linear restoring mooring force. By assuming a 3^{rd} order polynomial fit of the load-excursion curve, the mooring force can be expressed as:

$$F_{1m}(t) = k_1 x_1(t) + k_2 x_1^2(t) + k_3 x_1^3(t) \tag{3.11}$$

Where k_1, k_2 and k_3 are constant values corresponding to shape of the load-excursion curve.

3.2.3. Coupled equation of motion

The EoM of the coupled system, shown in Figure 3.4, including vessel and mooring system can now be derived by combining Equation 3.8 with Equation 3.10 or 3.11:

$$(m + a_{11})\ddot{x}_1(t) + b_{11}\dot{x}_1(t) = F_{1wave}(t) + F_{1wind}(t) + F_{1current}(t) - F_{1m}(t) \tag{3.12}$$

The motions of a moored vessel induced by the described environment in irregular waves consists of small wave frequent motions and large low frequent surge motions. The high wave frequent motions are caused by first order wave forces $F^{(1)}$ proportional to the wave elevation and low frequent motions by second order wave forces $F^{(2)}$ proportional to the square of the wave elevation. Therefore, the total wave force $F_{1wave}(t)$ can be written as a summation of these forces:

$$F_{1wave}(t) = F_{1wave}^{(1)}(t) + F_{1wave}^{(2)}(t) \tag{3.13}$$

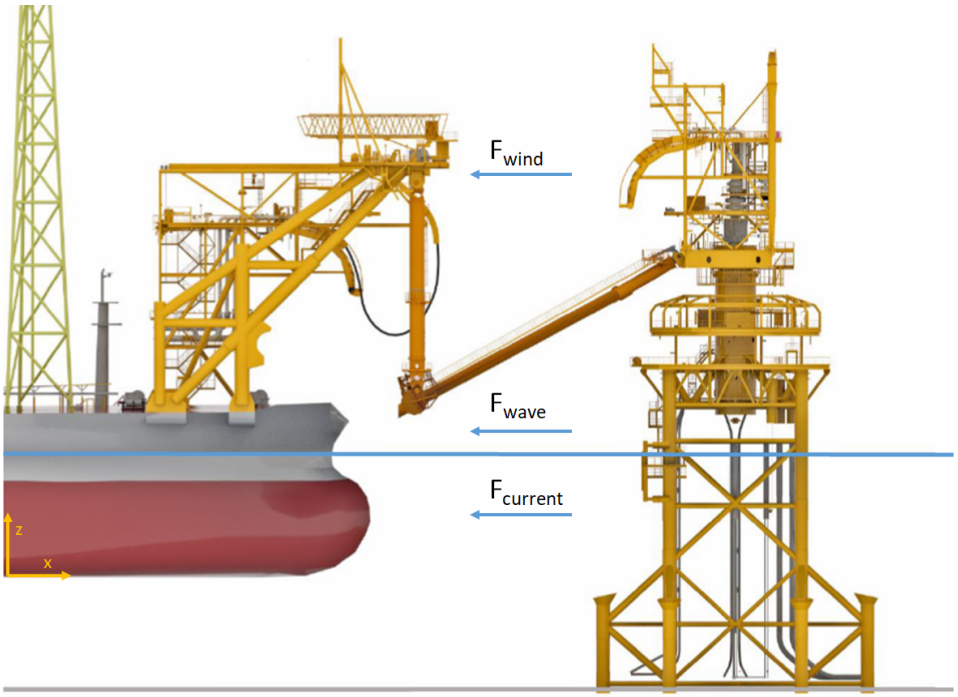

Figure 3.4: The coupled system

Linear system

For the linearized mooring system, the coupled EoM is given by:

$$\begin{aligned}(m+a_{11})\ddot{x}_1(t)+b_{11}\dot{x}_1(t) &= F_{1wave}(t)+F_{1wind}(t)+F_{1current}(t)-F_{1m}(t)\\ (m+a_{11})\ddot{x}_1(t)+b_{11}\dot{x}_1(t)+c_{1m}x_1(t) &= F^{(1)}_{1wave}(t)+F^{(2)}_{1wave}(t)+F_{1wind}(t)+F_{1current}(t)\end{aligned} \tag{3.14}$$

Let us consider the right hand side of the equation as the total environmental force $F_{1e}(t)$ and that the behaviour of the vessel is linearly related to its displacement, velocity and acceleration. Now, the EoM may be converted in the frequency domain by assuming solutions for $x_1(t)$ and $F_e(t)$:

$$\begin{aligned}x_1(t) &= \Re\left\{\hat{\zeta}_a e^{i\omega t}\right\}\\ F_{1e}(t) &= \Re\left\{\hat{F}_a e^{i\omega t}\right\}\end{aligned} \tag{3.15}$$

Here, $\Re$ is the real part and $\hat{\zeta}_a$ and $\hat{F}_a$ are the complex amplitudes of the motion and force respectively. By substituting the derivatives of Equation 3.15 into Equation 3.14 and by taking into account that the added mass a_{11} and potential damping b_{11} are frequency dependent, the EoM in the frequency domain becomes:

$$\begin{aligned}\Re\left\{\left[-\omega^2(m+a_{11})+b_{11}i\omega+c_{1m}\right]e^{i\omega t}\hat{\zeta}_a\right\} &= \Re\left\{\hat{F}_a e^{i\omega t}\right\}\\ \left[-\omega^2(m+a_{11}(\omega))+b_{11}(\omega)i\omega+c_{1m}\right]\hat{\zeta}_a &= \hat{F}_a(\omega)\end{aligned} \tag{3.16}$$

Non-linear system

Considering the system with a non-linear restoring mooring force $F_{1m}(t)$ described in Equation 3.11, the EoM cannot be converted in the frequency domain. Therefore, the non-linear EoM in the time domain stays:

$$(m+a_{11})\ddot{x}_1(t)+b_{11}\dot{x}_1(t)+F_{1m}(t) = F^{(1)}_{1wave}(t)+F^{(2)}_{1wave}(t)+F_{1wind}(t)+F_{1current}(t) \tag{3.17}$$

3.3. Rayleigh model

This section describes the linear model, referred to as the Rayleigh model, in more detail. It describes the assumptions and calculations done to calculate the surge response of the system. Modelled FPSO properties and the extreme collinear environment including wind, waves and current are described in Appendix C. Referring back to Figure 3.2, the environmental forces acting on the FPSO are estimated using spectral analysis. Using the estimated environmental forces and linearized mooring system, a MPM surge excursion can be estimated if it is assumed that the excursion behaviour is Rayleigh distributed and resonant. This means that N peaks in a surge excursion time signal of duration T have a Probability Density Function (PDF) given by:

$$P\left(x_1,\sigma_{x_1}\right) = \frac{x_1}{\sigma^2_{x_1}} e^{-\left(\frac{x_1^2}{2\sigma^2_{x_1}}\right)} \tag{3.18}$$

Where x_1 and σ_{x_1} are the surge excursion and standard deviation respectively. The MPM of the low frequent surge excursion is defined as the summation of the mean and oscillating part[6]:

$$x_{MPM} = \overline{x_1} + \sigma_{x_1}\sqrt{2\ln N} \tag{3.19}$$

Here it is assumed that the wave elevations are normally distributed and the excursion peaks Rayleigh distributed. Equation 3.19 is based on the dominant low frequent surge excursions only induced by low frequent second order wave drift forces. To include a correction of the small wave frequent surge motions as well, the surge motion RAO is used. The significant surge amplitude $\overline{x_{1a_s}}$, defined as the mean value of the highest one-third part of the amplitudes, resulting from first order wave forces is added to Equation 3.19:

$$x_{MPM} = \overline{x_1} + \sigma_{x_1}\sqrt{2\ln N} + \overline{x_{1a_s}} \tag{3.20}$$

The following sections describe the consecutive steps to be taken to calculate the MPM surge excursion according to Equation 3.20. A more detailed calculation procedure including applied equations is described in Appendix D.

3.3.1. Mean environmental force

As described in Section 3.1, the governing low frequent motion is influenced by the second order wave drift forces in irregular waves. As derived in Appendix A.3, the second order wave drift forces consists of a mean, low frequent and high wave frequent part. The mean second order wave drift force results in a mean displacement of the moored vessel, while the low frequent part of the second order wave drift force results in a large oscillation around the mean displacement as shown in Figure 3.1. Since current and wind forces are included, and considered constant, the mean excursion $\overline{x_1}$ is induced by a summation of the mean second order wave drift, mean current and mean wind force. Calculation of the mean environmental force $\overline{F_{1e}}$, resulting in a mean excursion, is the first step in the Rayleigh model.

3.3.2. Mooring stiffness approximation

Since the Rayleigh model assumes a mooring system with linear restoring properties, the next step is to linearize the restoring mooring force. According to Equation 3.19, the expected MPM surge excursion x_{MPM} is a result of a low frequent oscillation around the mean excursion $\overline{x_1}$. This implies that the stiffness of the mooring system has to be estimated at the mean excursion. Using the load-excursion curves for ballast and fully loaded condition, the mean excursions can be read at the intersection point of the mean environmental force and the expected mean excursion. By calculating the gradient of the curve a small step left and right with respect to the mean excursion, the stiffness of the mooring system c_m at the mean surge excursion $\overline{x_1}$ can be estimated.
The approximation of the mooring stiffness c_m for ballast and fully loaded condition is visualized in Figure 3.5. Note that the mean environmental force $\overline{F_{1e}}$ is dependent on the draft of the FPSO, which means that the estimate mooring stiffness c_m for ballast and fully loaded condition is different. Estimating the mooring stiffness at the mean surge excursion is the second step in the Rayleigh model.

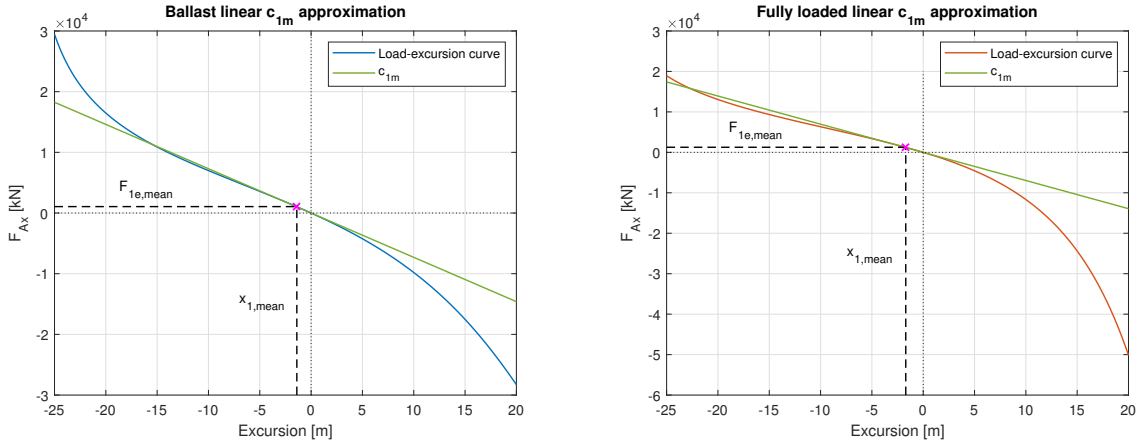

(a) Ballast (b) Fully loaded

Figure 3.5: Surge mooring stiffness approximation of the mooring system at $\overline{x_1}$

3.3.3. Added mass and damping estimation

Section 3.1 points out, that the expected period of the surge motion will be close to the natural surge period of the single point moored FPSO. Accordingly, using this assumption the frequency dependent added mass and potential damping can be estimated as a constant at the natural surge frequency. Since the natural surge period is very large, the constant added mass and potential damping values can be estimate at $\omega \approx 0$. Normally, the damping of the vessel include the summation of viscous and potential damping. However, according to Figure C.2b, the potential damping of the Stena Surprise FPSO at $\omega \approx 0$ can be considered zero. This means that the potential damping in this project can be considered as viscous damping only. Wichers *et al.* shows that the constant still water surge damping for single point moored structures can be estimated by viscous damping only, which agrees that the potential damping in this project can be neglected. Additionally, Wichers *et al.* shows that the viscous damping for single point moored structures consists of an additional term, the wave drift damping.

The damping term now consists of the damping provided by friction as it moves to still water and an additional frictional damping of waves when the vessel is moving through it with a slow drifting velocity. The damping term b_{11} in Equation 3.14 should now be replaced by the summation of still water and time dependent wave drift damping, $\left(b_{11}+b_1(t)\right)$. It has been show that the wave drift damping, equal to the wave drift force, consist of a mean and oscillating part. The oscillating part has a very small contribution to the surge wave drift damping force[15]. Therefore, the final damping term becomes $\left(b_{11}+\overline{b_1}\right)$. Estimation of the added mass and damping values is the third step in the Rayleigh model.

3.3.4. Rayleigh parameter estimation

The Rayleigh parameter, also known as the standard deviation of the distributed values, can be estimated in the frequency domain by using the wave drift force spectrum. Since the low frequent surge motion of the system are dominant, the spectral analysis of the low frequencies are considered only. These low frequencies μ are defined as the difference frequency of wave groups i and j resulting in $\omega_i - \omega_j = \mu$. Applying Newman's approximation, the low frequency wave drift force spectrum can be estimated using the group spectrum and main diagonal of the wave drift force QTF given in Equation D.16. In many cases, single point moored structures are slightly damped which implies that the motion response will be near the natural surge frequency ω_{1n}. Since the natural surge frequency of large moored vessels is close to zero, the main assumption results in $\mu \approx \omega_{1n} \approx 0$. By simplifying the low frequency wave drift force spectrum $S_F(\mu)$ to $S_F(0)$ and using the motion RAO $\left|\frac{\hat{\zeta_a}}{\hat{F_a}}(\omega_{1n})\right|$, resulting from Equation 3.16, the standard deviation of the surge motion σ_{x1} can be calculated.
Using the same natural surge excitation assumption, the number of resonant surge oscillations N in a storm duration of 3 hours can be estimated. Eventually, the MPM surge excursion can be calculated according to Equation 3.20.

3.3.5. Stiffness adjustment by energy correction

Now the MPM surge excursion can be calculated, the corresponding restoring mooring force has to be estimated using the load-excursion curve. According to Equation 3.20, the surge motion of the FPSO for benchmark mooring design parameters is illustrated in Figure 3.6:

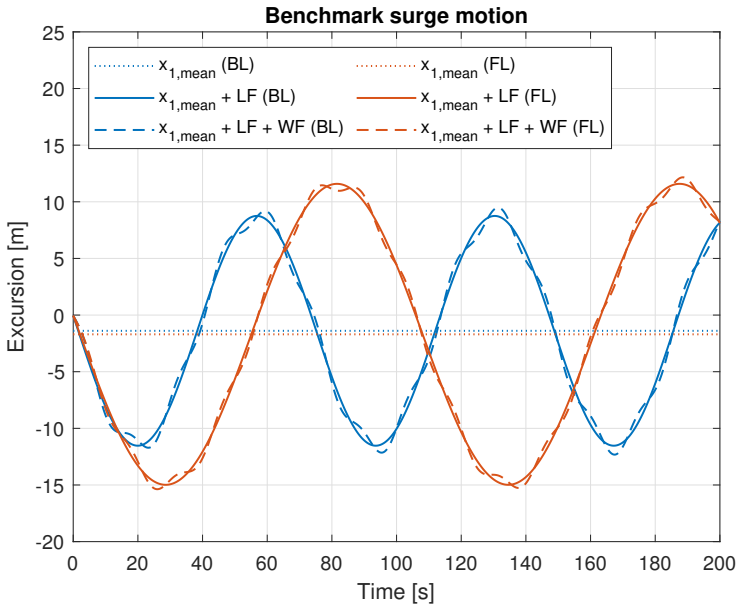

Figure 3.6: Dominant low frequent motion for benchmark mooring design parameters in ballast and fully loaded condition

As can be seen, the vessel is oscillating around the mean surge excursion, away from (-) and towards (+) the tower. Since it is expected that the frequency of excitation is at the natural surge frequency, the low frequent motion shown in Figure 3.6 is equal to ω_{1n}. It is assumed that the wave frequent

motion is at the peak frequency ω_p. Note that ω_p is dependent on the analysed wave spectrum.
The corresponding maximum horizontal mooring force is estimated using the load-excursion curve for the vessel in fully loaded condition as illustrated in Figure 3.7. By finding the intersection point between the maximum calculated excursion and the corresponding non-linear load-excursion curve, the maximum horizontal mooring forces are estimated. However, since the system is linearized, it is expected that the calculated maximum positive surge excursion and corresponding horizontal mooring force (F_{Push}) are overestimated. This can be imagined by comparing the gradient of the linearized and non-linear mooring force. The gradient represents the stiffness of the mooring system at a certain excursion. If the gradient is larger, the mooring system is more stiff resulting in an earlier movement in the opposite direction. This is caused, since the restoring mooring force can overcome the environmental forces earlier.

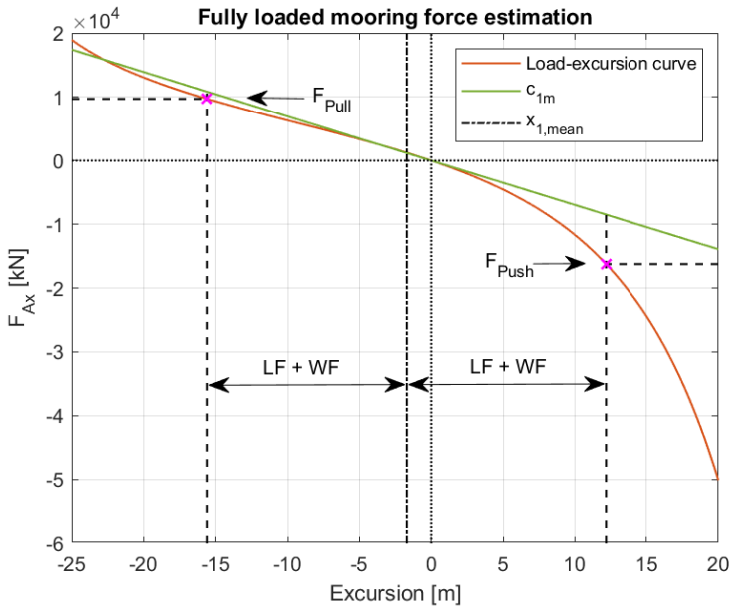

Figure 3.7: Estimated forces F_{Pull} and F_{Push} in fully loaded condition by using the non-linear load-excursion curve

Keeping this in mind, an adjustment of the stiffness should be made using a correction of energy. The stiffness can be adjusted by calculating the difference in energy absorbed by the linear and non-linear load-excursion curve. Eventually, depending on the gradient difference between both curves, energy can be added or subtracted to the non-linear system. This can be done for both positive and negative excursions, nonetheless it will have more impact on the system for positive excursions. This is caused by the high non-linearity of the curve at positive excursions. The method of stiffness adjustment is illustrated in Figure 3.8 by using the calculated surge excursions for fully loaded condition shown in Figure 3.6. Note that the gradient difference between the linear and non-linear mooring force is different for every set of design parameters.
As can be seen from Figure 3.8, the blue area represents the contrast in energy absorbed by the system by using the linear mooring force compared with the non-linear mooring force. The green and the red areas are both equal to the corresponding blue area in negative and positive excursions respectively. Recall that positive and negative excursions are defined towards and away from the tower respectively measured from the mean position. Since the gradient for positive excursion of the non-linear mooring force is larger, calculations of the maximum excursion and mooring force by using the gradient of c_{1m} will lead to an overestimation. These values are shown as x_{old} and F_{old}. Therefore, the part of the curve indicated in red should be disregarded resulting in the new values x_{new} and F_{new}. The other way around, for negative excursions, the opposite applies.
By using the stiffness adjustment by energy correction for every set of design parameters, it is expected that the calculations of the maximum surge excursion and mooring force will be more accurate by still using a linearized system.

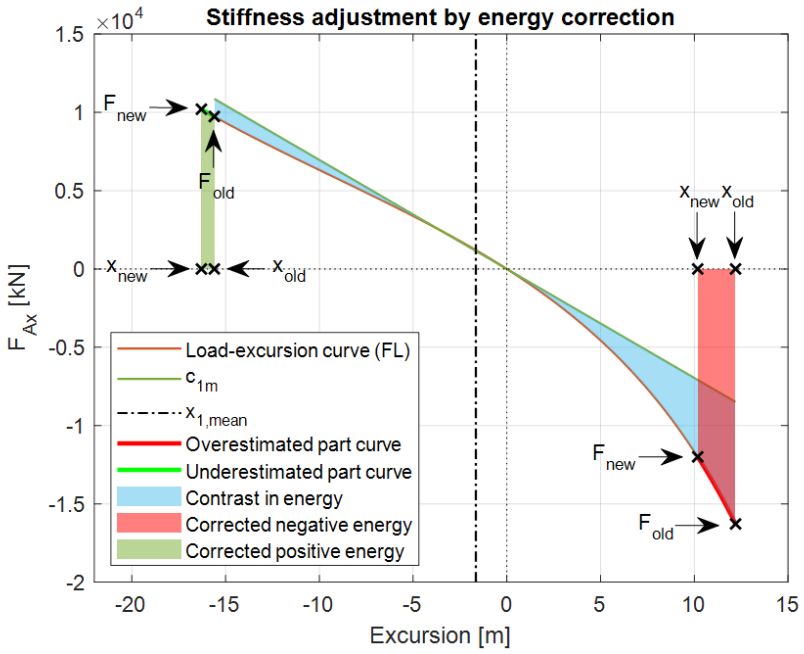

Figure 3.8: Visualization of the principle of stiffness adjustment by energy correction

3.4. Harmonic Balance Method

This section describes the non-linear model, referred to as the Harmonic Balance Method, in more detail. It describes the assumptions and calculations done to calculate the maximum surge amplitude. The Harmonic Balance Method assumes that the response of the system is periodic, so that the process will repeat in a certain way. By assuming that the surge excitation will be close to the natural surge frequency of the vessel, one can expect the approximate solution of the system in the form of a Fourier series $f_H(t)$ truncated to order H[8]:

$$f_H(t) = \sum_{k=-H}^{H} \hat{f}(k) e^{ik\omega t} \tag{3.21}$$

Where $\hat{f}(k)$ are the Fourier coefficients and k the harmonic index. It is expected, that with $k = 1$ a reasonable first approximation of the maximum surge excursion is made. Dependent on the analysed mooring design parameters, a n^{th} order polynomial fit of the load-excursion curve is made and implemented as non-linear mooring stiffness $F_{1m}(t)$. By substituting the expected response with frequency ω given in Equation 3.21 in the non-linear EoM 3.17 and by applying an integration method to vanish the time dependent terms, an algebraic equation system is established which can be solved for $\hat{f}(k)$. The following sections describe the steps to be taken to calculate the maximum amplitude of the surge excursion.

3.4.1. Environmental force

As described in Section 3.1.2, a time signal of the environmental force is required. Using OrcaFlex, this forcing signal on a fixed FPSO can be collected and used in the analysis. The FPSO has to be constraint fixed at equilibrium position, otherwise possible damping and added mass forces are included in the time signal. A three hour second order wave load on the fully loaded fixed FPSO is shown in Figure 3.9. Note that the first order wave, current and wind forces are not included in this signal and should be added as well. The total environmental force can easily be obtained from an OrcaFlex simulation. For more information on OrcaFlex modelling, please refer to Chapter 4. Obtaining the total environmental force on the FPSO from OrcaFlex for both ballast and fully loaded condition is the first step in the Harmonic Balance Method.

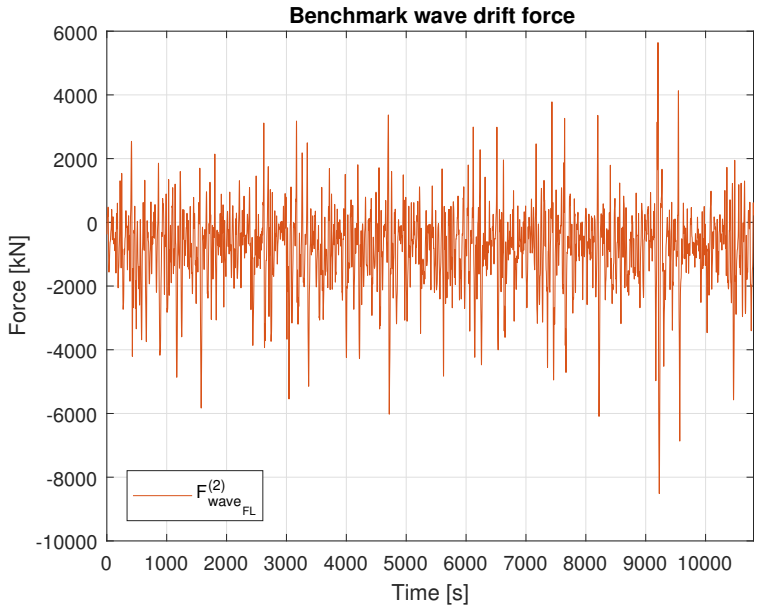

Figure 3.9: Second order wave force on the fully loaded FPSO

3.4.2. Mooring stiffness approximation

Since the Harmonic Balance Method uses the non-linear mooring characteristics, the next step is to define the restoring mooring force as a function of the surge excursion x_1. To do so, a n^{th} order polynomial fit of the restoring mooring force is made using MATLAB by retrieving the fitting parameters k_1, k_2 and k_3. To show the fit for benchmark mooring design parameters, a 3rd order polynomial fit is created for ballast and fully loaded condition of the FPSO and shown in Figure 3.10. Note that the fit has to be forced through the origin [0,0]. Describing the restoring mooring force as a n^{th} order polynomial fit is the second step in the Harmonic Balance Method.

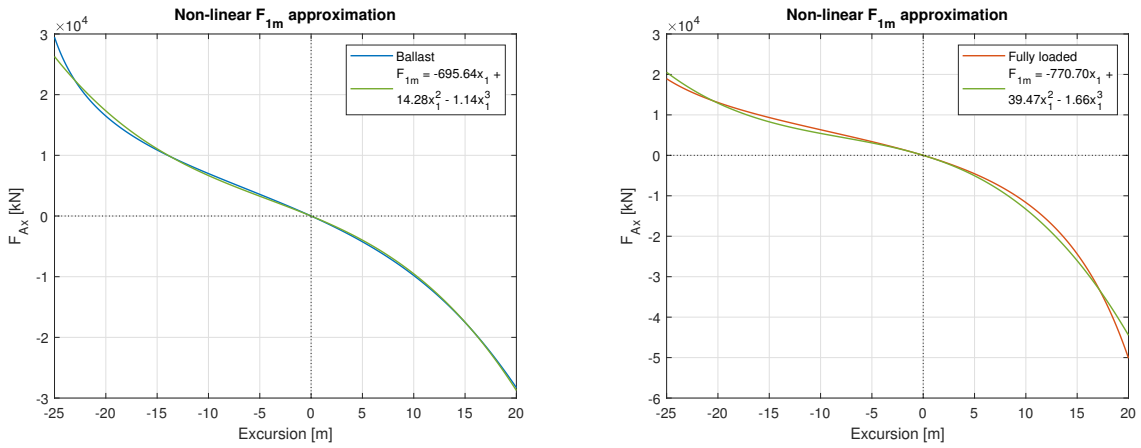

(a) Ballast (b) Fully loaded

Figure 3.10: Non-linear 3rd order polynomial fit through the origin [0,0] of the benchmark load-excursion curves

3.4.3. Maximum amplitude estimation

The last step is to determine the maximum amplitude of the surge excursion. By taking Equation 3.21 and rewriting using the Euler's formula $e^{ix} = \cos(x) + i\sin(x)$ including the first harmonic $(k = 1)$ results in:

$$\sum_{k=-1}^{1} \hat{f}(1)e^{i\omega t} = \hat{f}(0) + \hat{f}_c(1)\cos(\omega t) + \hat{f}_s(1)\sin(\omega t) \tag{3.22}$$

By assuming zero initial displacement of the FPSO and the expected surge excitation at the natural surge frequency ω_{1n}, the solution of Equation 3.17 can be written in the form:

$$x_1(t) = \hat{f}_c \cos(\omega_{1n} t) + \hat{f}_s \sin(\omega_{1n} t) \tag{3.23}$$

Note that the added mass and damping are considered constant and equal as described for the Rayleigh model in Section 3.3.3. Substitution of Equation 3.23 into the equation of motion, results in one equation with two unknowns ($\hat{f}_c$ and $\hat{f}_s$). To obtain a second equation and to vanish the time dependency, integration over the natural period $T_{1n} = \frac{2\pi}{\omega_{1n}}$ of every term in the equation of motion is performed using:

$$\begin{aligned} &\int_0^{T_{1n}} EoM \cdot \cos(\omega_{1n} t)dt \\ &\int_0^{T_{1n}} EoM \cdot \sin(\omega_{1n} t)dt \end{aligned} \tag{3.24}$$

Special care is required when integrating the total environmental force obtained from OrcaFlex. A workaround is executed by integration of the whole storm period T where a number of surge oscillations N are expected. By dividing the integral over N oscillations, a constant value is obtained:

$$\begin{aligned} &\frac{1}{N}\int_0^{N \cdot T_{1n}} F^{(2)}_{1wave}(t) \cdot \cos(\omega_{1n} t)dt \\ &\frac{1}{N}\int_0^{N \cdot T_{1n}} F^{(2)}_{1wave}(t) \cdot \sin(\omega_{1n} t)dt \end{aligned} \tag{3.25}$$

Eventually, by solving the set of equations for $\hat{f}_c$ and $\hat{f}_s$ and maximum amplitude of the surge excursion should become:

$$x_{1max} = \sqrt{\hat{f}_c^2 + \hat{f}_s^2} \tag{3.26}$$

A more detailed calculation procedure for the Harmonic Balance Method can be found in Appendix D.

3.5. Optimization

This section describes the optimization procedure by finding the set of mooring design parameters resulting in the lowest absolute maximum mooring force at the calculated surge excursion. Analysing the surge motion of a single point mooring system in head waves, it shows a large low frequent motion compared to the wave frequent heave and pitch motions, shown in Figure 3.6. The large surge motion will result in pulling and pushing forces away from and towards the moored point respectively. By reason of the non-linearity of the load-excursion curve shown in Figure 3.7, it can be imagined that it is not evident if the absolute pulling or pushing force will be larger. In addition, the calculated surge excursion is affected by the shape of the mooring system which is influenced by the chosen design parameters. Hence, the objective is to minimize the maximum restoring mooring force, the optimization procedure should minimize the absolute difference between pushing and pulling force. In this way, it is expected that the absolute maximum restoring mooring force corresponding to a maximum surge excursion will be lowest and close to the restoring mooring force when the vessel is surging in opposite direction. Note that for both the linear and non-linear model, depicted schematically in Figure 3.2, the optimization procedure will be the same.

Let us consider an optimization procedure with n number of different design parameter sets s. The stiffness of the mooring system has to be estimated n times, likewise for the maximum surge excursion and related restoring mooring force in two directions. First, within n number of sets the absolute difference between the pulling and pushing force has to be found as follows:

$$\Delta F_{Ax} = \left|\left(F_{Ax_{Pull}(-x_i)} - \left|F_{Ax_{Push}(x_i)}\right|\right)\right| \qquad \text{for} \qquad (s_1, s_i, .., s_N) \tag{3.27}$$

However, when ΔF_{Ax} is lowest, this does not mean that the absolute maximum restoring mooring force is at the minimum value. Therefore, the mean value of the summed absolute pulling and pushing force should be at the minimum value too. Consequently, the final optimization procedure consists of two criterion, giving the most efficient set of design parameters s_i which will minimize the absolute maximum mooring force:

$$\min\left(\Delta F_{Ax}\right) \qquad \& \qquad \min\left(\frac{F_{Ax_{Pull}(-x_i)} + \left|F_{Ax_{Push}(x_i)}\right|}{2}\right) \qquad \text{for} \qquad (s_1, s_i, .., s_N) \tag{3.28}$$

3.6. Chapter summary

This chapter describes the Rayleigh model and Harmonic Balance Method to estimate the surge response for a linear and non-linear system respectively in a given extreme collinear environment. The major assumptions made in both models are described below:

- Analyse single degree of freedom system only
- Analyse governing resonant low frequent surge motions, resulting from second order wave drift forces
- Due to low damping at the natural surge frequency, the frequency dependent added mass and damping can be considered constant
- The resulting restoring mooring force is estimated using the load-excursion curve

The assumptions made in the Rayleigh model are:

- The wave elevations are normally distributed and the surge motion Rayleigh distributed
- The restoring mooring force is linearized at the expected mean excursion of the surge motion, resulting in the mooring stiffness c_{1m}
- The low frequency part of the wave drift force spectrum can be calculated using the spectral density and the main diagonal QTF only, by assuming the difference frequency of wave groups $\omega_i - \omega_j = \mu = 0$
- By calculating the surge response with a linear system, the stiffness is adjusted using energy correction

The assumptions made in the Harmonic Balance Method are:

- The restoring mooring force is described using a n^{th} order polynomial fit
- The expected surge motion is periodic and can be reasonably estimated using a single harmonic with natural surge frequency ω_{1n}.

In Chapter 4, a choice between the two models is made by comparing surge response results of the benchmark system between OrcaFlex and both models. Ultimately, the chosen model will be implemented in the design tool and results of the proposed optimum set of mooring design parameters are validated by OrcaFlex as well.

4

Results & Validation

4.1. Introduction

In Chapter 3, two simplified models are proposed to be integrated in the design tool in order to estimate the surge response of the moored system. To confirm the most suitable model for our application, which needs to be simple and computational efficient, an OrcaFlex model is created to validate the output of both models. OrcaFlex is a fully coupled numerical simulation program which is normally used in the assessment of mooring design loads. The output of the OrcaFlex model can be considered close to reality, since within BES the settings of this program have been refined over the years to match model tests results [Bluewater Energy Services].
This chapter briefly describes the modelled parts in the OrcaFlex model, including relevant required simulation time. Based on comparing results of the surge response between OrcaFlex and both proposed models with benchmark mooring properties, shown in Table D.1, a final model choice is made. Implementing the chosen model in the design tool, the sensitivity assessment of the surge response related to design parameter variation of the mooring system can be compared with OrcaFlex results. In addition, a proposed set of optimized design parameters by OrcaFlex and by the design tool can be compared. A schematic overview of the validation procedure is shown in Figure 4.1.
First, the description of the OrcaFlex model used for validation is given in Section 4.2. Section 4.3 defines the method to obtain comparable results from OrcaFlex in order to validate both models with benchmark mooring characteristics. In Section 4.4, the final model is chosen based on an analysis with the Runge-Kutta method and is implemented in the design tool. After that, Section 4.5 describes the validation of surge response results including sensitivity assessment and optimization procedure for both design tool and OrcaFlex. Eventually, the chapter summary is given in Section 4.6.

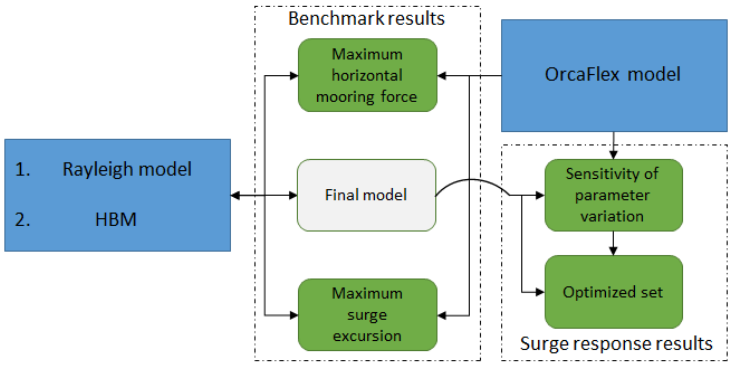

Figure 4.1: Validation procedure

4.2. OrcaFlex model

This section presents the modelling approach for the time domain analyses, and covers the various elements that are included in the numerical model. For convenience, the coordinate system in OrcaFlex is equal to the coordinate system shown in Figure 3.3.

4.2.1. FPSO

The FPSO is modelled as a free floating body. Its hydrodynamic properties are incorporated through a hydrodynamic database that follows from radiation/diffraction analysis with Hydrostar. The actual water depth and loading conditions have been taken into account in the calculation. Same as described in Chapter 3 two loading conditions are analysed, the ballast and fully loaded FPSO. Likewise, the FPSO properties described in Appendix C.1 are integrated in the OrcaFlex model. Note that a six-dimensional vessel response is analysed.

4.2.2. Mooring system

The mooring system is included by modelling of the various SYMS components available in OrcaFlex. The modelled mooring system consists of objects and lines, that can be connected to each other rigidly or by constraints. The mooring system consists of a yoke, two pendulums and a ballast weight connecting the FPSO to the tower. Table 4.1 describes the various modelled objects in OrcaFlex.
By rigidly connecting certain objects of the mooring system, different sets of design parameters resulting in different local axis locations can easily be adjusted. Adjustments of the mooring dimensions and weights can be made in a batch processing sheet implemented in Microsoft Excel.

Name	Object type	Connections
FPSO	Vessel	Free floating, with two connection points (pendulum) at the MSS
Tower	6D buoy	Earth fixed
Turntable	6D buoy	Attached to the tower, with one connection point (yoke)
Ballast box	3D buoy	Free object, with two connection points (yoke) at each side
Yoke	Line	Consisting of two lines, each attaching the turntable to the ballast weight on either side
Pendulum	Line	Consisting of two lines, each attaching the FPSO to the ballast weight on either side

Table 4.1: OrcaFlex objects

4.2.3. Environment

Irregular wave realizations are generated by OrcaFlex based on user input such as wave spectrum, significant wave height, peak period and peak enhancement factor. Different wave realization can be obtained by varying the seed number. The JONSWAP spectrum, wind and current speed described in Appendix C.2 are also used in the OrcaFlex model.

4.2.4. Simulation time

A three-hour simulation time is required to achieve a reasonable storm representation. However, each time domain simulation will last 3.5 hours. The first 30 minutes of the simulation are a swell-up period in which the waves build up and the system can reach its static state condition. By static state, a mean equilibrium offset and heading is meant. For example, if a vessel is modelled in beam waves (90°) it is expected that the vessel needs some time to weathervane to approximately head waves (180°). The swell-up period is excluded from all the analyses.

4.3. Comparison of results

This section describes the output of OrcaFlex obtained and how the results can be compared to both the Rayleigh model and Harmonic Balance Method. The benchmark system is implemented in OrcaFlex as described in Section 4.2. Results of the fully loaded surge, heave and pitch motion responses are shown in Figure 4.2. Clearly, the surge motion shows indeed a large low frequent motion compared to the heave and pitch motions. Since there is interest in the maximum surge response, within the 3 hour time frame, the maximum surge motion has to be found. Note that the motion responses in Figure 4.2 are of one wave seed only. Normally, in dynamic storm analyses a statistic approach is required to deliver acceptable predictions of the maximum responses. Accordingly, multiple wave seeds are desired. In OrcaFlex, these wave seeds can be implemented by specifying a random seed number. For all the analyses in OrcaFlex, these seed numbers are kept identical to allow for a fair comparison between different mooring design parameters.

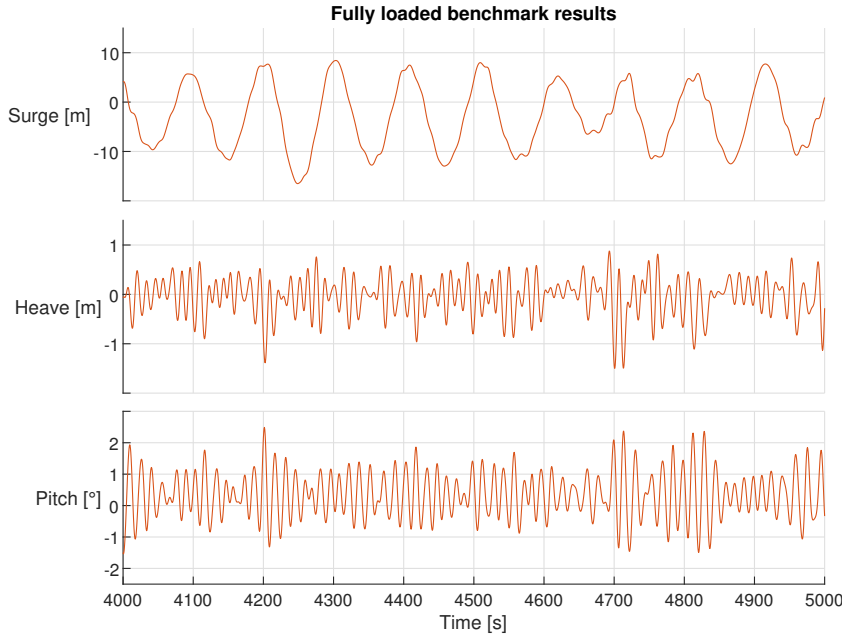

Figure 4.2: Motion response of the fully loaded benchmark system

4.3.1. Statistic analysis

To make an acceptable approximation of the maximum surge response, a set of 15 different wave realizations are generated by varying the wave seed. Wind and current parameters are kept constant. Using these 15 storm realizations, the maximum values of the surge responses for each wave seed are collected. In line with offshore rules and regulations, extreme values are reported as MPM values approximated by a Gumbel distribution [Bluewater Energy Services]. This can be achieved by applying a Gumbel distribution fit to the maxima by acquiring an appropriate Gumbel scale and location parameter. These parameters influence the shape of the Gumbel distribution. Based on the Cumulative Distribution Function (CDF) of the fitted Gumbel distribution, the MPM value follows from the 0.63 probability of exceedance. The cumulative probability of 15 wave seeds of the benchmark fully loaded surge excursion and restoring mooring force maxima including fitted Gumbel CDF are shown in Figure 4.3. The MPM value is indicated by the 0.37-percentile value, that is equivalent to the 0.63 probability of exceedance. Note that the procedure has to be executed twice for both the surge excursion and restoring mooring force, since distinction is made between surging away and towards the tower. A detailed description of MPM evaluation based on a Gumbel distribution fit is described in Appendix D.

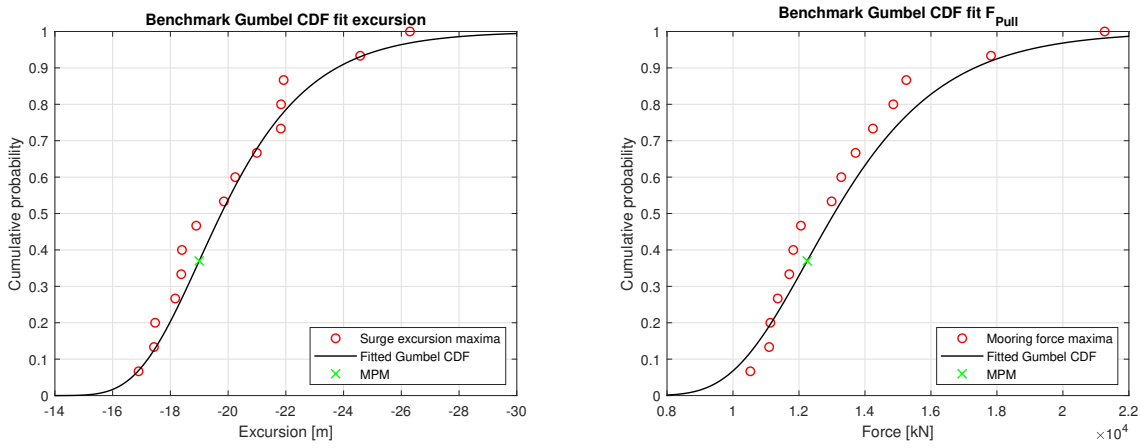

(a) Surge excursion (b) Mooring force

Figure 4.3: Fitted Gumbel CDF for 15 benchmark fully loaded surge excursion and restoring mooring force maxima

4.3.2. Compare Rayleigh model results

The Rayleigh model approximates the MPM value based on the variance of the surge excursion. In a process with N surge excursion peaks, the Rayleigh MPM is based on the probability of exceedance $P = \frac{1}{N}$. This probability corresponds to the cumulative probability $P = 1 - \frac{1}{N}$. The MPM value calculated in the Rayleigh model is not influenced by the a seed number, since it uses the fixed spectral shape of the wave elevations in the calculations. However, OrcaFlex uses multiple seeds to estimate the MPM value. Therefore, it have to be shown that the MPM values of both models can be compared with each other. To find out, it have to be shown that the surge excursion peaks in OrcaFlex are Rayleigh distributed, so that the value corresponding to the cumulative probability $P = 1 - \frac{1}{N}$ is equal to the Gumbel MPM value. Since 15 wave seeds are used in the OrcaFlex calculations, the surge excursion peaks resulting from 15 different wave seeds have to be collected and fitted with a Rayleigh distribution. The peaks are defined as global peaks which are defined by the largest peak between two mean crossings as indicated in Figure 4.4.

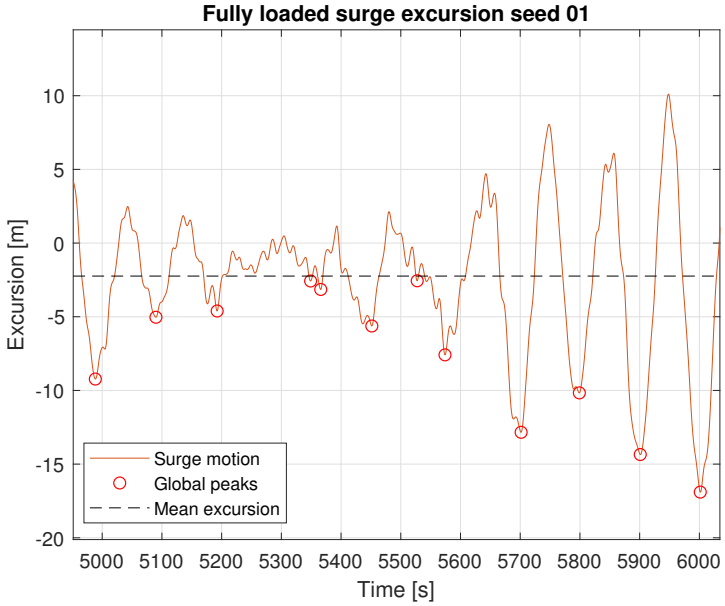

Figure 4.4: Global peaks for fully loaded benchmark system

All the 15 surge excursion time signals are imported from OrcaFlex and the global peaks are collected using MATLAB software. By sorting the global peaks and plotting them on Rayleigh probability paper, an horizontal line can be fitted as shown in Figure 4.5. All the global peaks are measured from zero excursion. Since the MPM value for a 3 hour storm has to be evaluated, the MPM of the Rayleigh distribution has to be equal to the cumulative probability $P = 1 - \frac{1}{N/15}$. The MPM value is depicted at the green cross. By comparing the MPM value of Figure 4.3a, it shows equivalence.
Now, it is shown that the global surge excursion peaks can be fitted with a Rayleigh distribution, within a 95% prediction interval. Therefore, it is fair to say that the MPM values calculated according to the OrcaFlex and Rayleigh model can directly be compared with each other.

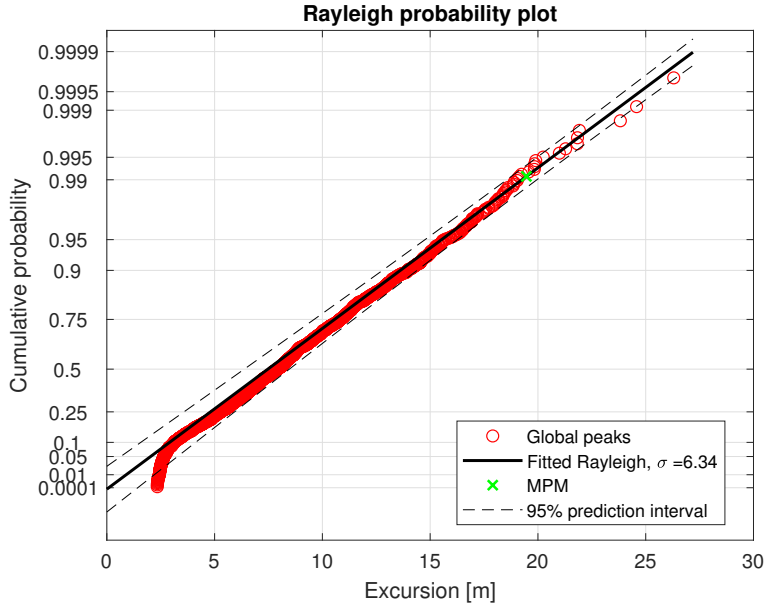

Figure 4.5: Rayleigh distribution fit of global surge excursion peaks

4.3.3. Compare HBM results

The Harmonic Balance Method approximates the maximum value of the particular wave seed, using the same forcing signal as in OrcaFlex. Therefore the result of the harmonic balance can be compared directly with the maxima of the particular seed in OrcaFlex. In the same way as described in Appendix D, the MPM value can be calculated using a Gumbel distribution fit.

4.4. Model choice

This section describes the final model chosen to be implemented in the design tool. The MPM surge excursion away from the tower and mooring pull force resulting from 15 wave seeds in OrcaFlex are compared with MPM values calculated by the two proposed models. Eventually, using the Runge-Kutta method the final model is chosen to be implemented in the design tool.

4.4.1. Benchmark results

Figure 4.6 shows the MPM values calculated with the three different models for the excursion away from the tower and the related mooring force. Comparing the ballast results from the Rayleigh model with OrcaFlex, it clearly shows an overestimation in both the excursion and mooring force. Contrarily, the fully loaded results are underestimated. Still, the Rayleigh model shows a structurally higher excursion and mooring force for fully loaded compared to ballast condition, equal to OrcaFlex.
When studying the results of the Harmonic Balance Method, it shows an extreme underestimation in both excursion and mooring force. This indicates that multiple iterations shall be done in order to give reliable results. The Harmonic Balance Method assumes that the response of the system is periodic and that the response of the system can be estimated as a truncated Fourier series. This results shows

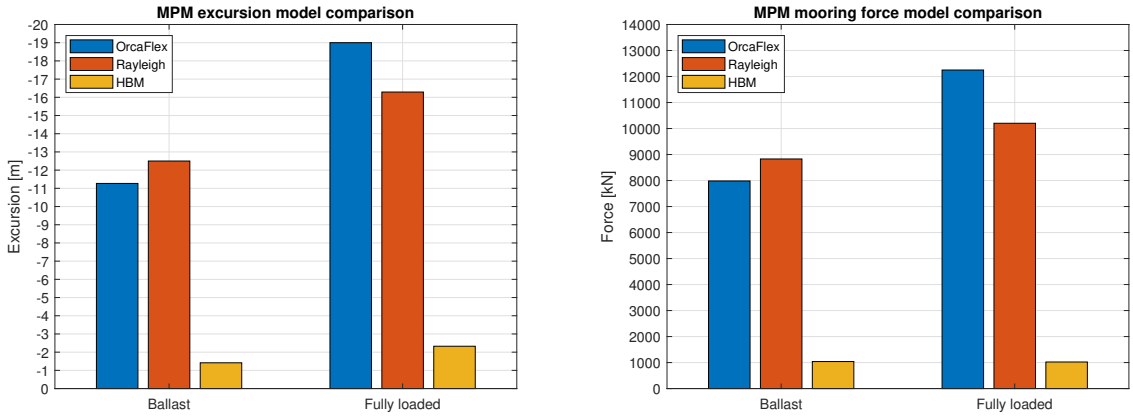

(a) Surge excursion (b) Mooring force

Figure 4.6: MPM surge excursion and restoring mooring force comparison

that either the response is not periodic or additional harmonics should be included. To check if the Harmonic Balance Method is able to improve results compared to the Rayleigh model, the accuracy of the results that can be obtained with the non-linear equation of motion used has to be investigated. Accordingly, the numerical solution of the one-dimensional non-linear equation of motion should be obtained. To achieve this, the Runge-Kutta method is applied. The procedure is described below in Section 4.4.2.

4.4.2. Runge-Kutta Method

The Runge-Kutta Method is a numerical iterative integration method used to find approximate solutions of an Ordinary Differential Equation (ODE). The ODE solved here is equal to Equation D.29. By writing Equation D.29 in state space form and applying zero initial conditions, the ODE can be reduced to first order and MATLAB is able to solve the response per time step. The result of the single degree of freedom ODE45 solver in MATLAB for fully loaded benchmark system is shown and compared with the single degree of freedom surge motion obtained from OrcaFlex in Figure 4.7.

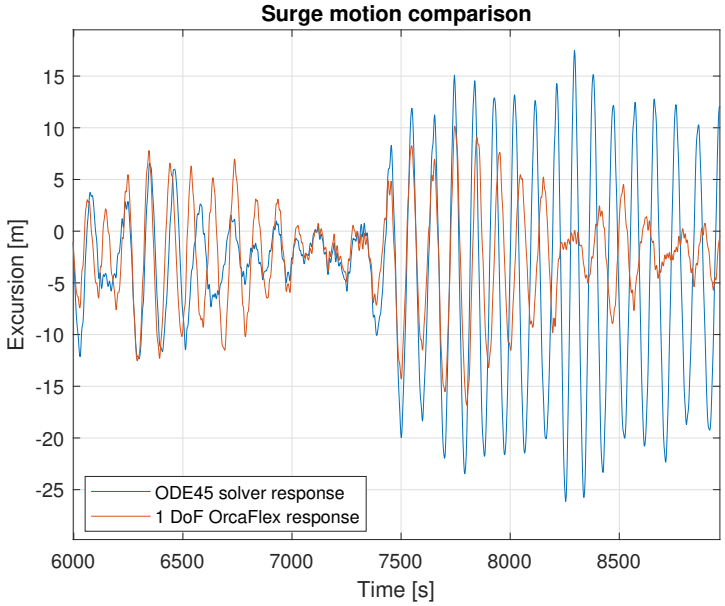

Figure 4.7: Surge motion comparison of the ODE45 solver and OrcaFlex for fully loaded benchmark system with wave seed 01

Note that the right hand side of Equation D.29 is replaced by the exact same force time signal used in the OrcaFlex model. The surge response from OrcaFlex depicted in orange includes the vessels pure surge motion only, which means that coupled vessel motions are excluded. This is done to make a fair comparison between the surge response in OrcaFlex and the ODE45 solver. At a certain point, it can be seen that the ODE45 solver extreme overestimates the surge excursion. The ODE45 solver and OrcaFlex both uses the same environmental forces and vessel mass. The only difference between both solvers is that OrcaFlex uses frequency dependent added mass and damping or possible discrepancies in mooring characteristics. By obtaining both load-excursion curves from both solvers, Figure 4.8 shows indistinguishability.

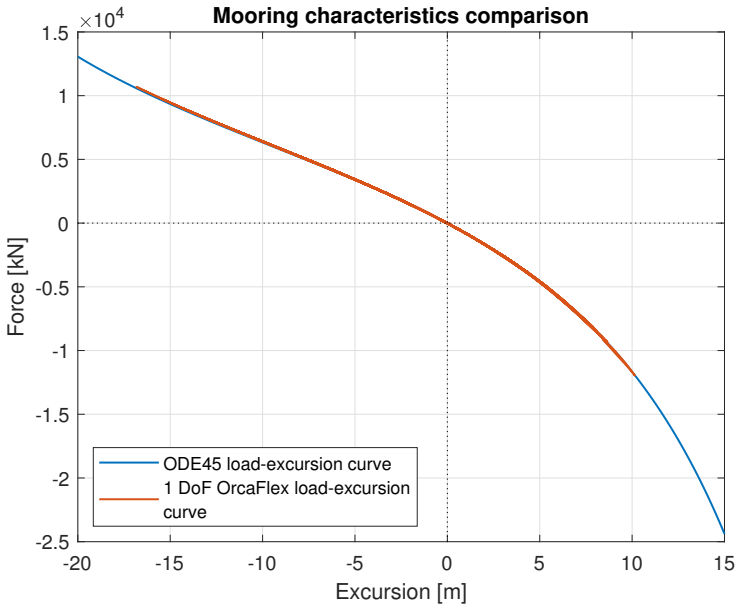

Figure 4.8: Mooring characteristics comparison between OrcaFlex and ODE45 solver for fully loaded benchmark system with wave seed 01

Using this information, it is expected that the mooring characteristics used in the ODE45 solver will not induce the large discrepancy shown in Figure 4.7. Therefore, the constant added mass and damping assumption may be of an influence. However, by having a closer look at the dominant frequency of excursion in Figure 4.2, it shows a dominant frequency close to the natural surge frequency of the vessel. To obtain the frequency spectrum, a Fast Fourier Transform (FFT) is applied on the surge motion response obtained from OrcaFlex. Figure 4.9 shows that the dominant frequency indeed is close to the natural surge frequency of the vessel. Accordingly, it sounds impossible that the assumed constant added mass and damping at this natural surge frequency will induce the large differences between both models.
Ultimately, if both solvers use the same or comparable numerical method to calculate the response of the system, it can not be explained why there is such an inconsistency. Though, possible explanations may be:

- The environmental force obtained from OrcaFlex does not show zero initial conditions. Since the vessel is excited from equilibrium position, OrcaFlex may include some non-zero initial conditions which cannot be retrieved
- Additional feedback effects between FPSO, environmental force and structure which is not included in the ODE45 solver

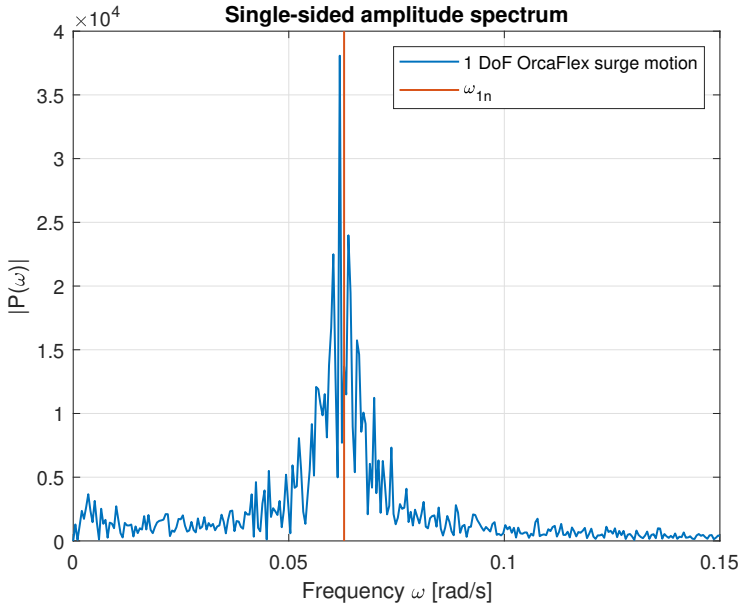

Figure 4.9: Frequency spectrum of the 1 DoF surge excursion from OrcaFlex with wave seed 01

4.4.3. Conclusion

It is shown that the numerical solution of a non-linear single degree of freedom system used in the Harmonic Balance Method will not improve results compared to the statistical Rayleigh model. Due to large differences in calculated surge motion response between OrcaFlex and the Runge-Kutta method, it can be said that the assumed non-linear equation of motion is not the correct one. However, it can not be explained, within the provided information from OrcaFlex, why the large differences occur. Therefore, simulating the system with either the Harmonic Balance or Runge-Kutta Method is not the optimal choice. With the assumed non-linear equation of motion, surge response results will be improve compared to the linear Rayleigh model without the computational costs. In addition, Harmonic Balance and Runge-Kutta methods require an input force signal obtained from OrcaFlex to work properly, which is undesired. Conclusively, in this project, the Rayleigh model is chosen to be implemented in the design tool.

As the results in Figure 4.6 demonstrates, exact results with the Rayleigh model will not and are not required to be obtained, because the ultimate goal is the determination of efficient mooring design parameters. In a design process, actual mooring design loads will yet be evaluated with OrcaFlex software.

4.5. Design tool results

This section shows surge response results and compares them with results obtained from OrcaFlex. As described in Section 2.5, the design tool is able to optimize mooring design parameters by finding the set of mooring parameters within the reported range resulting in the lowest horizontal mooring load. By defining a certain design parameter step between mooring design parameter limits, the optimum design parameters can be recovered. However, the design tool is able to find this optimum extremely fast compared to OrcaFlex. The design tool is able to calculate the surge response of one set of mooring design parameters within a second, while OrcaFlex needs at least one and a half hour for one wave seed. Therefore, in order to validate surge responses results and the optimized set of mooring design parameters proposed by the design tool, a suitable step between individual mooring design parameters should be chosen. First, it is important to define a minimum number of wave seeds required for reliable results and to save computational time.

4.5.1. Required number of wave seeds

The minimum number of wave seeds S required to obtain a reliable estimate of the extreme response in OrcaFlex is given by:

$$S = \left(20\frac{\sigma_{max}}{\mu_{max}}\right)^2 \tag{4.1}$$

Where μ_{max} and σ_{max} are the mean and standard deviation of the maxima respectively. The objective of the formula is that the requested extreme value will fall within 10% on either side of the true extreme value. In addition, the error tolerance of the estimated extreme value will be achieved within 95% probability[16]. By obtaining μ_{max} and σ_{max} from the 15 surge excursion maxima of the benchmark system shown in Figure 4.3a, the minimum number of wave seeds is estimated at $S = 10$.

4.5.2. Required number of design parameter sets

The design tool is able to calculate the surge response of 10,000 different sets of mooring design parameters within minutes. Contrarily, OrcaFlex requires 10 simulations of 1,5 hour each per single set of mooring design parameters. The objective is to capture the sensitivity of the surge response when mooring design parameters are modified. In addition, the optimum set of mooring design parameters has to be found. Therefore, to validate results of the design tool, a minimum combination of mooring design parameter sets have to be found that can be modelled in OrcaFlex within a reasonable time frame. The limits defined for the mooring design parameters are reported in Table 2.2. Note that the yoke arm length is kept constant at YL = 40.2 m.

As stated in Section 2.4, the variation of pendulum length influences the linear part of the curve, while the hang-off height does not. Therefore, it is expected that the sensitivity of the surge response related to the pendulum length variation is higher compared to the hang-off height. Hence, the step size for pendulum length is chosen smaller than the step size of the hang-off height. According to Section 2.4, the ballast weight influences the slope of the load-excursion curve, and thus the surge response. Since the benchmark system uses a ballast weight of 1800 tons, it is chosen to analyse this ballast weight here too. By varying the ballast weight approximately 10 % on either side, it is expected that significant sensitivity will be shown.

As mentioned above, OrcaFlex will simulate 10 wave seeds per set of mooring design parameters. Using an 8 core desktop PC, the required simulation time T in hours for ballast and fully loaded condition of the FPSO can be calculated using:

$$T = \frac{2 \cdot 10 \cdot n_{L_C} n_{HC} n_{BW}}{8} \cdot 1.5h \tag{4.2}$$

By taking n_{L_C} = 4, n_{HC} = 3 and n_{BW} = 3 the simulation time will take a reasonable 6 days for one analysed environment. The simulated mooring design parameters in OrcaFlex are given in Table 4.2. Note that per loading condition, 36 mooring design parameter sets can be analysed.

Mooring design parameter	Symbol	Unit	Ballast	Fully loaded
Pendulum length	L_C	[m]	25 - 28.3 - 31.6 - 35	
Hang-off height	HC	[m]	14 - 19 - 24	7 - 12 - 17
Ballast weight	BW	[te]	1600 - 1800 - 2000	

Table 4.2: Modelled design parameter sets in OrcaFlex

4.5.3. Sensitivity of the surge response

Equal to the benchmark surge response results shown in Figure 4.6, the FPSO in ballast condition shows lower MPM values for surge excursion and mooring force when compared to fully loaded FPSO. Consequently, the main focus here will be on the fully loaded surge response results. Additional results for ballast FPSO can be found in Appendix E.

To map the sensitivity of the surge response related to variation of design parameters, the results will be shown by either keeping the pendulum length or hang-off height constant. Surge response results of L_C = 28.3 m and HC = 12 m are given in Figure 4.10. Each bar includes three different ballast

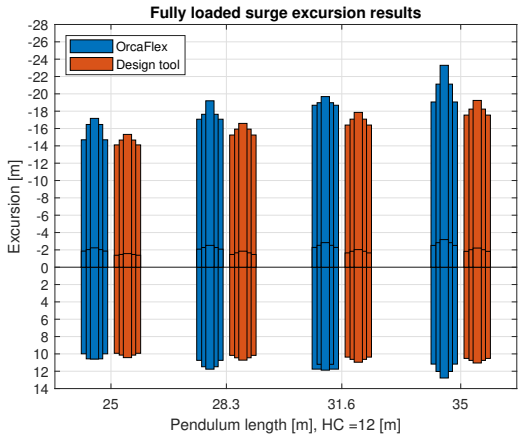

(a) Pendulum length variation, surge excursion

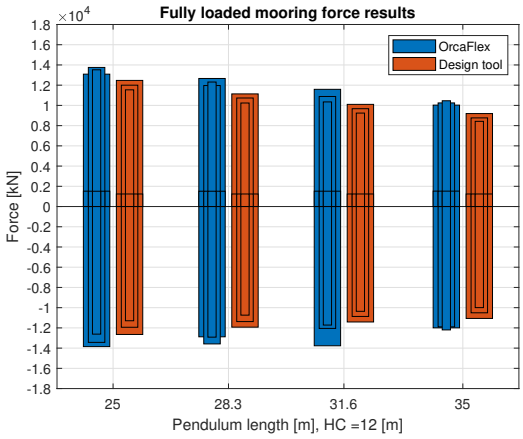

(b) Pendulum length variation, mooring force

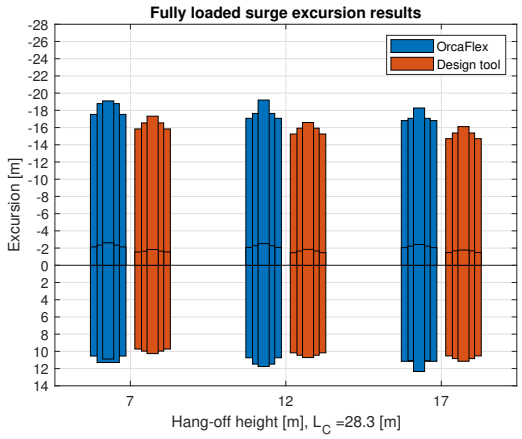

(c) Hang-off height variation, surge excursion

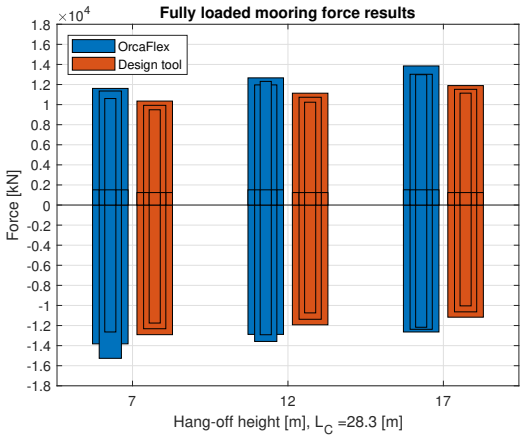

(d) Hang-off height variation, mooring force

Figure 4.10: Schematic sensitivity of the surge response related to mooring design parameter variation for OrcaFlex and design tool. The thickest bar represents largest ballast weight and the mean values are depicted as horizontal lines

weights, where the thickest corresponds to the largest ballast weight of 2000 tons. Observations of the surge response results will be given below by separating results from OrcaFlex and design tool.

Design tool

- Figure 4.10a: Both positive and negative excursion show a gradual increase when increasing pendulum length. The increase of ballast weight results in a decrease in both negative and positive excursion.
- Figure 4.10b: Exact opposite to the item above. The mooring force gradually decreases when increasing the pendulum length. The increase of ballast weight results in an increase of both the pull and push force.
- Figure 4.10c: When increasing hang-off height, negative excursion decreases while positive excursion increases. The increase of ballast weight results in a decrease for negative excursion and increase in positive excursion.
- Figure 4.10d: The mooring pull force gradually increases, while the push force decreases when increasing the hang-off height. The increase of ballast weight results in an increase of both the pull and push force.

OrcaFlex

- Figure 4.10a: Only negative excursion shows a general increase when increasing pendulum length. The increase of ballast weight does not necessarily results in a decrease in both negative and positive excursion.
- Figure 4.10b: Only the mooring pull force shows a general decrease when increasing the pendulum length. The increase of ballast weight does not necessarily result in an increase of both the pull and push force.
- Figure 4.10c: Only negative excursion shows a general decrease when increasing hang-off height. The increase of ballast weight does not necessarily results in a decrease in both negative and positive excursion.
- Figure 4.10d: The mooring pull force generally increases when increasing the hang-off height, while the push force does not. The increase of ballast weight does not necessarily result in an increase of both the pull and push force.

Overall, the design tool shows an underestimation of the surge response, including the calculated mean excursion and mooring force. The sensitivity of the negative surge excursion and related pull force can be well described by varying the pendulum length and hang-off height in the design tool. However, the influence of varying the ballast weight shows significant non-linearity to the response in OrcaFlex. In addition, the sensitivity of the positive surge excursion and related push force shows high non-linearity in results obtained from OrcaFlex when varying the pendulum length and hang-off height. This indicates the complexity of the analysed SYMS. Discrepancies in describing the sensitivity of the surge response related to mooring design parameter variation in the design tool and OrcaFlex, does not mean that the design tool is not able to proposed an efficient set of mooring design parameters. The proposed set of mooring design parameters which results in the lowest mooring force by both models is shown in the following section.
Note that results from ballast show the same sensitivity of the surge response when varying the design parameters. The main observation here is that the design tool in ballast condition consistently overestimates the surge response when compared to OrcaFlex.

4.5.4. Optimized design parameters

By applying the optimization procedure described in Section 3.5, the mooring design parameters proposed by the design tool and OrcaFlex are given in Table 4.3

Design tool	**Symbol**	**Unit**	**Ballast**	**Fully loaded**
Pendulum length	L_C	[m]	35	
Hang-off height	HC	[m]	24	17
Ballast weight	BW	[te]	1600	
Optimization factor	ΔF_{Ax}	[kN]	1211	163
OrcaFlex	**Symbol**	**Unit**	**Ballast**	**Fully loaded**
Pendulum length	L_C	[m]	31.6	
Hang-off height	HC	[m]	24	17
Ballast weight	BW	[te]	1600	
Optimization factor	ΔF_{Ax}	[kN]	1232	258

Table 4.3: Proposed optimized sets of mooring design parameters

It can be seen that both the hang-off height and ballast weight are proposed equal in the design tool and OrcaFlex. However, the pendulum length is different. When comparing the surge response of pendulum length 31.6 m and 35 m, it can be seen that a lower optimization factor ΔF_{Ax} for the pendulum length of 31.6 m results in the desired set of design parameters proposed by OrcaFlex. As Figure 4.11a shows, the calculated push force for a pendulum length of 35 m obtained from OrcaFlex suppresses the correct set of design parameters provided by the design tool. However, the difference between the absolute maximum mooring forces for pendulum length 31.6 and 35 m obtained from OrcaFlex is less than 2%. Therefore, the proposed set of mooring parameters by the design tool can be considered sufficient.

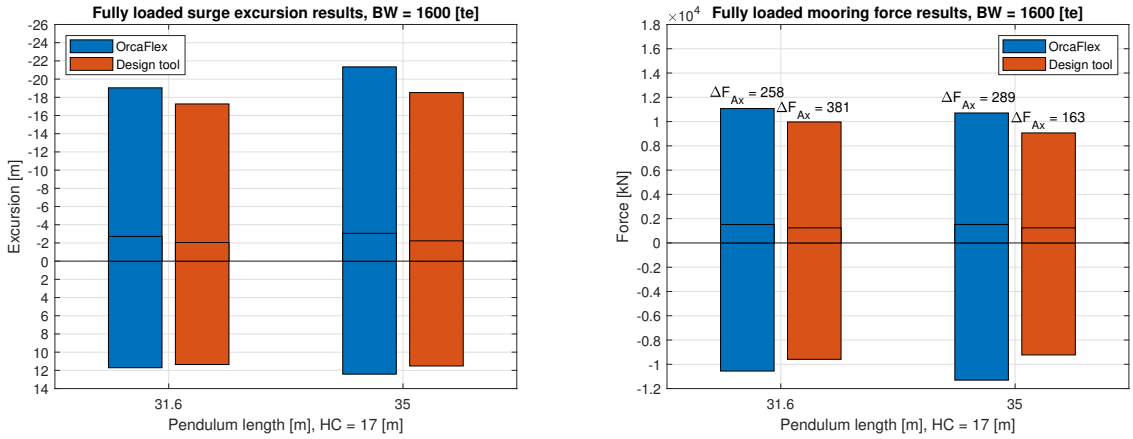

(a) Surge excursion

(b) Mooring force

Figure 4.11: Optimized set of mooring design parameters comparison between OrcaFlex and design tool

The proposed set of mooring design parameters by the design tool is implemented in OrcaFlex and surge response results are compared with the benchmark system. As Table 4.4 shows, the absolute maximum mooring force is decreased with approximately 25% while the surge excursion shows a moderate increase of 10%.

OrcaFlex	MPM excursion	MPM mooring force
Proposed set design tool	21.34 m	11305 kN
Benchmark system	19.00 m	14495 kN

Table 4.4: Comparison of surge response results obtained from OrcaFlex for the proposed mooring design parameters of the design tool and the benchmark system

4.5.5. GUI

To build an user friendly design tool, a GUI is developed. The user is able to implement own environment and vessel properties. By varying mooring design parameters using sliding bars, the resulting influence on the mooring characteristics and surge response is shown. More information on the options and interface is given in Appendix F.

4.6. Chapter summary

This chapter describes the validation of surge response results for both the Rayleigh model and Harmonic Balance Method based on benchmark mooring design parameters using OrcaFlex software. Further analysis with Harmonic Balance Method is being avoided by reason of:

- Multiple harmonics are required in the solution of the truncated Fourier series that significantly increases computational time
- The surge response seems not to be periodic which indicates that it is not the most appropriate solution method for this system
- The results of the Runge-Kutta method showed that with the assumed non-linear equation of motion, it is not possible to improve results when compared to the linear Rayleigh model

Therefore, the Rayleigh model is chosen to be implemented in the design tool. To compare Rayleigh model results, in this chapter, it is shown that the global peaks of the surge excursion time signal are Rayleigh distributed. By comparing the MPM of the Rayleigh distribution and the Gumbel distributed MPM obtained from OrcaFlex, similarity is proven.
By validating the sensitivity of the surge response related to the modification of mooring design parameters, the design tool shows that:

- An overestimation of the surge response for the FPSO in ballast conditions
- An underestimation of the surge response for the FPSO in fully loaded condition
- An underestimation of the mean surge response for both fully loaded and ballast condition of the FPSO
- Equality of the sensitivity for negative excursions and related pulling forces for both fully loaded and ballast condition of the FPSO
- Some small inequality of the sensitivity for positive excursions and related pushing forces for both fully loaded and ballast condition of the FPSO
- The sensitivity of the ballast weight variation is difficult to describe

By validating the optimized mooring design parameters proposed by the design tool and OrcaFlex, it shows that:

- The hang-off height and ballast weight are correctly proposed by the design tool
- The pendulum length is proposed differently by the design tool, but the difference in absolute maximum mooring force between the two different pendulum lengths obtained from OrcaFlex is within 2%.
- The optimization procedure done by the design tool can be considered sufficient.

The ideal set of design parameters proposed by the design tool seems to be a long hang-off height and pendulum length in combination with a low ballast weight. It has to be kept in mind that these mooring design parameters are related with a large surge excursions.
In Chapter 5, the influence of the assumptions made in the Rayleigh model to the surge response are described. By creating a model in OrcaFlex close to the Rayleigh model and its assumptions, the influence of the assumptions can be identified.

5

Discussion

5.1. Introduction

In Chapter 4, the linear Rayleigh model is chosen to be implemented in the design tool. In this chapter, it is described how the major assumptions in the design tool influences the calculated surge response results. This is going to be achieved by comparing design tool and OrcaFlex MPM surge response results with identical mooring design parameters. By changing several calculation options in OrcaFlex, a model with equal assumptions to the Rayleigh model can be developed and the influence of these assumptions can be encountered. Section 4.3.2 describes that the global surge excursion peaks obtained from OrcaFlex can be described by a Rayleigh distribution. Therefore, the assumption of Rayleigh distributed surge excursion can be considered correct. Additional observations described in Section 4.5 showed that a ballast FPSO shows an overestimation of the surge response, while fully loaded vessel does not. Therefore, this is one of main objectives to be discussed. Related to the project goal, a sufficient sensitivity to the surge response is shown when varying design parameters in both ballast and fully loaded condition resulting in a correct optimized set of mooring design parameters proposed by the design tool. Since the optimized set of design parameters rely on the fully loaded surge response results, the main focus in this chapter will be on the fully loaded FPSO.
Figure 5.1 shows a flow diagram of the assumptions made in the Rayleigh model. The assumptions are shown in the red rectangles. The assumptions throughout this chapter are organized as follows:

- Single degree of freedom assumption
- Linearization of the mooring force
- Natural excitation assumption
  - Constant added mass and damping
  - Low frequency wave drift force spectrum

The influence of the depicted assumptions in Figure 5.1 to the surge response results obtain from the design tool are described in Sections 5.2, 5.3 and 5.4. In this project, the analyses done so far are based on a single extreme collinear environment. To show the robustness of the developed design tool, two moderate collinear environments are analysed as well. A comparison of surge response results from OrcaFlex and design tool is made, by validating the sensitivity of the surge response related to mooring design parameter variation and the proposed optimum mooring design parameters. The robustness analysis is described in Section 5.5. Eventually, the chapter summary is given in Section 5.6.

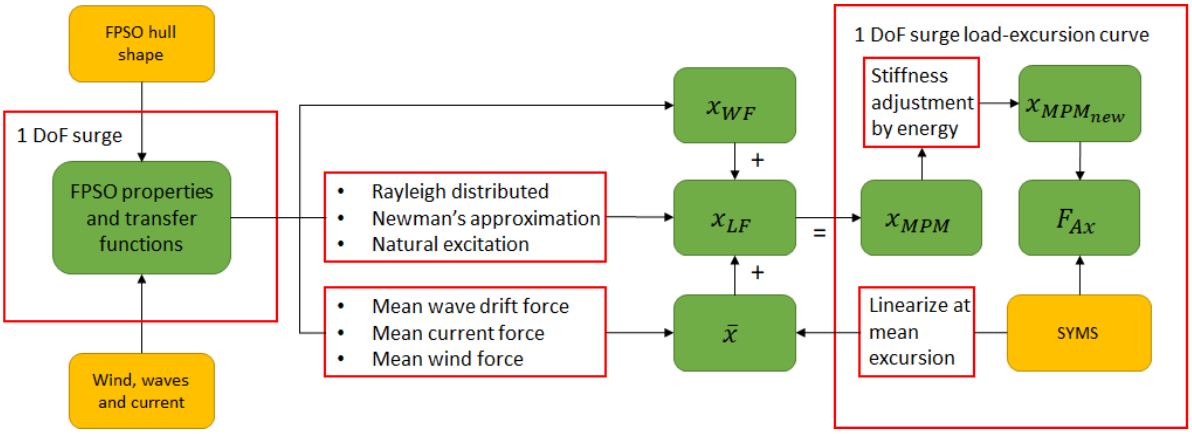

Figure 5.1: Rayleigh model assumptions

5.2. Influence of the single degree of freedom assumption

The first major assumption is the single degree of freedom assumption. Since an extreme collinear environment in head waves, wind and current is analysed, the assumption of a surge dominant system seems fair. To study the influence of this assumption to the calculated surge response, a single degree of freedom system in OrcaFlex is modelled by constraining all motions except surge. In this way, the influence of the assumption can be verified when compared to the original six-degree of freedom OrcaFlex model. The ballast results show the same surge response sensitivity when mooring characteristics are changed. Since the optimized set of design parameters are based on fully loaded results, this section will describe only the influence of the assumption to the fully loaded FPSO. The possible proof for overestimation for ballast surge response results may be explained by the next sections.
The fully loaded Rayleigh model results described in Section 4.5.3 show an underestimation of both the excursion and mooring force when compared to a six-degree of freedom OrcaFlex system. To show the difference in surge excursion and mooring force, a part of the time signal of a single degree of freedom surge and six-degree of freedom system from OrcaFlex are plotted in Figure 5.2. It shows that the systems response is surge dominant, since both responses are close to identical. It can be seen that indeed, the maximum surge excursion and mooring force are higher for a six-degree of freedom system compared to a single degree of freedom system. However, the wave frequent motions starting at 3400 seconds, show higher values for the single degree of freedom system. This may be explained by additional damping of other motions.

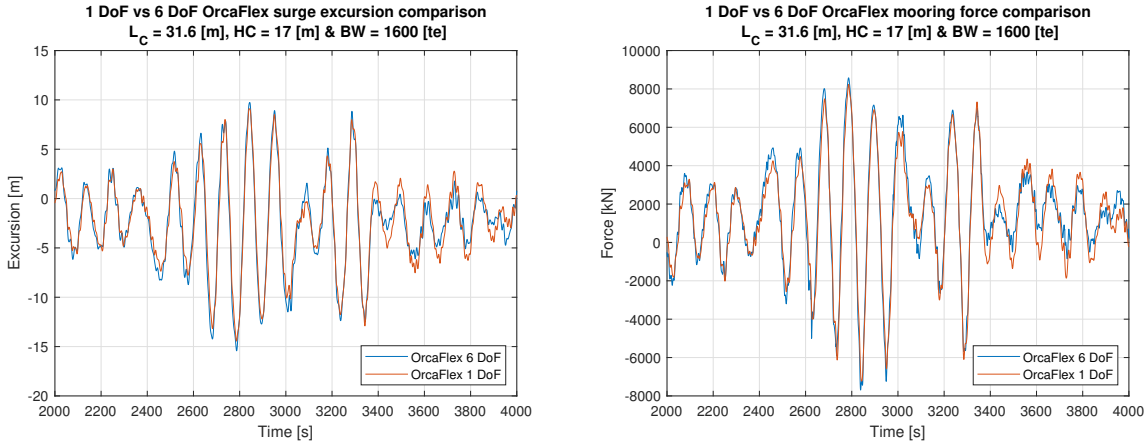

(a) Surge excursion

(b) Mooring force

Figure 5.2: Single degree of freedom system compared to a six-degree of freedom system in OrcaFlex with wave seed 01

In addition, the sensitivity of the surge response related to the variation in mooring design parameters show some high non-linearity's for positive excursions and push forces in Figure 4.10. To verify if this is affected by the single degree of freedom assumption, results of the pendulum length variation with constant hang-off height is shown in Figure 5.3. The hang-off height is chosen to be the same as in the optimized set of design parameters shown in Figure 4.11. Just as the results there, the calculated MPM values are based on 10 wave seeds. Again, it can be seen that both the surge excursion and mooring force are underestimated by using the single degree of freedom model in OrcaFlex. Also the mean excursion and mooring force are underestimated. Reasonably, it may be said that a small part of the underestimation of fully loaded results are influenced by other motions of the vessel. This underestimation is more predominant for negative excursions. However, when comparing the forces in Figure 5.3, the push force (negative force) suddenly shows a large difference even though the positive excursion results are identical. This observation indicates that, especially for the push force, the other motions may have a significant influence.

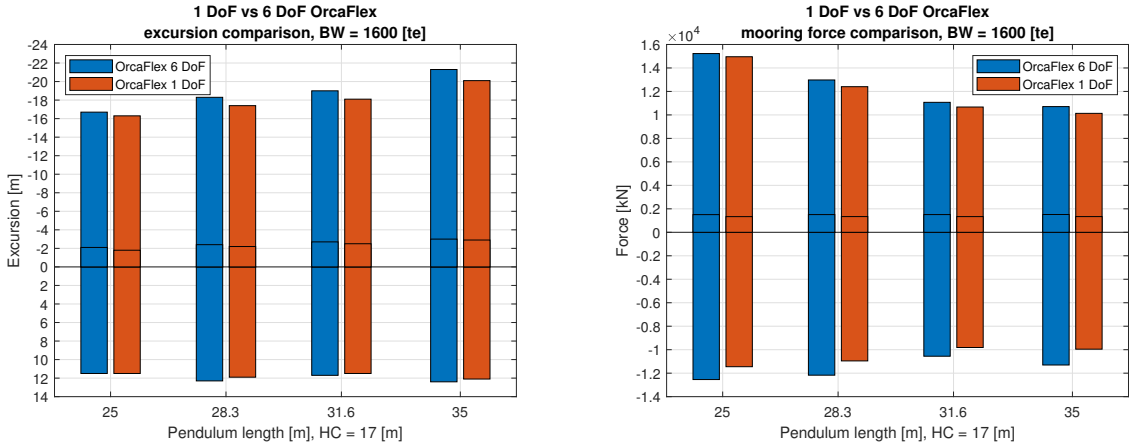

(a) Surge excursion

(b) Mooring force

Figure 5.3: Single degree of freedom system compared to a six-degree of freedom system in OrcaFlex

To find out which motions induces these significant difference, the load-excursion time trace for a six-degree of freedom system should be compared to the load-excursion curve in the design tool. It is chosen to do this for the optimized set of design parameters followed from the OrcaFlex analysis. The comparison is depicted in Figure 5.4. It can be noticed that the mooring force deviates more when the FPSO is moving towards the tower. Indeed, as mentioned before, other motions seems to affect the push force more than the pull force. Now, the force difference $\Delta F_{Orca/Tool}$ at every time step between the six-degree of freedom OrcaFlex time history and design tool can be evaluated. By obtaining the time signals of the other motions and plotting them against $\Delta F_{Orca/Tool}$, the most influential motions can be identified. This is done by finding the motion-force plots which show a symmetry around zero equal to Figure 5.4. It means that the the motion-force plot should go through the origin [0,0] and should show a wider range of force deviation at either side of the origin. By plotting the sway, heave, roll, pitch and yaw motions against the force difference $\Delta F_{Orca/Tool}$, only heave and pitch motions show the described symmetry around the origin. Results of the heave and pitch motion-force plots are shown in Figure 5.5. The pitch motion shows a dense area around the origin with a wider range of $\Delta F_{Orca/Tool}$ for positive pitch angle. Further, negative heave motions result in a wider range of $\Delta F_{Orca/Tool}$. Recall the coordinate system from Figure 3.3. Positive pitch is when the nose of the vessel dives down and negative heave is a downward motion. The wider range of force deviation for positive surge excursions may be explained by the positive pitch and negative heave motions, since the ballast weight is capable to push the nose of the FPSO down when surging towards the tower. As illustrated in Figure 5.6, this pitch in combination with the heave motion will results in a decrease in hang-off height. According to Chapter 2, the modification of the hang-off height shows high sensitivity to the shape of the load-excursion curve for positive excursions. Therefore, the combined heave and pitch motions towards the tower may be of significant influence to the maximum push force.

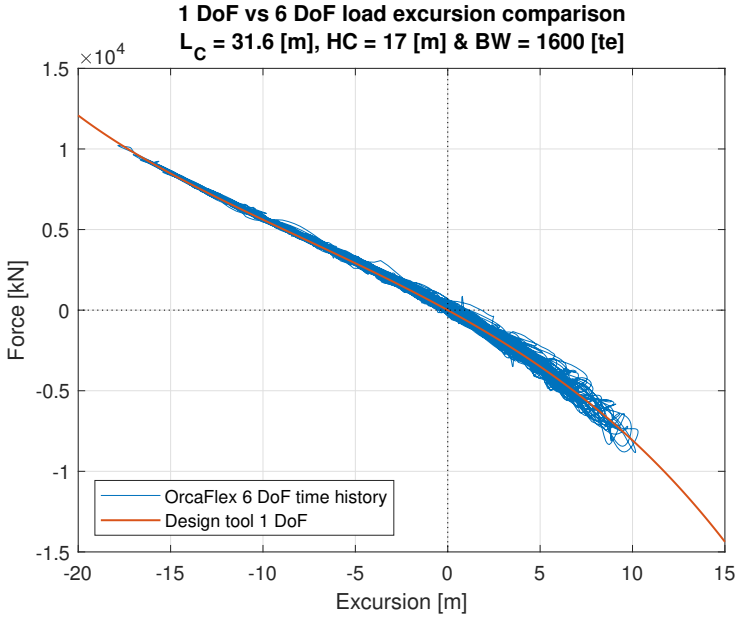

Figure 5.4: 6 DoF 3 hour time history load-excursion for wave seed 01 compared with 1 DoF design tool load-excursion curve

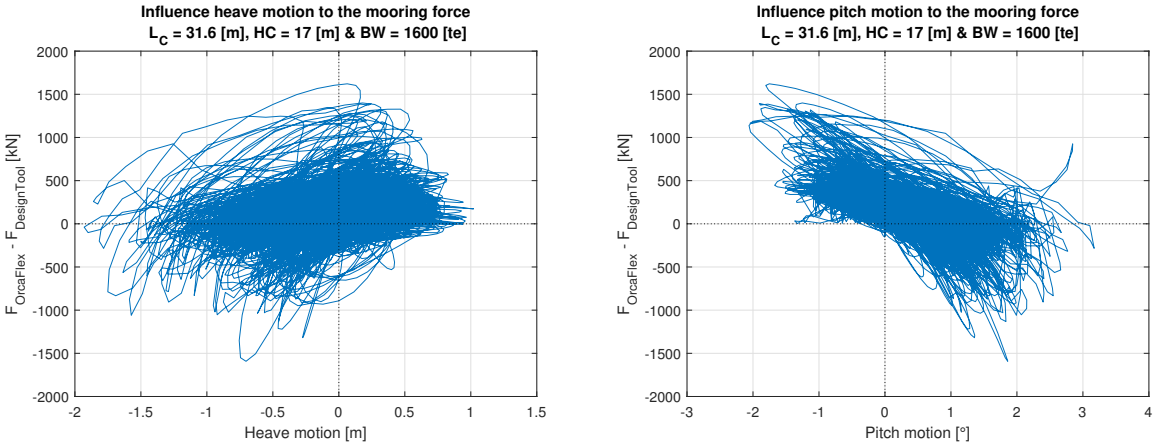

(a) Heave motion (b) Pitch motion

Figure 5.5: Dominant other motions with wave seed 01

With this information, the high sensitivity to the push force can be explained by a small increase in surge excursion. Reason one may be the non-linearity of the part of the load-excursion curve towards the tower. In general it shows a more non-linear shape compared to the part of the curve away from the tower, especially in fully loaded condition. Equal increase in surge excursion contributes to a larger push compared to pull force variation. The second reason may be that possible combined heave and pitch motions significantly increase the mooring force when surging towards the tower. By using the motion RAO for pitch and heave, as described for surge in Appendix A.2, the change in hang-off height can be calculated. Using a combined 2° pitch angle and 1 m heave motion results in a shift of approximately 7 m in hang-off height. The consequence to the load-excursion curve is illustrated in Figure 5.7 for both directions. Using the figure, it may be said that the surge, heave and pitch motions are dominant in defining the maximum mooring force. It is expected that the sway, roll and yaw motions influence the general force deviation over the entire load-excursion curve. These motions may be caused by the asymmetry of the frontal wind area of the Stena Surprise FPSO indicated in Figure C.1.

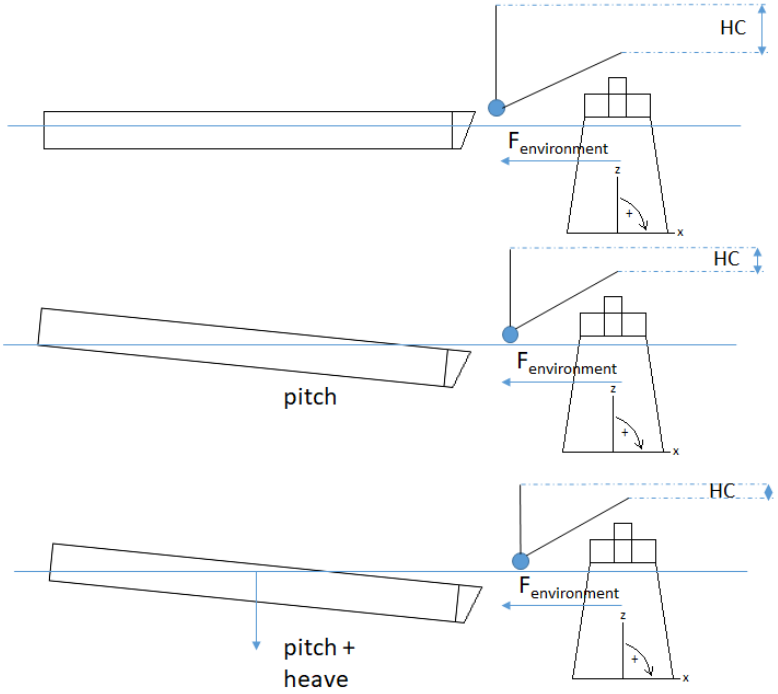

Figure 5.6: Combined heave and pitch motion influence to the hang-off height

Nevertheless, the other motions do not seem to influence the sensitivity to the surge response when varying mooring design parameters as shown in Figure 5.3. At a pendulum length of 31.6 m, the single degree of freedom system shows the lowest push force, equal to the six-degree of freedom system. However, when finding the optimized set by minimizing the absolute maximum mooring force, the single degree of freedom system proposes the pendulum length of 35 m instead of 31.6 m for the six-degree of freedom system. Again, the difference between the absolute maximum mooring force for a pendulum length of 31.6 and 35 m is less than 2%. Therefore, may be said that the single degree of freedom assumption is sufficient to achieve the project goal.

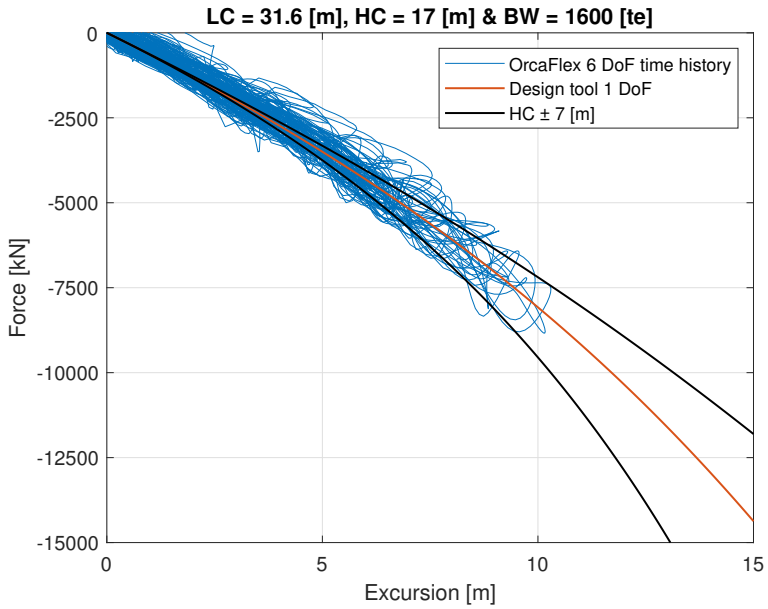

Figure 5.7: Combined heave and pitch motion influence to the hang-off height in wave seed 01

Concluding, by comparing a six-degree of freedom system with a single degree of freedom system in OrcaFlex it can be said that:

- A small part of the underestimation for fully loaded surge response is induced by other motions
- Equal sensitivity to the surge response when varying mooring design parameters is shown
- The high sensitivity of the push force can be explained by the combined heave and pitch motion caused by the ballast weight when the FPSO is surging towards the tower
- The optimized set of design parameters may be influenced by other motions, but the absolute maximum mooring force difference is still within 2% accuracy
- A single degree of freedom assumption is sufficient to achieve the project goal

5.3. Influence of the linearization of the mooring system

The second major assumption is the assumption of linear mooring characteristics. As described in Section 3.3.2, the mooring force is linearized at the expected mean surge excursion. It is assumed that the mean surge excursion results from the mean environmental force. The mean environmental force consist of the mean current, wind and second order wave drift force. By comparing the mean environmental force obtained from OrcaFlex and the design tool, it shows a small difference in the mean second order wave drift force. The mean environmental force from OrcaFlex and the design tool for ballast and fully loaded condition are given in Table 5.1

Mean force ballast	**Symbol**	**Unit**	**Design tool**	**OrcaFlex**
Current	$\overline{F_{1current}}$	[kN]	13.94	13.94
Wind	$\overline{F_{1wind}}$	[kN]	534.40	534.40
Wave drift force	$F^{(2)}_{1wave}$	[kN]	489.81	558.35
Total	$\overline{F_{1e}}$	[kN]	1038.2	1106.7
Mean force fully loaded	**Symbol**	**Unit**	**Design tool**	**OrcaFlex**
Current	$\overline{F_{1current}}$	[kN]	30.13	30.13
Wind	$\overline{F_{1wind}}$	[kN]	453.51	453.41
Wave drift force	$F^{(2)}_{1wave}$	[kN]	757.07	840.56
Total	$\overline{F_{1e}}$	[kN]	1240.7	1324.2

Table 5.1: Mean environmental force comparison

The second order wave drift force in OrcaFlex is generated in the time domain using the full QTF $|T(\omega+\mu,\omega)|$. The design tool estimates the mean wave drift force using only the main diagonal QTF $P(\omega,\omega)|$ in the frequency domain. For every wave seed, there is a small variation in mean second order wave drift force obtained from OrcaFlex. Apparently, the generation of the wave drift force in OrcaFlex using the full QTF results in a higher mean value. Still, the difference between design tool and OrcaFlex is very minor. The small underestimation of the mean environmental force has no significant influence on the linearized mooring force and thus the MPM value. When comparing the mean mooring force from a six-degree of freedom system with a single degree of freedom system in Figure 5.3, other motions may increase the mean mooring force. The mean environmental force from the design tool in Table 5.1 is identical to the mean mooring force for a single degree of freedom system in OrcaFlex. Possibly, due to the asymmetry of the vessels wind surge area, the vessel has a constant sway offset increasing the mean mooring force for the six-degree of freedom system. However, when using the mean environmental force from the single degree of freedom OrcaFlex model and read the mean excursion from the load-excursion curve, the mean excursion obtained in the design tool is slightly lower. Since the load-excursion curves of the design tool and single degree of freedom system are identical, this means that the mean surge excursion in OrcaFlex is not fully described by the mean environmental force. The mean surge excursion from the six-degree of freedom OrcaFlex model is approximately 10% higher compared to the design tool. In the end this will make 0.2 m difference in the calculation of the MPM, which can be considered insignificant.

As shown in Figure 3.5, the linearization of the mooring force is based on the part of the curve for surge excursion away from the tower. Since the shape of the other part of the curve is different, the linearization at one part of the curve should not be sufficient to estimate the positive surge excursion. To illustrate this, the Rayleigh probability plot for positive and negative surge excursion peaks are given in Figure 5.8. It can be seen that both positive and negative excursion can be described by a Rayleigh distribution, however the standard deviation σ_{x_1} of the surge response is different. This standard deviation is dependent on the damping of the vessel in waves, the spectral density of the low frequency wave drift force and the stiffness of the mooring system. In theory, two linearizations of the mooring force should be executed, each for away and towards the tower. Nonetheless, the expected surge excursion towards the tower is unknown. Together with the high non-linearity of the mooring characteristic, linearization for the part of the curve towards the tower is very challenging.

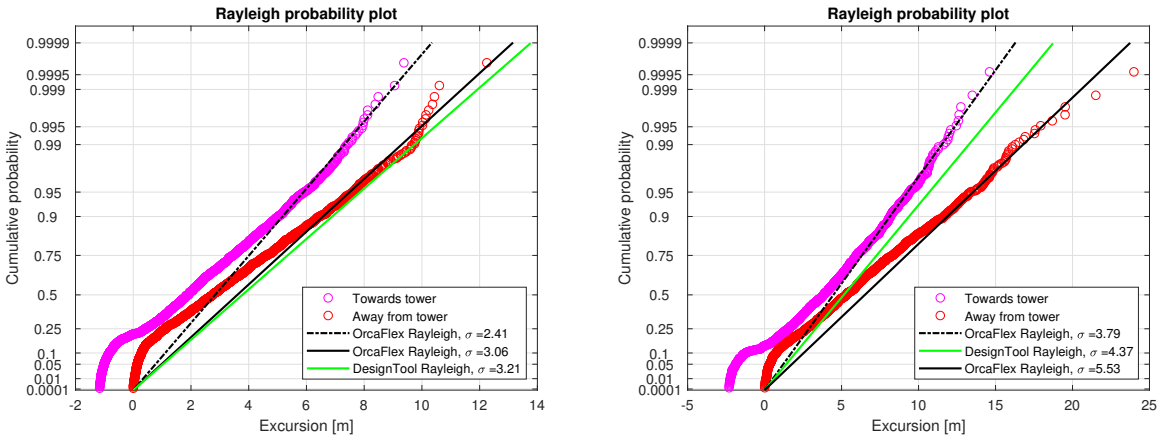

(a) Ballast surge excursion

(b) Fully loaded surge excursion

Figure 5.8: Rayleigh probability plots for surge excursion away and towards the tower for benchmark mooring properties. The standard deviation calculated by the design tool is depicted in green

Note that the surge excursion peaks away from the tower are estimated with respect to zero and for towards the tower with respect to the mean surge excursion. Also note that the standard deviation of the surge excursion in the design tool is related to the linearized mooring force and thus the stiffness adjustment, described in Section 3.3.5, is not yet executed. It can be seen that standard deviation for ballast loading condition overestimates the surge response, while fully loaded condition underestimates. Possible explanations for this may be explained in the following sections.

As a result of the linearization for one part of the load-excursion curve, a correction of the stiffness is executed as described in Section 3.3.5. The influence of the stiffness adjustment method can be evaluated using the single degree of freedom OrcaFlex surge response by reverse engineering. The corrected energy under the load-excursion curve is checked for a fully loaded system with L_C = 31.6 m, HC = 17 m and a ballast weight of 1600 tons shown in Figure 5.3. The results shows that the correct negative area, depicted in red in Figure 3.8, is 20% smaller in OrcaFlex when compared to the design tool. As can be seen from Figure 5.3, the surge excursion away from the tower for a six-degree of freedom system increases even more while obtaining approximately the same positive surge excursion. With this observation, it is expected that the error by using the stiffness adjustment method increases when comparing it to the six-degree of freedom OrcaFlex model. For the FPSO in ballast condition, the same observation applies. Depending on the shape of the load-excursion curve, the stiffness adjustment method may have significant influence to the estimated MPM value. Yet, the design tool is able to correctly propose efficient mooring design parameters.

Concluding, by linearization of the load-excursion curve at the mean surge excursion induced by the mean environmental force it can be said that:

- The mean environmental force in OrcaFlex is slightly higher than estimated in the design tool, resulting in a insignificantly small underestimation MPM surge excursion.
- In theory, the MPM positive and negative surge excursion can be estimated exactly by a Rayleigh distribution. However, a linearization of the negative part of the load-excursion curve should be executed as well. Although, this might be very challenging.
- The stiffness adjustment method executed in the design tool leads to an underestimation of the MPM surge excursion. Depending on the shape and location at the load-excursion curve, this may have significant effect calculated MPM values.

5.4. Influence of the natural excitation assumption

The design tool assumes that the vessel will surge at the natural surge frequency. This major assumption results in simplification of the damping terms, added mass and low frequency wave drift force spectrum. It also impacts the number of surge excursion peaks N in an expected 3 hour simulated storm. Recall the surge excursion time trace obtained from OrcaFlex depicted in Figure 5.2a. Here it shows also high frequent surge components, which may influence the total number of peaks. When comparing the number of fully loaded surge excursion peaks from Figure 5.8 and the design tool in a 3 hour storm, the difference is 10%. An error of 10% for N in calculation of the MPM surge excursion according to Equation 3.20 is insignificantly small. Therefore, the assumption of excitation at the natural surge period can be considered appropriate in estimation of the number of oscillations in a 3 hour storm.
In the following sections, the influence of the constant damping, added mass and low frequency wave drift force spectrum according to the natural excitation assumption is analysed.

5.4.1. Influence of constant damping and added mass

Section 3.3.3 describes the assumption of constant added mass and damping. The damping term consists of a summation of viscous damping by the FPSO when it moves to still water and by viscous damping when the FPSO is moving through waves with a slow drifting velocity. Using FFT analysis, it is shown that the dominant frequency of the vessels surge response is close to the natural surge frequency. Using this assumption, frequency dependent potential damping and added mass may be considered constant.
Figure 5.8a indicates that computed ballast results in the design tool lead to an overestimation when compared to OrcaFlex. According to the last sections, an underestimation is expected. Therefore, this may indicate that the assumption of constant potential damping and added mass are incorrect for the ballast FPSO. Figure 5.9 demonstrates the surge frequency components for ballast and fully loaded surge motion obtained from OrcaFlex. It shows that the relative contribution of wave frequent components are higher and more spread out for the FPSO in ballast condition. More influential wave frequent components for ballast FPSO could contribute to additional frequency dependent potential damping and added mass that is neglected in the design tool. This may explains the overestimation of ballast results in the design tool.
In OrcaFlex, the still water damping is constant and the wave drift damping is estimated by scaling the wave drift QTF values. This scaling factor is dependent on the slowly drifting velocity. As Appendix D.1.3 describes, the approximation of the mean wave drift damping in deep water may result in unreliable results. Therefore, Appendix A.4 describes an additional derivation of the mean wave drift damping in finite water depth. The values for the deep water and finite depth approximation are given in Table D.1. To check the influence of the mean wave drift damping used in the design tool, the mean wave drift damping estimation in OrcaFlex is disregarded. As a replacement, the constant values for deep water and finite depth are added to the constant still water damping of the vessel. Now, OrcaFlex does not scale the wave drift QTF values so that only constant damping is included, eqaul to the design tool. Results of these test are compared to the original wave drift damping method in the OrcaFlex model for ballast and fully loaded condition and are given in Table 5.2. The results show good agreement with the original model, by replacing the wave drift damping method in OrcaFlex by a constant value.

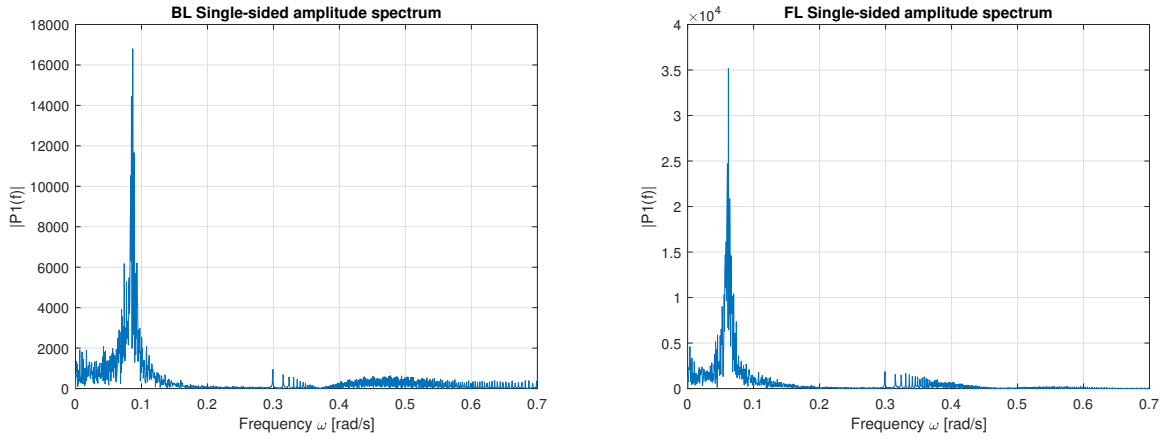

(a) Ballast (b) Fully loaded

Figure 5.9: Frequency spectra for ballast and fully loaded condition for benchmark mooring properties in wave seed 01

Results ballast FPSO	**Maximum excursion** [m]	**Minimum excursion** [m]	**Maximum F_{Pull}** [kN]	**Maximum F_{Push}** [kN]
Original model	-13.42	9.11	9825	-8964
Deep water	-14.61	10.09	10847	-10167
Finite depth	-13.70	9.22	10047	-9033
Results fully loaded FPSO	**Maximum excursion** [m]	**Minimum excursion** [m]	**Maximum F_{Pull}** [kN]	**Maximum F_{Push}** [kN]
Original model	-16.90	10.10	10525	-10544
Deep water	-17.10	10.13	10666	-10598
Finite depth	-15.84	9.36	9851	-9421

Table 5.2: Mean wave drift damping influence test for the benchmark system in wave seed 01

The results for ballast condition show that the finite depth approximation coincides with the original model. On the other hand, the fully loaded condition prefers the deep water approximation of the mean wave drift damping. Since the deep water approximation is used in the design tool, the influence of the deep water approximation for ballast FPSO may also result in the overestimation of the surge response. By applying the mean wave drift damping for finite water depth in the design tool and plotting Figure 5.8a again, it now shows the expected underestimation of the surge response in Figure 5.10. The possible reason for this higher wave drift damping in ballast condition, is that the vessels acceleration is higher. Since mass of the FPSO is lower, the enhanced restoring mooring force will induce a higher surge acceleration. Since the wave drift damping is dependent on velocity of the FPSO relative to the waves, ballast results are more sensitive to the wave drift damping approximation. Note that the increase of wave drift damping will not influence the goal of the project, since the optimized set of mooring design parameters are based on fully loaded results. All other possible explanations in this chapter still apply.

Concluding, by testing the influence of the mean wave drift damping for finite depth and deep water it can be said that:

- The wave drift damping method in OrcaFlex can be replaced with constant mean wave drift damping either for deep water or finite depth.
- The deep water approximation of the mean wave drift damping is too conservative for the ballast loading condition of the analysed vessel
- The possible reason for overestimation of ballast results is due to the incorrect assumption of either deep water mean wave drift damping or additional potential damping and added mass.

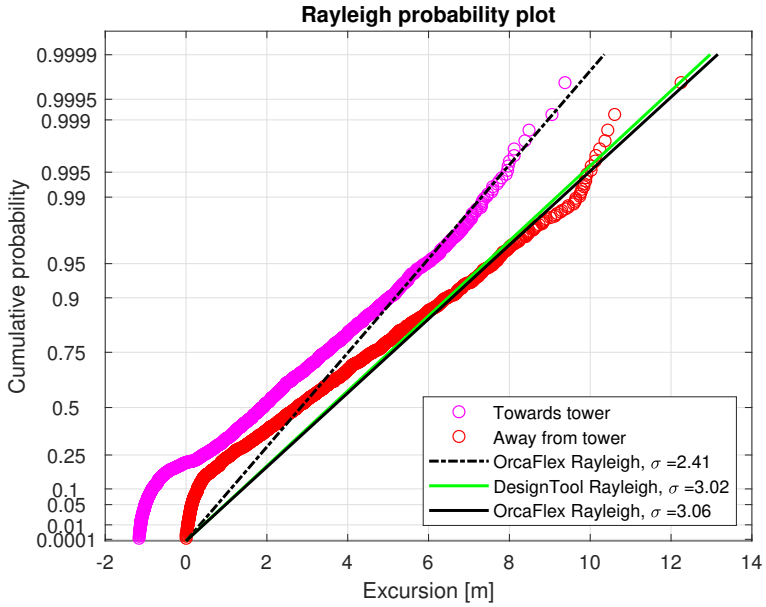

Figure 5.10: Ballast Rayleigh parameter with finite wave drift damping

5.4.2. Influence on the low frequency wave drift force spectrum

As described in Section D.1.4, a part of the Rayleigh parameter or standard deviation of the surge response σ_{x_1} is calculated using the spectral density of the low frequency wave drift force. It can be estimated with the wave group spectrum and the wave drift force QTF. By using Newman's approximation, the 'off-diagonal' terms of the low frequency wave drift QTF $Q(\omega+\mu,\omega)$ can be fully described by the 'diagonal' terms of the wave drift QTF P as given in Equation D.16. According to the natural excitation assumption, the difference frequency μ may be approximated by zero. This assumption results in the total exclusion of the off-diagonal term of the wave drift force QTF. By using low frequency wave drift spectrum in Figure D.2, the use of $S_F(\mu = \omega_{1n})$ and $S_F(0)$ will have insignificant influence to the Rayleigh parameter. However, the depicted low frequency wave drift spectrum is based on the Newman's approximation. To indicate the influence of the Newman's approximation to the surge response, another test in OrcaFlex is to be performed.
OrcaFlex provides the option to either use Newman's approximation (only P) or the full QTF (P and Q) method in order to estimate second order wave drift loads on the FPSO. Resulting from these loads, the large slow drifting motions will appear. Since the original OrcaFlex model uses the full QTF method, the influence of the Newman's approximation versus the use of the full wave drift force QTF is evaluated in OrcaFlex by a single run for benchmark mooring characteristics in ballast and fully loaded condition of the FPSO. The results are shown in Table 5.3. As can be seen, Newman's approximation underestimates the results of both excursion and mooring force by approximately 30% when compared to the original model. This may be caused the shallow water depth analysed in this project. In shallow waters, depending on the analysed environment, the Newman's approximation may give unreliable results[17]. With this information, it is expected that the influence of the off-diagonal' terms Q for the analysed water depth is significant. The use of Newman's approximation in the design tool may be the main reason for the underestimation of the surge response results.

Concluding, by comparing the Newman's approximation versus the full QTF method to specify the second order wave drift loads it can be said that:

- Newman's approximation underestimates both surge excursion and mooring force in the analysed environment.
- Since the design tool uses only a part of the wave drift force QTF by using Newman's approximation, it is expected that this is the main reason for the recurring underestimation by the design tool.

Results ballast FPSO	**Maximum excursion** [m]	**Minimum excursion** [m]	**Maximum F_{Pull}** [kN]	**Maximum F_{Push}** [kN]
Original model (full QTF)	-13.42	9.11	9825	-8964
Newman's approximation	-9.72	5.61	6835	-5635
Results fully loaded FPSO	**Maximum excursion** [m]	**Minimum excursion** [m]	**Maximum F_{Pull}** [kN]	**Maximum F_{Push}** [kN]
Original model (full QTF)	-16.90	10.10	10525	-10544
Newman's approximation	-12.67	7.38	8029	-7008

Table 5.3: Newman's approximation test for the benchmark system in wave seed 1

5.5. Robustness

During this project, an extreme collinear environment with a return period of approximately 100 years is analysed. In order to discuss the robustness of the developed design tool, two additional moderate collinear environments are analysed as well. These environments are determined by equal wave steepness S_w and current and wind speeds are unchanged. The wave steepness is defined by the characteristic wave height divided by the characteristic wave length given as:

$$S_w = \frac{H_s}{gT_p^2/2\pi} \tag{5.1}$$

Using the equation and subtracting two times one meter H_s from the original wave height, two T_p values are obtained. Using Figure C.4, these less extreme environments fall within a 5-year and 1-year return period respectively. The additional analysed environments are given in Table 5.4. Note that the peak enhancement factor γ stays identical to Environmental Case (EC) 1. By doing the same analysis in OrcaFlex as described in Section 4.5, the robustness of the design tool can be estimated with two additional environments. Results of the analyses are shortly described below.

Environment	**H_s** [m]	**T_p** [s]	**V_c** [m/s]	**V_w** [m/s]	γ [-]
Case 1 (original)	7.38	14.26			
Case 2	6.40	13.26	0.35	19.11	1.4
Case 3	5.40	12.18			

Table 5.4: Analysed extreme collinear environments

5.5.1. Environmental case 2

Results of the sensitivity analysis for environmental EC 2 are given in Appendix E. The sensitivity of the surge excursion related to the variation of mooring design parameter change can be well described with the design tool. The optimization procedure in the design tool obtains the exact same set of mooring design parameters as for EC 1. OrcaFlex proposes, in comparison to EC 1, a lower hang-off height of HC = 12 m. Yet, the same longest pendulum length and lowest ballast weight are preferred by both models. The optimized mooring design parameters are indicated in the figures given in Appendix E. The absolute difference between the maximum mooring forces obtained from OrcaFlex for a hang-off height of 12 m and 17 m is less than 10%. Therefore, the optimization procedure done by the design tool can still be considered sufficient.

The same described observations in Section 4.5.3 apply for EC 1. However, it can be seen that the absolute surge response results of the design tool and OrcaFlex match closely. No underestimation of the surge response is shown anymore. This may be explained by the fact that in a less extreme environment, other motions are less severe and contribute less to the surge excursion and mooring force. Due to lower excursions, forces are estimated at the more linear part of the load-excursion curve. This means that the force is less sensitive to a small excursion difference. In addition, when comparing

the included surge frequencies for the two additional environmental load cases in Figure 5.11, it shows a increasing relative contribution of the wave frequent components. In addition, the frequencies of the wave frequent components are increasing when the environment becomes more moderate. Recall the potential damping graph of the Stena Surprise FPSO from Figure C.2b. Here it can be seen that the damping rapidly increases with increase frequency. Therefore, it is expected that the increasing frequency of the wave frequent motions will influence the contribution of frequency dependent potential damping in OrcaFlex. Accordingly, it is expected that mild environments will require more damping in the design tool when compared to OrcaFlex, since frequency dependent potential damping is neglected.

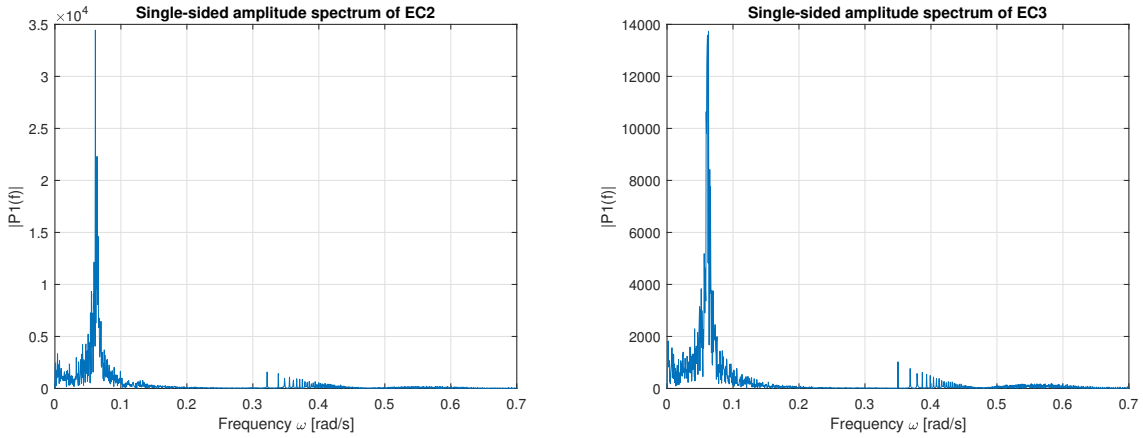

(a) Environmental case 2 (EC2)

(b) Environmental case 3 (EC3)

Figure 5.11: Frequency spectra of the surge motion response for benchmark EC2 and EC3 for wave seed 01

5.5.2. Environmental case 3

Results of the sensitivity analysis for environmental EC 3 are given in Appendix E. As expected, the design tool now slightly overestimates the surge response for EC 3, possibly due to the frequency dependent potential damping. For this case, the design tool proposes the same set of mooring design parameters as OrcaFlex did for EC 2. However, for EC 3, OrcaFlex proposes a hang-off height of HC = 7 m. Again, the longest pendulum and lowest ballast weight are preferred for both models. When comparing the absolute maximum mooring force results for both HC = 7 m and HC = 12 m in OrcaFlex, the difference is less than 2%. Therefore, the proposed set of mooring design parameters proposed by the design tool can be considered sufficiently accurate.

Concluding, by doing the robustness analysis it can be said that:

- Frequency dependent damping may become increasingly important when a moderate environment is analysed.
- Long pendulum and low ballast weight are preferred in all environmental cases
- According to results from OrcaFlex, the hang-off height can be decreased in a moderate environment, since other motions have a lower impact to the surge response of the system
- The design tool is capable to describe the sensitivity of the surge response related to mooring design parameter variation and proposes the correct set of mooring design parameters within 2~10% accuracy.

5.6. Chapter summary

This chapter discusses the influence of the assumptions made in the Rayleigh model by doing several checks in OrcaFlex. By modifying the OrcaFlex model such that it uses the same assumptions as in the Rayleigh model, the effect of the assumptions can be assessed.

First, the single degree of freedom assumption will underestimate the surge response compared to a six-degree of freedom system. Other motions are influencing the frontal area of the FPSO, resulting in higher loads and larger excursions. Especially, with large excursions, the mooring characteristic is very non-linear which results in a high sensitivity of other motions to the restoring mooring force. The heave and pitch motions may be considered as most critical in this case. Yet, the project goal can be achieved by using the single degree of freedom system only.

Second, it is shown that both the positive and negative excursion can be described using a Rayleigh distribution with different Rayleigh parameters. However, the linearization of the mooring force can only be done at the mean environmental force. Therefore, the stiffness adjustment method is used to estimate the mooring force for positive excursion too. Depending on the non-linearity of the load-excursion curve, a small error between OrcaFlex and design tool can have significant influence to the calculated mooring force. Yet, results of the optimized set of mooring design parameters show that the method of stiffness adjustment in the design tool can be considered sufficient.

Third, it has been shown that the constant wave drift damping in the design tool is able to describe the frequency dependent wave drift damping method used in OrcaFlex very well. With estimations of the constant deep and finite wave drift damping, it has been shown that the wave drift damping in finite depth applies for the vessel in ballast condition for EC 1. The possible lack of either frequency wave drift or potential damping in the design tool may be the result of the overestimation of ballast surge response results when compared to the OrcaFlex.

Fourth, it is shown that the out-of-phase part of the low frequency wave drift force may have a significant influence on the estimation of the surge response in shallow water when the difference frequency μ is assumed to be zero. Therefore, it can be said that the Newman's approximation, implemented in the design tool, is most likely to underestimate the surge response when compared to OrcaFlex.

Lastly, by doing a robustness check by analysing two additional environmental cases, it has been observed that frequency dependent damping may become increasingly important when the environment is more moderate. Therefore, this can be one of the reasons why the design tool slightly overestimates the surge response when compared to OrcaFlex, since it uses constant damping only. Nevertheless, the results of the design tool are sufficient to show the sensitivity of the surge response related to mooring design parameter variation. In addition the design tool is able to propose an optimum set of mooring design parameters for given environment and FPSO within an accuracy of 2~10%.

6

Conclusion & Recommendations

Soft yoke moored FPSO systems used for offshore field developments are known by its high dynamic complexity. Therefore, the design process of such systems often consists of small adjustments to proven mooring solutions in the past by using computationally expensive dynamic simulations. To increase the efficiency of the design process, by decreasing the amount of required dynamic simulations, the following goal was set:

Develop an efficient design tool, to be used before dynamic modelling, which is able to assess the sensitivity of dynamic surge response related to variation of mooring design parameters and provide the designer with an optimum set of mooring design parameters in a given environment.

To achieve this goal two separate models were developed; a linear frequency domain statistic Rayleigh model and a non-linear time domain Harmonic Balance model evolved in an extended Runge-Kutta method. By comparing both models to fully coupled numerical simulation software OrcaFlex for an extreme collinear environment, one model is selected and implemented in the design tool. This chapter will reflect upon the goal set by providing the conclusion and recommendations in Sections 6.1 and 6.2 respectively.

6.1. Conclusion

Despite the high dynamic complexity of the analysed system, both models adopt a single degree of freedom mooring system. Single point moored structures can often be considered as surge dominant, induced by the low frequency wave drift forces. Due to low damping, these forces actuate the system close to the natural surge frequency, followed by large slowly oscillating motions. These motions induces the maximum loads in the mooring system to be optimized. By defining a single degree of freedom system, the surge response can be fully described by the load-excursion characteristics of the mooring system.

The static analyses indicated that the pendulum length, hang-off height and ballast weight significantly affect the mooring characteristics. Variation of these mooring design parameters are required to minimize the maximum restoring mooring force in a given environment. By describing optimization limits to the mooring design parameters, the stiffness of the mooring system is linearized in the Rayleigh model or described by a n^{th} order polynomial fit in the Harmonic Balance and Runge-Kutta method.

By comparing the MPM surge response of the benchmark mooring system from OrcaFlex to the MPM values for both proposed models, it showed that Harmonic Balance was unable to describe the surge response by one single harmonic so that multiple iterations were required. To investigate the accuracy of the results that could be obtained with the non-linear equation of motion used, the Runge-Kutta method was applied. By implementing the exact same environmental forces from OrcaFlex, it was observed that the surge response of the assumed non-linear system is unable to match the output from OrcaFlex and unable to increase accuracy compared to the Rayleigh model. In combination with

untraceable numerical differences in OrcaFlex software, further analyses with Harmonic Balance nor Runge-Kutta method was avoided. The Rayleigh model was to be implemented in the design tool.

Thirty-six (36) different sets of mooring design parameters for three different environmental cases were analysed in OrcaFlex. To achieve a reliable MPM, 10 wave seeds for both ballast and fully loaded FPSO were analysed resulting in 720 cases per environmental case. Each environmental case required a computational time of approximately 6 days. By comparing MPM surge responses from OrcaFlex with the design tool, it demonstrated capability of correctly proposing a set of mooring design parameters for every environmental case within a minute by minimizing the restoring mooring force with 2~10% accuracy. By obtaining surge response results from OrcaFlex for the optimized set of mooring design parameters and comparing them with the benchmark system, it showed a decrease of 25% in mooring load with a moderate increase of 10% in MPM surge excursion.

Although the absolute MPM surge responses of the Rayleigh model shows differences with OrcaFlex results, it is capable to describe the sensitivity of the surge response related to mooring design parameter variation quite well. Increasing the ballast weight and decreasing the pendulum length generally results in a decrease of surge excursion, though a raise in mooring load. An increase of hang-off height results in a decrease in surge excursion away from the tower and an increase in mooring load, while the motion towards the tower results in an increase of surge excursion and a decrease in mooring load. Since the sensitivity of the surge response can be well described, accurate calculations of the surge response to propose an optimum set of mooring design parameters are not necessary.

It is proven that a simple, computational efficient single degree of freedom linear Rayleigh model is able to describe the dynamic surge response of an FPSO with SYMS in an extreme collinear environment by varying mooring design parameters. By introducing the design tool including GUI in the design process, the designer has access to a quick and efficient tool that proposes an adequate set of mooring design parameters which limits the required computational time in comprehensive dynamic modelling.

6.2. Recommendations

Eventually, OrcaFlex software is used to obtain the actual design loads for the moored system. Therefore, it was not an objective to achieve accurate surge response results with the design tool. It has been shown that by minimizing the restoring mooring force, the maximum surge excursion is high. Therefore, the most important recommendation for future development of the design tool is to improve the optimization procedure by including a limiting surge excursion. This can only be accomplished by attaining more accurate surge response results. The following recommendations are focused on this improvement:

- *Include combined pitch and heave motions*
  Especially for extreme wave environments, the contribution of heave and pitch motions to the surge response become increasingly important since they influence the relative hang-off height. Depending on the non-linearity of the mooring characteristic, a slight variation in hang-off height could induce an extreme build-up of maximum load in the mooring system.
- *Investigate two part linearization of the mooring force*
  It has been shown that the surge response peaks away from and towards the tower indicate a different Rayleigh distribution. Therefore, as an alternative to the energy balance method a way has to be found to linearize the part of the load-excursion curve towards the tower as well. Accordingly, a reliable Rayleigh parameter can be estimated for either part of the load-excursion curve.
- *Investigate the influence of frequency dependent damping and added mass*
  Constant damping and added mass of the FPSO is adjusted for in ballast and fully loaded condition. However, in more moderate environmental conditions the relative contribution of wave frequent surge components seems to increase, resulting in a higher frequency dependency of damping and added mass. It should be indicated for which H_s/T_p combinations the frequency dependent damping and added mass has to be adjusted for in both ballast and fully loaded condition of the FPSO.
- *Investigate the implementation of the full or influential parts of the wave drift QTF*
  It is shown that Newman's approximation underestimates the surge response in shallow waters. It should be investigated how and for which water depths additional QTF values should be implemented while preserving the high computational efficiency.
- *Perform model tests*
  Model tests with varying mooring design parameters should be performed in order to validate the accuracy of the results obtained by OrcaFlex.

The following recommendations are focused on research outside the scope of the project. In future extended projects, these recommendations could be useful:

- *Extend validation to multiple FPSO shapes and sizes*
  The current design tool is limited to one FPSO only. By including multiple FPSO shapes and sizes, valuable extension would be achieved.
- *Define sensitivity of the surge response to multiple non-collinear environments*
  The computations done in the current design tool are based on collinear environments only. Favourable extension of the design tool can be accomplished by including a sensitivity study for non-collinear environmental cases as well.

A

Theory

This appendix will provide some background information on how diffraction and radiation software programs like Hydrostar are able to calculate frequency dependent vessel properties, related to the shape and draft of the hull.

A.1. Added mass and potential damping

This section describes the calculation of frequency dependent added mass and potential damping values that. Note that the added mass and potential damping values are directional independent.
The added mass and potential damping can be estimated using either model tests or the radiation potential of the waves caused by the surge motion of the vessel. For more information on the radiation potential, please refer to M J Journée and W Massie. If we assume that the radiation potential for surge direction is known, the surge added mass and potential damping coefficients can be estimated by:

$$\begin{aligned} a_{11} &= -\Re\left[\rho \iint_{S_0} \phi_1 n_1 \, dS_0\right] \\ b_{11} &= -\Im\left[\rho\omega \iint_{S_0} \phi_1 n_1 \, dS_0\right] \end{aligned} \tag{A.1}$$

Where, S_0 is the mean wetted surface of the vessel, ϕ_1 is the radiation potential of the waves due to the motion in surge direction and n_1 is the normal vector.

A.2. Derivation of the motion RAO in regular waves

In this section, calculation of the response amplitude operator for the surge motion in regular waves is described. Using this RAO, the significant surge amplitude in irregular waves can be estimated. This motion is induced by the first order wave force. The force can be obtained by the integration of the pressures on the body of the FPSO in an undisturbed wave. Due to diffraction of waves, the total first order wave force can be written as a summation of force components proportional to the acceleration, velocity and position of the water particles:

$$F^{(1)} = a\ddot{\zeta} + b\dot{\zeta} + c\zeta \tag{A.2}$$

Where the wave elevation for a regular wave approaching from 180° is given can be written as:

$$\zeta = \zeta_a \cos(\omega t - kx) \tag{A.3}$$

Where k is the wave number and ζ_a the amplitude of the wave elevation. By defining the equation of motion including the first order wave force, the following is obtained:

$$(m + a)\,\ddot{x} + b\dot{x} + cx = a\ddot{\zeta} + b\dot{\zeta} + c\zeta \tag{A.4}$$

The surge response to the regular wave excitation including phase shift $\epsilon_{x\zeta}$ is given by:

$$x = x_a \cos\left(\omega t + \epsilon_{x\zeta}\right) \tag{A.5}$$

By substitution of Equation A.5 and A.3 with their derivatives in Equation A.4 and by collection of the in-phase and out-of-phase terms, two equation with two unknowns are obtained. The surge amplitude of the response $\frac{x}{\zeta_a}$ can be obtained by adding the squares of the in-phase terms (C) and out-of-phase terms (S):

$$\frac{x}{\zeta_a} = \sqrt{C^2 + S^2} \tag{A.6}$$

The phase can be calculated using:

$$\epsilon_{x\zeta} = \tan^{-1}\left(\frac{S}{C}\right) \tag{A.7}$$

Note that this procedure is dependent on the propagation direction of the incoming waves.

A.3. Derivation of the wave drift force QTF in irregular waves

In this section, calculation of the second order wave force in irregular waves is described. Using this second order wave force, the QTF of the second order wave force can be derived. First, the pressure p can be calculated when the wave velocity potential Φ is known using the non-linear Bernoulli equation given as:

$$p = -\rho g z - \rho \frac{\partial \Phi}{\partial t} - \frac{1}{2}\rho\left(\vec{\nabla}\Phi\right)^2 \tag{A.8}$$

It can be seen that p consist of hydrostatic, first order and second order pressure given as:

$$p = p^{(0)} + p^{(1)} + p^{(2)} \tag{A.9}$$

Where the hydrostatic pressure $p^{(0)}$ is proportional to the hydrostatic force measured vertically from the surface elevation (z), $p^{(1)}$ to the first order force and $p^{(2)}$ to the second order force. Next, the fluid force excited on the vessel can be determined by direct pressure integration over the instantaneous wetted surface S of the hull by:

$$\vec{F} = \iint_S p\vec{n}dS \tag{A.10}$$

Where $\vec{N}$ is the normal vector to the surface element dS, defined by the mesh created for the FPSO. Note that when calculating the second order wave force, every part of the Bernoulli equation needs to be integrated over the vessels hull. In the following, only one term in the Bernoulli equation is integrated in order to show the procedure on how software programs derive the QTF values for vessels in irregular waves. Thus, the QTF derived in this section is only a part of the full QTF.
Let's consider the first order pressure $p^{(1)}$ times a oscillatory wetted surface dS of the hull at the waterline (WL). The surface element $dS = dz \cdot dl$ is defined as the vertical varying distance dz times the varying horizontal distance dl on the hull, caused by the incoming waves. The second order force can be calculated using Equation A.10 by integrating first between the surface elevation ζ and the motion of the vessel at the waterline $x_{3_{WL}}$:

$$F_{WL}^{(2)} = \int_{WL}\int_{x_{3_{WL}}}^{\zeta} p^{(1)}\vec{n}dz \cdot dl \tag{A.11}$$

The first order pressure $p^{(1)}$ at the waterline can be written as:

$$p^{(1)} = -\rho g x_3 - \rho\frac{\partial \Phi}{\partial t} = -\rho g x_3 + \rho g \zeta \tag{A.12}$$

Equation A.11 becomes:

$$F_{WL}^{(2)} = \int_{WL} \int_{x_{3_{WL}}}^{\zeta} \rho g \left(\zeta - x_3\right) \vec{n} dz \cdot dl = -\oint_{WL} \frac{1}{2} \rho g \left(\zeta - x_{3_{WL}}\right)^2 \vec{n} \cdot dl \tag{A.13}$$

Now, the term inside the brackets can be considered as the relative surface elevation ζ_r at the waterline which is defined as the superposition of the surface elevation and vertical motion of the hull at the location of the waterline. In the end, the second order wave force at the waterline F_{WL}^2 can be written as:

$$F_{WL}^{(2)} = -\oint_{WL} \frac{1}{2} \rho g \left(\zeta_r\right)^2 \vec{n} \cdot dl \tag{A.14}$$

In irregular waves, the surface elevation can be considered as a summation of large numbers (N) of harmonic components with surface elevation ζ with random frequencies ω and phases ϵ:

$$\zeta(t) = \sum_{i=1}^{N} \zeta_i(t) \cos\left(\omega_i t + \epsilon_i\right) \tag{A.15}$$

The relative surface elevation ζ_r can be written as a summation of large number of harmonic components with surface elevation $\zeta \cdot \zeta_r$, random frequencies, phases and relative phases ϵ_r:

$$\zeta_r(t) = \sum_{i=1}^{N} \zeta_i(t)\zeta_{ir}(t) \cos\left(\omega_i t + \epsilon_i + \epsilon_{ir}\right) \tag{A.16}$$

Substituting Equation A.16 into Equation A.14 for two wave components i and j and by taking $\vec{n}$ as 1 results in:

$$\begin{aligned} F_{WL}^{(2)} = -\frac{1}{2}\rho g \oint_{WL} \Big[& \zeta_i^2 \zeta_{ir}^2 \cos^2\left(\omega_i t + \epsilon_i + \epsilon_{ir}\right) + \\ 2\zeta_i \zeta_j \zeta_{ir} \zeta_{jr} & \cos\left(\omega_i t + \epsilon_i + \epsilon_{ir}\right) \cos\left(\omega_j t + \epsilon_j + \epsilon_{jr}\right) + \\ & \zeta_j^2 \zeta_{jr}^2 \cos^2\left(\omega_j t + \epsilon_j + \epsilon_{jr}\right) \Big] dl \end{aligned} \tag{A.17}$$

By using the trigonometry rules $\cos^2(x) = \frac{1}{2} + \frac{1}{2}\cos(2x)$ and $2\cos(x)\cos(y) = \cos(x-y) + \cos(x+y)$, Equation A.17 can be written as:

$$\begin{aligned} F_{WL}^{(2)} = -\frac{1}{2}\rho g \oint_{WL} \Big[& \zeta_i^2 \zeta_{ir}^2 \left(\frac{1}{2} + \frac{1}{2}\cos\left(2\omega_i t + 2\epsilon_i + 2\epsilon_{ir}\right)\right) + \\ & \zeta_i \zeta_j \zeta_{ir} \zeta_{jr} \cos\left(\left(\omega_i - \omega_j\right) t + \left(\epsilon_i - \epsilon_j\right) + \left(\epsilon_{ir} - \epsilon_{jr}\right)\right) + \\ & \zeta_i \zeta_j \zeta_{ir} \zeta_{jr} \cos\left(\left(\omega_i + \omega_j\right) t + \left(\epsilon_i + \epsilon_j\right) + \left(\epsilon_{ir} + \epsilon_{jr}\right)\right) + \\ & \zeta_j^2 \zeta_{jr}^2 \left(\frac{1}{2} + \frac{1}{2}\cos\left(2\omega_j t + 2\epsilon_j + 2\epsilon_{jr}\right)\right) \Big] dl \end{aligned} \tag{A.18}$$

It can clearly be seen that the second order wave force consist of a mean part $\left(\frac{1}{2}\right)$, low frequency part $(\omega_i - \omega_j)$ and high frequency part $(\omega_i + \omega_j)$.
By using the trigonometry rules $\cos(x+y) = \cos(x)\cos(y) - \sin(x)\sin(y)$ and $\cos(x-y) = \cos(x)\cos(y) +$

$\sin(x)\sin(y)$, the parts of the incoming waves and relative waves can be separated:

$$F_{WL}^{(2)} = -\frac{1}{2}\rho g \oint_{WL} \left[\zeta_i^2 \zeta_{ir}^2 \left(\frac{1}{2} + \frac{1}{2} \left\langle \cos\left(2\omega_i t + 2\epsilon_i\right) \cos\left(2\epsilon_{ir}\right) - \sin\left(2\omega_i t + 2\epsilon_i\right) \sin\left(2\epsilon_{ir}\right) \right\rangle \right) + \right.$$
$$\zeta_i \zeta_j \zeta_{ir} \zeta_{jr} \left\langle \cos\left(\left(\omega_i - \omega_j\right) t + \left(\epsilon_i - \epsilon_j\right) \right) \cos\left(\epsilon_{ir} - \epsilon_{jr}\right) - \sin\left(\left(\omega_i - \omega_j\right) t + \left(\epsilon_i - \epsilon_j\right) \right) \sin\left(\epsilon_{ir} - \epsilon_{jr}\right) \right\rangle +$$
$$\zeta_i \zeta_j \zeta_{ir} \zeta_{jr} \left\langle \cos\left(\left(\omega_i + \omega_j\right) t + \left(\epsilon_i + \epsilon_j\right) \right) \cos\left(\epsilon_{ir} + \epsilon_{jr}\right) - \sin\left(\left(\omega_i + \omega_j\right) t + \left(\epsilon_i + \epsilon_j\right) \right) \sin\left(\epsilon_{ir} + \epsilon_{jr}\right) \right\rangle +$$
$$\left. \zeta_j^2 \zeta_{jr}^2 \left(\frac{1}{2} + \frac{1}{2} \left\langle \cos\left(2\omega_j t + 2\epsilon_j\right) \cos\left(2\epsilon_{jr}\right) - \sin\left(2\omega_j t + 2\epsilon_j\right) \sin\left(2\epsilon_{jr}\right) \right\rangle \right) \right] dl \tag{A.19}$$

By writing this final form as a double summation and by taking only the difference frequencies $\omega_i - \omega_j$ and $\omega_i + \omega_j$ into account, the second order wave force can be written as:

$$\begin{aligned} F_{WL}^{(2)} = & \sum_i \sum_j \zeta_i \zeta_j P_{ij}^{-} \cos\left(\left(\omega_i - \omega_j\right) t + \left(\epsilon_i - \epsilon_j\right) \right) + \\ & \sum_i \sum_j \zeta_i \zeta_j Q_{ij}^{-} \sin\left(\left(\omega_i - \omega_j\right) t + \left(\epsilon_i - \epsilon_j\right) \right) + \\ & \sum_i \sum_j \zeta_i \zeta_j P_{ij}^{+} \cos\left(\left(\omega_i + \omega_j\right) t + \left(\epsilon_i + \epsilon_j\right) \right) + \\ & \sum_i \sum_j \zeta_i \zeta_j Q_{ij}^{+} \sin\left(\left(\omega_i + \omega_j\right) t + \left(\epsilon_i + \epsilon_j\right) \right) \end{aligned} \tag{A.20}$$

Where P and Q are:

$$\begin{aligned} P_{ij}^{-} &= -\frac{1}{4}\rho g \oint_{WL} \zeta_{ir} \zeta_{jr} \cos\left(\epsilon_{ir} - \epsilon_{jr}\right) dl \\ Q_{ij}^{-} &= +\frac{1}{4}\rho g \oint_{WL} \zeta_{ir} \zeta_{jr} \sin\left(\epsilon_{ir} - \epsilon_{jr}\right) dl \\ P_{ij}^{+} &= -\frac{1}{4}\rho g \oint_{WL} \zeta_{ir} \zeta_{jr} \cos\left(\epsilon_{ir} + \epsilon_{jr}\right) dl \\ Q_{ij}^{+} &= +\frac{1}{4}\rho g \oint_{WL} \zeta_{ir} \zeta_{jr} \sin\left(\epsilon_{ir} + \epsilon_{jr}\right) dl \end{aligned} \tag{A.21}$$

P and Q are parts of the QTF's of the system in irregular waves, where P are the in-phase and Q the out-of-phase parts. P^{-} and Q^{-} are the in-phase and out-of-phase part of the low frequency part of the square of the incident waves respectively. These QTF parts values can be considered as the most important ones, since these are related to the low frequency wave drift force resulting in the large low frequency surge motions. Since P_{ij} and Q_{ij} are the in-phase and out-of-phase part of the QTF, the amplitude of the QTF is $|T(\omega_i, \omega_j)| = \sqrt{P(\omega_i, \omega_j)^2 + Q(\omega_i, \omega_j)^2}$. The low-frequency part of the QTF is often described in terms of μ, where $\omega_i - \omega_j = \mu$. Applying this, the amplitude of the QTF is written as:

$$|T(\omega + \mu, \omega)| = \sqrt{P(\omega + \mu, \omega)^2 + Q(\omega + \mu, \omega_j)^2} \tag{A.22}$$

A.4. Derivation of the mean surge wave drift damping in irregular waves

In this section the surge wave drift damping is estimated using the heuristic approach first introduced by Clark *et al.* and Aranha. This heuristic formula can be used for estimation of the damping quadratic transfer function, or wave drift damping coefficient $B(\omega)$ in deep water if the waves and the speed of the surging vessel are co-linear. Since in this project, head waves and the surge response is analysed, this formula can be applied. However, since the waterdepth at the location analysed is 32.6 m, deep water approximations may result in unreliable surge damping estimations. Therefore, by using the extended formula for finite depth[20], two derivations related to the surge mean wave drift damping are described.

A.4.1. Deep water approximation

Since the second order wave drift forces on the hull of a vessel are dependent on the its speed U, they can be written as a Taylor expansion[20]:

$$F_{wave}^{(2)}(U,\omega) = F_{wave}^{(2)}(0,\omega) + \frac{\partial F_{wave}^{(2)}}{\partial \omega} U + O(U^2) \tag{A.23}$$

Where the first term $F_{wave}^{(2)}(0,\omega)$ is the wave drift force at zero speed and the term $\frac{\partial F_{wave}^{(2)}}{\partial \omega}$ can be considered as a damping term $B(\omega)$. Now the Taylor expansion can be written as[15]:

$$F_{wave}^{(2)}(U,\omega) = F_{wave}^{(2)}(0,\omega) + B(\omega)U + O(U^2) \tag{A.24}$$

By applying the heuristic approach introduced by Clark *et al.* and Aranha, the wave drift damping coefficient $B(\omega)$ can be written as:

$$B(\omega) = \frac{\partial F_{wave}^{(2)}(\omega)}{\partial U} = -\frac{4\omega}{g} F_{wave}^{(2)}(\omega) - \frac{\omega^2}{g}\frac{\partial F_{wave}^{(2)}}{\partial \omega} \tag{A.25}$$

By substitution Equation A.25 into the formula of the mean wave drift damping estimation results in:

$$\begin{aligned} \overline{b_1} &= 2\int_0^\infty S_\zeta(\omega) B(\omega) d\omega \\ \overline{b_1} &= -2\int_0^\infty S_\zeta(\omega)\left(\frac{4\omega}{g} F_{wave}^{(2)}(\omega) + \frac{\omega^2}{g}\frac{\partial F_{wave}^{(2)}}{\partial \omega}\right) d\omega \end{aligned} \tag{A.26}$$

Now, by splitting the integral up in two parts and by partial integration of the second integral, the surge mean wave drift damping becomes:

$$\begin{aligned} \overline{b_1} &= -2\left(\int_0^\infty S_\zeta(\omega)\frac{4\omega}{g} F_{wave}^{(2)}(\omega) d\omega + \int_0^\infty S_\zeta(\omega)\frac{\omega^2}{g}\frac{\partial F_{wave}^{(2)}}{\partial \omega} d\omega\right) \\ \overline{b_1} &= -2\left(\int_0^\infty S_\zeta(\omega)\frac{4\omega}{g} F_{wave}^{(2)}(\omega) d\omega + \left(S_\zeta(\omega)\frac{\omega^2}{g} F_{wave}^{(2)}(\omega)\right|_0^\infty - \right. \\ &\quad \left.\int_0^\infty \left(\frac{dS_\zeta}{d\omega}\frac{\omega^2}{g} + \frac{2\omega}{g} S_\zeta(\omega)\right)\left(\int_0^\infty \frac{\partial F_{wave}^{(2)}}{\partial \omega} d\omega\right) d\omega\right)\right) \\ \overline{b_1} &= -2\left(\int_0^\infty S_\zeta(\omega)\frac{4\omega}{g} F_{wave}^{(2)}(\omega) d\omega + \left(S_\zeta(\omega)\frac{\omega^2}{g} F_{wave}^{(2)}(\omega)\right|_0^\infty - \right. \\ &\quad \left.\int_0^\infty \left(\frac{dS_\zeta}{d\omega}\frac{\omega^2}{g} + \frac{2\omega}{g} S_\zeta(\omega)\right) F_{wave}^{(2)}(\omega) d\omega\right)\right) \\ \overline{b_1} &= -2\int_0^\infty \left(\frac{2\omega}{g} S_\zeta(\omega) - \frac{\omega^2}{g}\frac{dS_\zeta}{d\omega}\right) F_{wave}^{(2)}(\omega) d\omega \end{aligned} \tag{A.27}$$

Where

$$S_\zeta(\omega)\frac{\omega^2}{g}F_{wave}^{(2)}\Big|_0^\infty = 0 \tag{A.28}$$

Since the wave spectrum $S_\zeta(\omega)$ is approximately zero at both $\omega = 0$ and $\omega = \infty$ as can be seen in Figure C.5. As can be seen, the surge mean wave drift damping can now be fully described by the wave spectrum $S_\zeta(\omega)$ and a force term $F_{wave}^{(2)}$. Since the mean part of the wave drift damping has to be calculated and to agree with the units of damping, the force term can be replace by the mean wave drift coefficient $P(\omega,\omega)$ resulting in the final form of the surge mean wave drift damping estimation:

$$\overline{b_1} = -2\int_0^\infty \left(\frac{2\omega}{g}S_\zeta(\omega) - \frac{\omega^2}{g}\frac{dS_\zeta}{d\omega}\right)P(\omega,\omega)d\omega \tag{A.29}$$

A.4.2. Finite depth approximation

The useful Equation A.25 was extended to be used in finite depth by implementing the drift velocity in the horizontal plane $U(X',Y')$ caused by monochromatic waves under an angle β. The expression of the surge damping quadratic transfer function $B_{xx}(\omega,\beta)$ in finite depth d and waves (ω,β) can be written as[20]:

$$B_{xx}(\omega,\beta) = \frac{\partial F_{wave}^{(2)}}{\partial X'} = \left(-\frac{2\kappa}{C_g}F_{wave}^{(2)}(\omega) - k\frac{\partial F_{wave}^{(2)}}{\partial\omega}\right)\cos\beta + \frac{1}{C_g}\frac{\partial F_{wave}^{(2)}(\omega)}{\partial\beta}\sin\beta \tag{A.30}$$

With $\kappa(\omega)$, a factor, described by Trassoudaine and Naciri, wavenumber $k(\omega)$[21] and the group velocity $C_g(\omega)$[22] given by:

$$\begin{aligned}
k(\omega) &= \frac{\omega^2}{g}\left(1 - e^{-\left(\sqrt{\frac{\omega^2 d}{g}}\right)^{\frac{5}{2}}}\right)^{-\frac{2}{5}} \\
C_g(\omega) &= \frac{1}{2}\frac{\omega}{k(\omega)}\left(1 + \frac{2k(\omega)d}{\sinh 2k(\omega)d}\right) \\
\kappa(\omega) &= 1 - \left(\frac{\omega}{2}\frac{\partial}{\partial\omega}\frac{C_g}{C}\right) = 1 - \left(\frac{\omega}{2}\frac{\partial n}{\partial\omega}\right) \\
n(\omega) &= \frac{C_g}{C}(\omega) = \frac{1}{2}\left(1 + \frac{2k(\omega)d}{\sinh 2k(\omega)d}\right)
\end{aligned} \tag{A.31}$$

Where $n(\omega)$ is the ratio between the group velocity $C_g(\omega)$ and phase velocity $C(\omega)$.
By substituting Equation A.30 with $\beta = 0°$ (co-linear with the drift velocity in our case) into the formula of the mean wave drift damping estimation results in:

$$\begin{aligned}
\overline{b_1} &= 2\int_0^\infty S_\zeta(\omega)B_{xx}(\omega,0)d\omega \\
\overline{b_1} &= -2\int_0^\infty S_\zeta(\omega)\left(\frac{2\kappa(\omega)}{C_g(\omega)}F_{wave}^{(2)}(\omega) + k(\omega)\frac{\partial F_{wave}^{(2)}}{\partial\omega}\right)d\omega
\end{aligned} \tag{A.32}$$

Now, by splitting the integral up in two parts and by partial integration of the second integral, the surge mean wave drift damping becomes:

$$\overline{b_1} = -2\left(\int_0^\infty S_\zeta(\omega)\frac{2\kappa(\omega)}{C_g(\omega)}F_{wave}^{(2)}(\omega)d\omega + \int_0^\infty S_\zeta(\omega)k(\omega)\frac{\partial F_{wave}^{(2)}}{\partial\omega}d\omega\right)$$

$$\overline{b_1} = -2\left(\int_0^\infty S_\zeta(\omega)\frac{2\kappa(\omega)}{C_g(\omega)}F_{wave}^{(2)}(\omega)d\omega + \left(S_\zeta(\omega)k(\omega)F_{wave}^{(2)}(\omega)\Big|_0^\infty - \int_0^\infty\left(\frac{dS_\zeta}{d\omega}k(\omega) + \frac{dk}{d\omega}S_\zeta(\omega)\right)\left(\int_0^\infty \frac{\partial F_{wave}^{(2)}}{\partial\omega}d\omega\right)d\omega\right)\right) \tag{A.33}$$

$$\overline{b_1} = -2\left(\int_0^\infty S_\zeta(\omega)\frac{2\kappa(\omega)}{C_g(\omega)}F_{wave}^{(2)}(\omega)d\omega + \left(S_\zeta(\omega)k(\omega)F_{wave}^{(2)}(\omega)\Big|_0^\infty - \int_0^\infty\left(\frac{dS_\zeta}{d\omega}k(\omega) + \frac{dk}{d\omega}S_\zeta(\omega)\right)F_{wave}^{(2)}(\omega)d\omega\right)\right)$$

$$\overline{b_1} = -2\int_0^\infty\left(\frac{2\kappa(\omega)}{C_g(\omega)}S_\zeta(\omega) - \frac{dS_\zeta}{d\omega}k(\omega) + \frac{dk}{d\omega}S_\zeta(\omega)\right)F_{wave}^{(2)}(\omega)d\omega$$

Where again, equal to Equation A.28:

$$S_\zeta(\omega)k(\omega)F_{wave}^{(2)}\Big|_0^\infty = 0 \tag{A.34}$$

By applying the Equations given in A.31 and by computing $\frac{dk}{d\omega}$ and $\frac{dS_\zeta}{d\omega}$, the final form of the mean surge wave drift damping in finite water depth for head waves can, similar to Equation A.29, be written as:

$$\overline{b_1} = -2\int_0^\infty\left(\frac{2\kappa(\omega)}{C_g(\omega)}S_\zeta(\omega) - \frac{dS_\zeta}{d\omega}k(\omega) + \frac{dk}{d\omega}S_\zeta(\omega)\right)P(\omega,\omega)d\omega \tag{A.35}$$

B

Soft Yoke Mooring System (SYMS)

This appendix shows the side and top view of the benchmark mooring system used throughout the project in figure B.1 and B.2 respectively. The corresponding parameters are given in Table B.1.

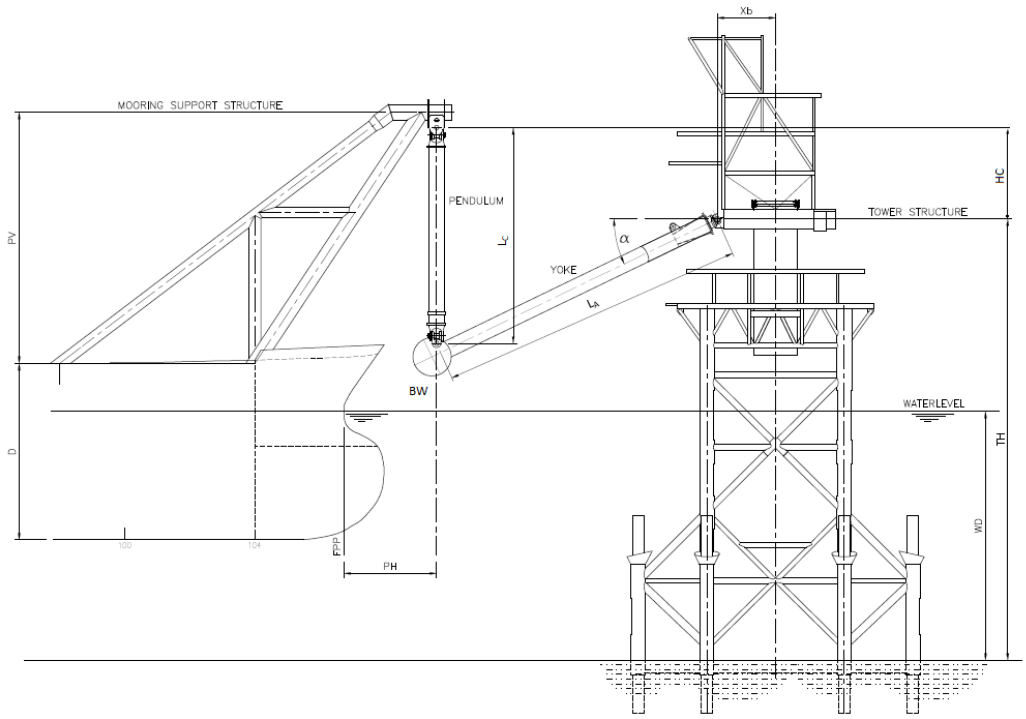

Figure B.1: Side view of the DYTMS [Bluewater Energy Services]

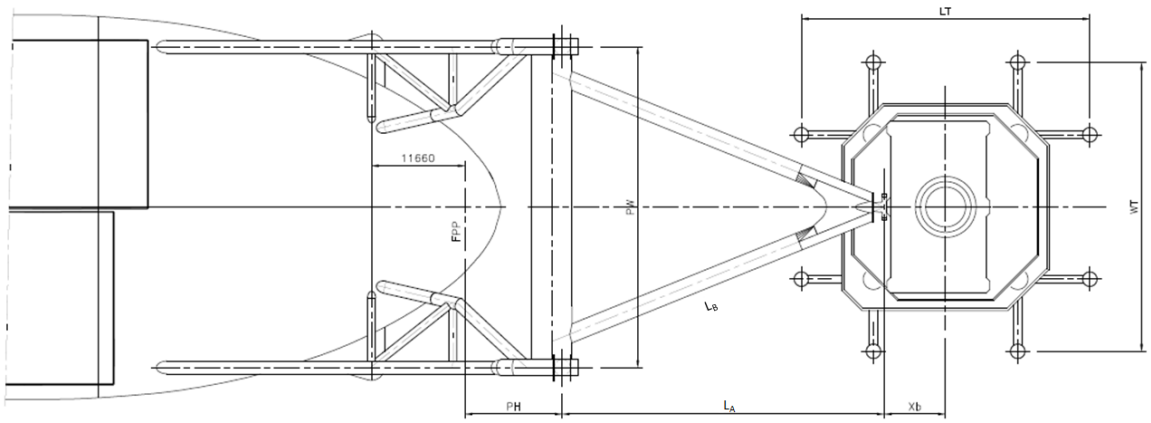

Figure B.2: Top view of the DYTMS [Bluewater Energy Services]

Parameter	Symbol	Unit	Dimension
Pendulum length	L_C	[m]	28.3
Pendulum hinge above deck	PV	[m]	32.9
Pendulum hinge forward of FPP	PH	[m]	12.2
Pendulum width w.r.t. centreline	PW	[m]	20.0
Yoke arm length (side view)	L_A	[m]	40.2
Yoke arm length (along side)	L_B	[m]	44.9
Ballast weight (in air)	BW	[te]	1800
Height yoke connection to tower	TH	[m]	57.8
Tower width	WT	[m]	36.0
Tower length	LT	[m]	36.0
Relative hang-off height	HC (Fully loaded)	[m]	8.78
Relative hang-off height	HC (Ballast)	[m]	15.8
Water depth	WD	[m]	32.6

Table B.1: Benchmark dimensions [Bluewater Energy Services]

C

FPSO and environment

This appendix describes the modelled FPSO properties and analysed extreme environment used in this project. All analyses done in this project are based on these properties. Note that two additional environments are analysed in Chapter 5.

C.1. FPSO properties

The vessel used in this project is the Stena Surprise FPSO. Using diffraction/radiation software Hydrostar, the frequency dependent added mass, potential damping and force QTF values can be estimated for ballast and fully loaded condition. Using model tests, dimensionless directional current and wind coefficients are evaluated. Results of the model tests are shown in Figure C.1. Since the calculations are done for a co-linear environment in head waves (180°), the added mass and potential damping values for this direction per frequency are shown in Figure C.2.
In spectral analysis, the main diagonal, or mean wave drift force coefficient $P(\omega, \omega)$ of the full wave drift force QTF is often used. This frequency and directional dependent force QTF can be calculated by taking $\omega_i = \omega_j$ in Equation A.20 described in Appendix A.3. The main diagonal of the surge force QTF in head waves for ballast and fully loaded condition of the Stena Surprise FPSO is shown in Figure C.3.

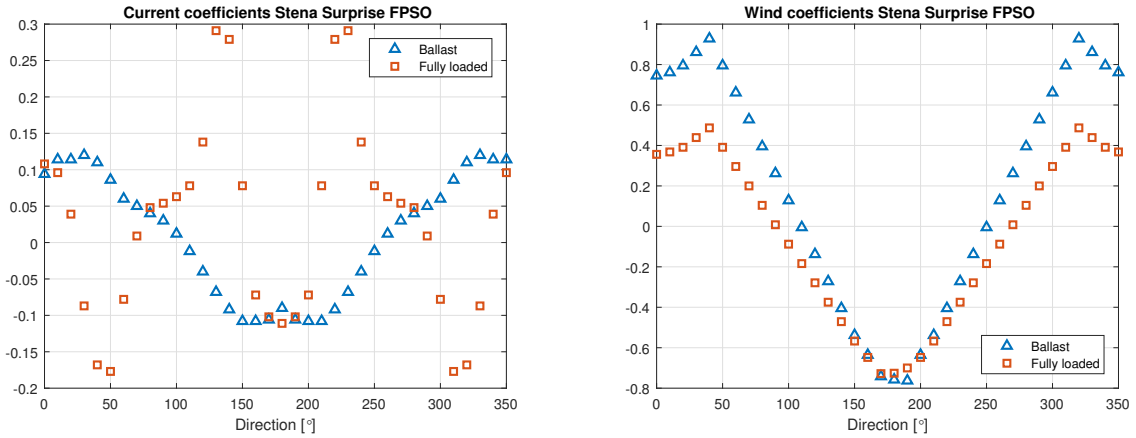

(a) Current coefficients

(b) Wind coefficients

Figure C.1: Directional dependent current and wind coefficients of the Stena Surprise FPSO for two load cases ballast and fully loaded

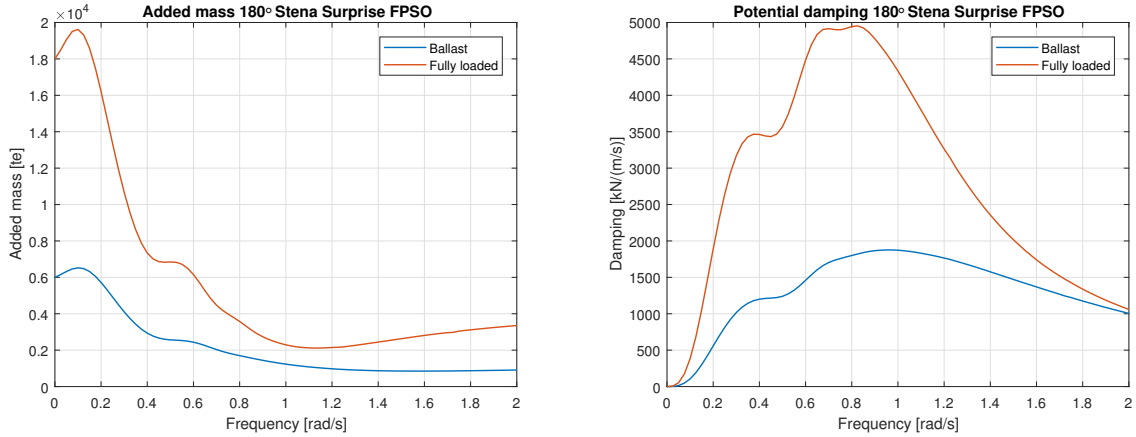

(a) Added mass (b) Potential damping

Figure C.2: Frequency dependent added mass and potential damping (180°) of the Stena Surprise FPSO for two load cases ballast and fully loaded

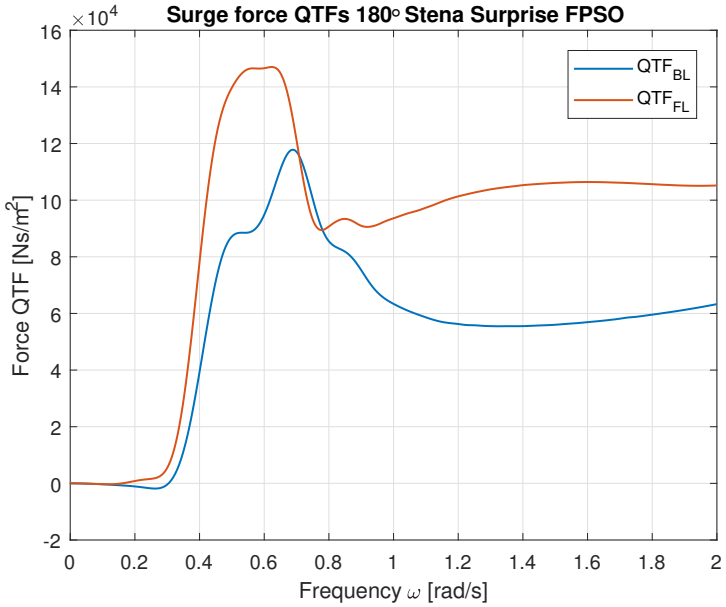

Figure C.3: Main diagonal of the surge force QTF in head waves (180°) of the Stena Surprise FPSO for ballast (BL) and fully loaded (FL) condition

The FPSO properties of the Stena Surprise used in this project are summarized in Table C.1.

Property	**Symbol**	**Unit**	**Ballast**	**Fully loaded**
Length between perpendiculars	L_{pp}	[m]	264.0	
Frontal aerial surface	A_{fa}	[m^2]	2970.02	2631.60
Frontal wetted surface	A_{fw}	[m^2]	2467.61	4323.92
Draft mean	Tm	[m]	9.562	16.578
Displacement mass	M	[te]	94,470	179,529
Current coefficient (180°)	C_c	[-]	-0.9	-0.111
Wind coefficient (180°)	C_w	[-]	-0.758	-0.7

Table C.1: Stena Surprise FPSO properties

C.2. Environment

The extreme co-linear environment analysed in this project is obtained from hindcast data for the Miztón field located in the Gulf of Mexico. The water depth at this location is 32.6 m. The modelled environment, including waves wind and current is discussed below.

C.2.1. Waves

The response of a system in irregular waves can be calculated if the distribution of the wave energy over the wave frequencies ω is known. This wave energy distribution, often called a wave spectrum $S_\zeta(\omega)$, describes the irregular wave history with a significant wave height H_s and peak period T_p. These are statistical values for the mean of the highest one-third of waves and period in a wave record respectively. The spectrum used in this project is the JONSWAP spectrum, which is a modified Pierson–Moskowitz spectrum by multiplying the Pierson-Moskowitz spectrum with a certain peak enhancement formula $G(\gamma, \omega)$. This peak enhancement formula is characterized by use of the peak enhancement factor γ[22]:

$$G(\gamma,\omega) = \gamma^{e^{\left(-\frac{\left(\frac{\omega}{\omega_p}-1\right)^2}{2\sigma\left(\omega,\omega_p\right)^2}\right)}} \tag{C.1}$$

Where $\omega_p = \frac{2\pi}{T_p}$ and $\sigma(\omega, \omega_p)$ the peak-width parameter which is given as:

$$\begin{aligned}\sigma\left(\omega,\omega_p\right) &= \sigma\left(\omega \le \omega_p\right) = 0.07\\ \sigma\left(\omega,\omega_p\right) &= \sigma\left(\omega > \omega_p\right) = 0.09\end{aligned} \tag{C.2}$$

Using the normalising constant $C(\gamma, T_p)$, the JONSWAP spectrum can be described by:

$$S_\zeta(\omega) = \frac{C\left(\gamma,T_p\right) H_s^2 G\left(\gamma,\omega\right) e^{\left(\frac{5}{4\left(\frac{\omega}{\omega_p}\right)^4}\right)}}{\left(\frac{\omega}{\omega_p}\right)^5} \tag{C.3}$$

Where the normalising constant is given by:

$$C(\gamma,T_p) = \frac{5}{\frac{16}{T_p}\left(1.15 + 0.168\gamma - \frac{0.925}{1.909+\gamma}\right)2\pi} \tag{C.4}$$

Note that when $\gamma = 1$ the Pierson-Moskowitz spectrum is created.

In this project, H_s and T_p are defined using hindcast H_s-T_p curves. These curves include return periods T_y which indicate the probabilty that a certain H_s-T_p combination will be exceeded in one year. Thus, a ten-year return period T_{10} will have a probability 1/10 to be exceeded in one year. The H_s-T_p curves for the Miztón field is given in Figure C.4. The chosen H_s-T_p combination for this project is defined between T_{50} and T_{100} and depicted in the red circle shown in Figure C.4. By using the values of H_s, T_p and the corresponding γ, the JONSWAP spectrum used is given in Figure C.5.

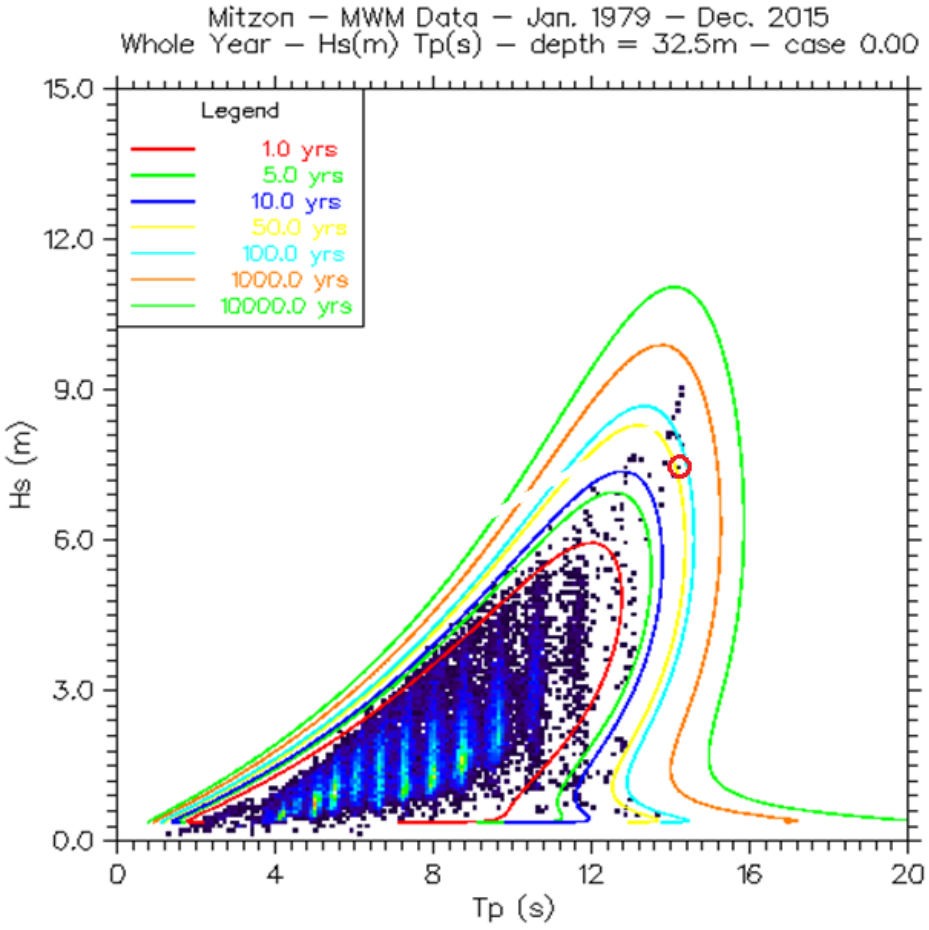

Figure C.4: H_s-T_p curves for the Miztón field [Bluewater Energy Services]

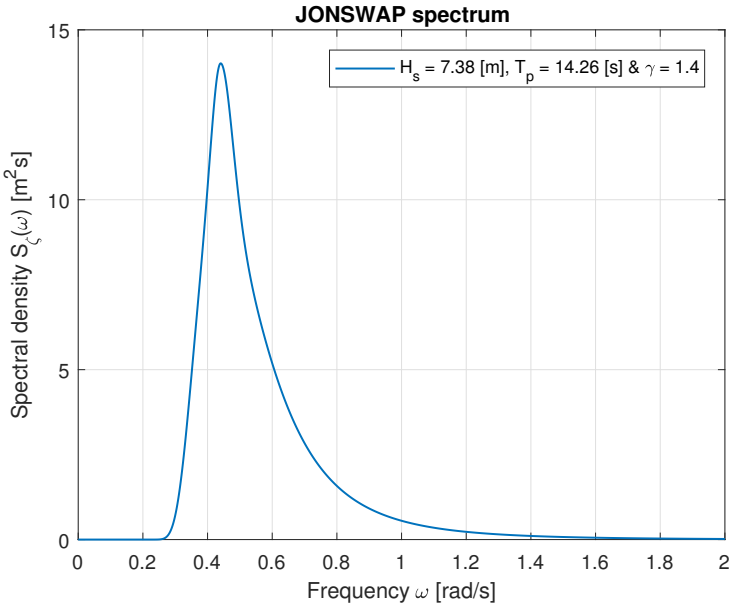

Figure C.5: Used JONSWAP spectrum

C.2.2. Current

The current condition is defined by a constant current speed over depth coming from the environmental direction 180°. The analysed current speed V_c for the Miztón field is defined at 0.35 m/s. The density of sea water ρ_{sea} used is 1025 kg/m^3.

C.2.3. Wind

The wind condition is defined, same as the current condition, by a constant wind speed over height coming from the environmental direction 180°. The analysed wind speed V_w for the Miztón field is defined at 19.11 m/s. The density of air ρ_{air} used is 1.3 kg/m^3.

The analysed extreme co-linear environment is summarized in Table C.2.

Property	**Symbol**	**Unit**	**Value**
Significant wave height	H_s	[m]	7.38
Peak period	T_p	[s]	14.26
Peak enhancement factor	γ	[-]	1.4
Current speed	V_c	[m/s]	0.35
Wind speed	V_w	[m/s]	19.11
Air density	ρ_{air}	[kg/m^3]	1.3
Sea water density	ρ_{sea}	[kg/m^3]	1025
Waterdepth	d	[m]	32.6

Table C.2: Analysed extreme co-linear environment

D

Model calculations

This appendix describes the steps and equations used to calculate the MPM surge response in the Rayleigh and OrcaFlex model. It also describes the steps and equations used to calculate the maximum amplitude of the surge motion for the Harmonic Balance Method.

D.1. Rayleigh model calculations

Same as Section 3.3, the appendix consists of five sections including the used equations to estimate the surge response of the analysed system.

D.1.1. Mean environmental force

The mean environmental surge force $\overline{F_{1e}}$ is calculated by the summation of the mean wave drift force $\overline{F_{1wave}^{(2)}}$, mean wind force $\overline{F_{1wind}}$ and mean current force $\overline{F_{1current}}$:

$$\overline{F_{1e}} = \overline{F_{1wave}^{(2)}} + \overline{F_{1wind}} + \overline{F_{1current}} \tag{D.1}$$

Where

$$\begin{aligned} \overline{F_{1current}} &= \frac{1}{2} C_c \rho_{sea} V_c^2 A_{fw} \\ \overline{F_{1wind}} &= \frac{1}{2} C_w \rho_{air} V_w^2 A_{fa} \\ \overline{F_{1wave}^{(2)}} &= 2 \int_0^\infty S_\zeta(\omega) P(\omega, \omega) d\omega \end{aligned} \tag{D.2}$$

The mean current and wind forces are calculated using the dimensionless coefficients C, velocity V, density of the medium ρ and the frontal area A. For the values, please refer to Table D.1 at the end of the section. The mean wave drift force is calculated using the wave spectral density $S_\zeta(\omega)$ and main diagonal of the wave drift force QTF $P(\omega, \omega)$. By finding the intersection point on the load-excursion curve between the mean environmental force and the excursion, the mean excursion $\overline{x_1}$ is estimated.

D.1.2. Mooring stiffness approximation

By calculating the mean environmental forces for ballast and fully loaded condition of the vessel, the load-excursion curves can be used to find the mean displacement. By calculating the gradient of the curve a small step left and right with respect to the mean displacement in MATLAB, the stiffness of the

mooring system c_m at the mean surge excursion $\overline{x_1(i)}$ at index i is estimated using:

$$\begin{aligned}\frac{dF_m}{d\overline{x_1}_{(i-1)}} &= \frac{F_{m(\overline{x_1}=i)} - F_{m(\overline{x_1}=i-1)}}{\overline{x_1}_{(i)} - \overline{x_1}_{(i-1)}} \\ \frac{dF_m}{d\overline{x_1}_{(i+1)}} &= \frac{F_{m(\overline{x_1}=i+1)} - F_{m(\overline{x_1}=i)}}{\overline{x_1}_{(i+1)} - \overline{x_1}_{(i)}} \\ \frac{dF_m}{d\overline{x_1}_{(i)}} &= \frac{\frac{dF_m}{d\overline{x_1}_{(i-1)}} + \frac{dF_m}{d\overline{x_1}_{(i+1)}}}{2} = c_{1m}\end{aligned} \tag{D.3}$$

D.1.3. Added mass and damping estimation

Now the stiffness of the mooring system is estimated by linearizing the non-linear restoring mooring force, the vessels added mass and damping can be approximated. As described in Section 3.3.3, the frequency dependent added mass and potential damping can be considered constant and estimated at $\omega \approx 0$ (Figure C.2). Since the potential damping is neglected, the total damping term in surge direction can be considered constant and consist of still water damping b_{11} and mean wave drift damping $\overline{b_1}$ only:

$$b_{tot} = b_{11} + \overline{b_1} \tag{D.4}$$

In many SPM offshore applications, according to Bureau Veritas (BV), the still water damping b_{11} is estimated using the mass M and length between perpendiculars L_{pp} of the vessel[23]:

$$b_{11} = 3.7E^{-3}M\sqrt{\frac{g}{L_{pp}}} \tag{D.5}$$

The mean wave drift damping $\overline{b_1}$ can be calculated in the frequency domain according to:

$$\overline{b_1} = 2\int_0^\infty S_\zeta(\omega)B(\omega)d\omega \tag{D.6}$$

Where $B(\omega)$ is the mean wave drift coefficient and $S_\zeta(\omega)$ the wave spectral density. However, first an estimation of the mean wave drift damping coefficient has to be made. According to Aranha and Clark *et al.*, the mean wave drift coefficient for deep water in head waves can be written as the derivative of the second order wave drift force over the drift velocity U, since the second order wave drift force is dependent on the drift velocity:

$$B(\omega) = \frac{\partial F_{wave}^2}{\partial U} = -\frac{4\omega}{g}F_{wave}^2 - \frac{\omega^2}{g}\frac{\partial F_{wave}^2}{\partial \omega} \tag{D.7}$$

Substituting Equation D.7 in Equation D.6 results after some rewriting in:

$$\overline{b_1} = -2\int_0^\infty \left(\frac{2\omega}{g}S_\zeta(\omega) - \frac{\omega^2}{g}\frac{dS_\zeta(\omega)}{d\omega}\right)P(\omega,\omega)d\omega \tag{D.8}$$

The derivation of the mean wave drift damping $\overline{b_1}$ is described in more detail in Appendix A.4.1
To check if deep water approximation can be made, the rule of thumb for deep water approximations $kd >> 1$ is applied, where kd is the wave number k times the waterdepth d. Using a factor α, kd can be estimated as[24]:

$$kd \approx \alpha\,(\tanh\alpha)^{\frac{1}{2}} \tag{D.9}$$

Where α can be estimated using the peak frequency $\omega_p \approx 0.44\ \frac{rad}{s}$ corresponding to the wave spectrum shown in Figure C.5 and the waterdepth d:

$$\alpha \approx \frac{\omega_p^2 d}{g} \tag{D.10}$$

Applying Equations D.9 and D.10 with the waterdepth given in Table C.2, it shows that $kd >> 1$ can not be met and no deep water approximations can be made. Therefore, the estimation of the deep water mean wave drift damping is questionable. In Appendix A.4.2, an estimation of the mean wave drift damping for finite water depth is derived as well and is given as:

$$\overline{b_{1_{finite}}} = 2\int_0^\infty \left(\frac{2\kappa(\omega)}{C_g(\omega)}S_\zeta(\omega) - \frac{dS_\zeta}{d\omega}k(\omega) + \frac{dk}{d\omega}S_\zeta(\omega)\right)P(\omega,\omega)d\omega \tag{D.11}$$

Where κ, C_g and k are a factor, the group velocity and the wavenumber respectively.
For first estimates, the deep water wave drift damping estimation is applied and changed to the finite approximation when required.

D.1.4. Rayleigh parameter estimation

Using the constant added mass, damping and stiffness parameters estimated in the sections above, the standard deviation of the surge response σ_{x1} or the Rayleigh parameter can be calculated.
The JONSWAP spectrum $S_\zeta(\omega)$ gives information on the distribution of the wave energy over different wave frequencies ω related to the wave elevation. However, in the analyses of low frequency motions of moored vessels, the spectral energy density of the square of the wave elevation over the low frequency part of the wave frequencies $\omega_i - \omega_j$ is of greater interest, since the second order wave forces are related to the square of the wave elevation. The low frequency part of the second order wave drift force results from simplifying Equation A.20:

$$\begin{aligned} F^{(2)} = &\sum_i\sum_j \zeta_i\zeta_j P_{ij}\cos\Big(\big(\omega_i-\omega_j\big)t + \big(\epsilon_i-\epsilon_j\big)\Big) + \\ &\sum_i\sum_j \zeta_i\zeta_j Q_{ij}\sin\Big(\big(\omega_i-\omega_j\big)t + \big(\epsilon_i-\epsilon_j\big)\Big) \end{aligned} \tag{D.12}$$

If it is assumed that the wave elevations are normally distributed, the spectral density (S_g) of the low frequency part (μ) of the square of the wave elevation (ζ^2), can be written by using the spectral density of the wave elevation S_ζ[5]:

$$S_g(\mu) = 8\int_0^\infty S_\zeta(\omega)S_\zeta(\omega+\mu)d\omega \tag{D.13}$$

$S_g(\mu)$ is often called, the low frequency group spectrum of the square of the wave record, since it says something about wave groups of $\omega_i - \omega_j = \mu$. The low frequency group spectrum corresponding to the JONSWAP spectrum shown in Figure C.5 is depicted in Figure D.1
Now the waves can be modelled using a wave spectrum, the wave forces on the FPSO can be calculated using the wave drift force QTF values described in Appendix A.3. Using the spectral density of the wave elevation S_ζ, the low frequency part of the drift force spectrum $S_F(\mu)$ can be calculated using:

$$S_F(\mu) = 8\int_0^\infty S_\zeta(\omega)S_\zeta(\omega+\mu)|T(\omega+\mu,\omega)|^2 d\omega \tag{D.14}$$

Where $|T(\omega+\mu,\omega)|$ is the amplitude the low frequency part of the QTF described in Appendix A.3. Using the in-phase and out-of-phase parts of the wave drift force QTF, the low frequency wave drift force spectrum can be written as:

$$S_F(\mu) = 8\int_0^\infty S_\zeta(\omega)S_\zeta(\omega+\mu)P(\omega+\mu,\omega)^2 d\omega + 8\int_0^\infty S_\zeta(\omega)S_\zeta(\omega+\mu)Q(\omega+\mu,\omega)^2 d\omega \tag{D.15}$$

However, the low frequency part of the full wave drift QTF $|T(\omega+\mu,\omega)|$ may be described by the Newman approximation consisting of the 'diagonal' values only[17]. These diagonal values consists of wave pairs with equal direction and equal phase. Applying Newman's approximation, the off-diagonal terms $Q(\omega+\mu,\omega)$ are described by an average of the diagonal terms $P(\omega+\mu,\omega)$ for those directions and periods. This reduces the calculation time significantly. Using Newman's approximation, Equation D.14 becomes:

$$S_F(\mu) = 8\int_0^\infty S_\zeta(\omega)S_\zeta(\omega+\mu)P\left(\omega+\frac{\mu}{2},\omega\right)^2 d\omega \tag{D.16}$$

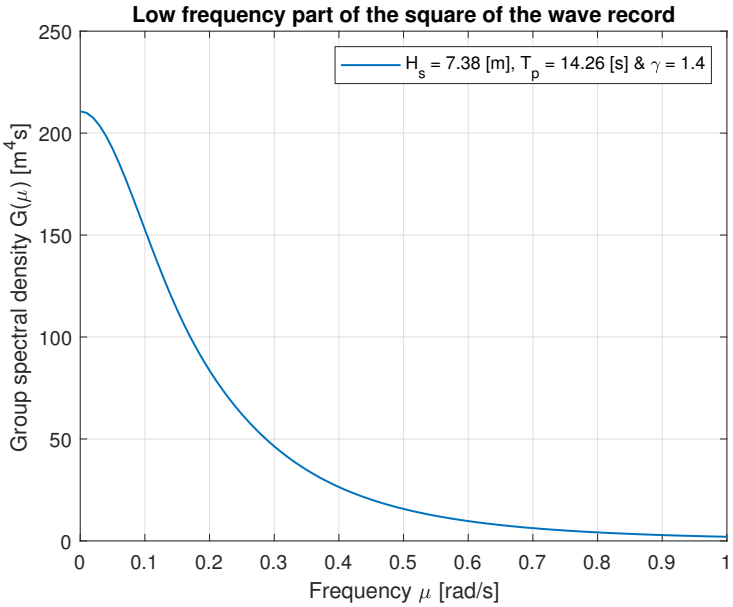

Figure D.1: The low frequency wave group spectrum of the square of the wave height

The low frequency wave drift force spectrum, corresponding to the main diagonal wave drift QTF from Figure C.3 and group spectrum from Figure D.1 is shown in Figure D.2.

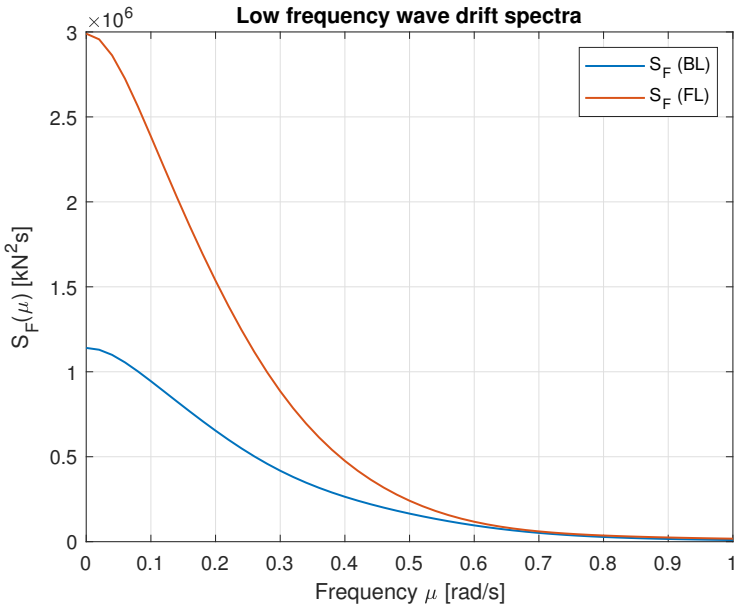

Figure D.2: The low frequency part of the wave drift force spectrum for ballast and fully loaded condition

Using the low frequency part of the wave drift force spectrum $S_F(\mu)$, the variance of the surge response spectrum related to this force spectrum can be calculated in the frequency domain using the motion RAO $\frac{x_{a1}}{F_{a1}}$. By rewriting the EoM in the frequency domain, shown in Equation 3.16, the motion RAO can be found. Since it is expected that the surge excitation will be close to the natural frequency of the FPSO, the wave frequency ω is replaced by the natural surge frequency ω_{1n}. The variance of the low

frequent surge response spectrum can now be written as:

$$\sigma_{x_1}^2 = \int_0^\infty \left|\frac{x_{a_1}}{F_{a_1}}\right|^2 S_F(\mu)d\mu \quad = \quad \int_0^\infty \frac{1}{(c_{1m} - (M + a_{11})\omega_{1n}^2)^2 + (b_{11} + \overline{b_1})^2\omega_{1n}^2} S_F(\mu)d\mu \tag{D.17}$$

Since the system has low damping, and the natural surge frequency of the moored FPSO is close to zero, the spectral density of the low frequency wave drift force can be estimated at $S_F(0)$, resulting in a constant value. By substitution of the natural surge frequency $\sqrt{\frac{M+a_{11}}{c_{1m}}}$ in Equation D.17 and after some rewriting, the variance of the surge response can be estimated by:

$$\sigma_{x_1}^2 = \frac{\pi}{2(b_{11} + \overline{b_1})c_{1m}} S_F(0) \tag{D.18}$$

Where after substitution of $\mu = 0$ in Equation D.16, $S_F(0)$ becomes:

$$S_F(0) = 8\int_0^\infty S_\zeta^2(\omega)P(\omega,\omega)^2 d\omega \tag{D.19}$$

$P(\omega,\omega)$ is often referred to as the mean wave drift coefficient. The mean wave drift force coefficient can be calculated by taking $\omega_i = \omega_j$ in Equation D.12 resulting in:

$$P(\omega,\omega) = \frac{F_{1wave}}{\zeta_a^2}(\omega) \tag{D.20}$$

The mean wave drift force coefficient in head waves for ballast and fully loaded condition of the FPSO is shown in Figure C.3.
The next step is to estimate the number of resonant surge oscillations (N) by dividing the total storm duration (T) by the natural surge period (T_{1n}) of the moored FPSO as:

$$N = \frac{T}{T_n} = \frac{T}{2\pi\sqrt{\frac{M+a_{11}}{c_{11}}}} \tag{D.21}$$

When it is assumed that the wave elevations are normally distributed and excursion peaks Rayleigh distributed, the most probable maximum surge excursion can be calculated using:

$$x_{MPM} = \overline{x_1} + \sigma_{x_1}\sqrt{2\ln N} \tag{D.22}$$

The calculation MPM surge excursion is based on the low frequent motion only. A correction is applied to include the significant high frequent motion $\overline{x_{1a_s}}$ as well. Although, the significant surge amplitude can be considered small compared to the low frequent motions it is included to make the surge response estimation as reliable as possible. To calculate significant surge amplitude, the surge motion RAO $\frac{x_1}{\zeta_a}$ is needed that is obtained from Hydrostar. The derivation of the motion RAO in regular waves is described in Appendix A.2.
First the surge response spectrum can be found using the motion RAO and wave spectrum:

$$S_{x_1}(\omega) = \left|\frac{x_1}{\zeta_a}\right|^2 S_\zeta(\omega) \tag{D.23}$$

The significant surge amplitude is defined by:

$$\overline{x_{1a_s}} = 2\sqrt{m_0} \tag{D.24}$$

Where m_0 is the zero order spectral moment of the surge response spectrum given as:

$$m_0 = \int_0^\infty S_{x_1}(\omega)d\omega \tag{D.25}$$

The most probable maximum surge excursion with the corrected high frequency surge motion included can be written as:

$$x_{MPM} = \overline{x_1} + \sigma_{x_1}\sqrt{2\ln N} + \overline{x_{1a_s}} \tag{D.26}$$

D.1.5. Stiffness adjustment by energy correction

Using the method of stiffness adjustment, it is assumed that potential over- or underestimations of the surge excursion are revised. Released and absorbed energy of the system can be calculated by determining the area under the load excursion curve measured from the mean excursion $\overline{x_1}$. Absorbed energy J is defined away from the tower, from $\overline{x_1}$ to negative excursion. Released energy is defined towards the tower, from $\overline{x_1}$ to positive excursion.
Recall Figure 3.8, the load-excursion curve $F_{Ax}(x)$ and linear mooring force $c_m(x)$ are described by defining an excursion vector $x(i)$ with index i. The calculated mean and MPM surge excursion by Equation D.26 is referred to as $\overline{x}$ and $\pm x_{old}$ respectively. The corresponding index is referred to as $i_{\overline{x}}$ and $\pm i_{x_{old}}$.
Since the linear stiffness of the mooring system is used to calculated the MPM surge excursion and the non-linear mooring force to estimate the restoring mooring force, it is expected that an significant error is implemented. To correct for this error, the first step is to calculate the difference in energy J_{diff} between the non-linear and linear mooring force.

$$\begin{aligned} J^{+}_{diff} &= J\left(F_{Ax}\left(i_{\overline{x}} \cdots -i_{x_{old}}\right)\right) - J\left(c_m\left(i_{\overline{x}} \cdots -i_{x_{old}}\right)\right) \\ J^{-}_{diff} &= J\left(F_{Ax}\left(i_{\overline{x}} \cdots +i_{x_{old}}\right)\right) - J\left(c_m\left(i_{\overline{x}} \cdots +i_{x_{old}}\right)\right) \end{aligned} \tag{D.27}$$

J_{diff} is depicted in Figure 3.8 by the blue area. Based on the sign of the energy difference, the restoring mooring force will be over- or underestimated and should be adjusted. To adjust for this energy difference, the index $i_{x_{new}}$ is found where $J^{\pm}_{diff}$ is equal to the absorption or release of energy of the non-linear system:

$$\begin{aligned} J^{+}_{diff} &= J\left(F_{Ax}\left(i_{\overline{x}} \cdots -i_{x_{old}}\right)\right) - J\left(c_m\left(i_{\overline{x}} \cdots -i_{x_{old}}\right)\right) &&= J\left(F_{Ax}\left(i_{\overline{x}} \cdots -i_{x_{new}}\right)\right) \\ J^{-}_{diff} &= J\left(F_{Ax}\left(i_{\overline{x}} \cdots +i_{x_{old}}\right)\right) - J\left(c_m\left(i_{\overline{x}} \cdots +i_{x_{old}}\right)\right) &&= J\left(F_{Ax}\left(i_{\overline{x}} \cdots +i_{x_{new}}\right)\right) \end{aligned} \tag{D.28}$$

$i_{x_{new}}$ is found by using MATLAB software. Using the adjusted x_{new}, the corrected restoring mooring force is estimated at $i_{x_{new}}$ using the non-linear load-excursion curve. The corrected energy, dependent on the sign, are depicted as red or green areas in Figure 3.8.

The estimated constant added mass and damping values corresponding to the Stena Surprise FPSO used in the models described in this appendix, together with the analysed extreme co-linear environment and benchmark mooring properties are summarized in Table D.1.

Vessel Properties	**Symbol**	**Unit**	**Ballast**	**Fully loaded**
Length between perpendiculars	L_{pp}	[m]	264.0	
Frontal aerial surface	A_{fa}	[m^2]	2970.02	2631.60
Frontal wetted surface	A_{fw}	[m^2]	2467.61	4323.92
Draft mean	Tm	[m]	9.562	16.578
Displacement mass	M	[te]	94,470	179,529
Added mass	a	[te]	6,154	18,495
Current coefficient (180°)	C_c	[-]	-0.9	-0.111
Wind coefficient (180°)	C_w	[-]	-0.758	-0.7
Viscous damping	b_{11}	[kN/(m/s)]	92.094	149.05
Environmental Properties	**Symbol**	**Unit**	**Ballast**	**Fully loaded**
Significant wave height	H_s	[m]	7.38	
Peak period	T_p	[s]	14.26	
Peak enhancement factor	γ	[-]	1.4	
Current speed	V_c	[m/s]	0.35	
Wind speed	V_w	[m/s]	19.11	
Air density	ρ_{air}	[kg/m^3]	1.3	
Sea water density	ρ_{sea}	[kg/m^3]	1025	
Waterdepth	d	[m]	32.6	
deep water mean wave drift damping	$\overline{b_1}$	[kN/(m/s)]	146.12	204.79
finite depth mean wave drift damping	$\overline{b_{1_{finite}}}$	[kN/(m/s)]	268.36	384.14
Mooring Properties (Benchmark)	**Symbol**	**Unit**	**Ballast**	**Fully loaded**
Pendulum length	L_C	[m]	28.3	
Yoke arm length	L_A	[m]	40.2	
Ballast weight	BW	[te]	1800	
Relative hang-off height	HC	[m]	15.80	8.78
Mooring stiffness	c_{1m}	[kN/m]	730.15	696.22

Table D.1: Model parameters

D.2. Harmonic Balance Method

This section contains a detailed calculation description of the maximum amplitude using the Harmonic Balance Method. The analysed equation of motion with 3rd order polynomial fit of the load-excursion curve is given below. The total environmental force F_{1e} is obtained from OrcaFlex and includes wind, wave and current forces:

$$(m + a_{11})\ddot{x}_1(t) + \left(b_{11} + \overline{b_1}\right)\dot{x}_1(t) + k_1 x_1(t) + k_2 x_1^2(t) + k_3 x_1^3(t) = F_{1e}(t) \tag{D.29}$$

By assuming the solution of the equation in the form of a truncated Fourier series with a frequency at the natural surge frequency ω_{1n}:

$$\begin{aligned} x_1(t) &= \hat{f}_c \cos(\omega_{1n} t) + \hat{f}_s \sin(\omega_{1n} t) \\ \dot{x}_1(t) &= -\omega_{1n}\hat{f}_c \sin(\omega_{1n} t) + \omega_{1n}\hat{f}_s \cos(\omega_{1n} t) \\ \ddot{x}_1(t) &= -\omega_{1n}^2\hat{f}_c \cos(\omega_{1n} t) - \omega_{1n}^2\hat{f}_s \sin(\omega_{1n} t) \end{aligned} \tag{D.30}$$

Substitution of the displacement, velocity and acceleration in the equation of motion results in:

$$\begin{aligned} &(m + a_{11})\left(-\omega_{1n}^2\hat{f}_c \cos(\omega_{1n} t) - \omega_{1n}^2\hat{f}_s \sin(\omega_{1n} t)\right) + \left(b_{11} + \overline{b_1}\right)\left(-\omega_{1n}\hat{f}_c \sin(\omega_{1n} t) + \omega_{1n}\hat{f}_s \cos(\omega_{1n} t)\right) + \\ &k_1\left(\hat{f}_c \cos(\omega_{1n} t) + \hat{f}_s \sin(\omega_{1n} t)\right) + k_2\left(\hat{f}_c \cos(\omega_{1n} t) + \hat{f}_s \sin(\omega_{1n} t)\right)^2 + k_3\left(\hat{f}_c \cos(\omega_{1n} t) + \hat{f}_s \sin(\omega_{1n} t)\right)^3 \\ &= F_{1e}(t) \end{aligned} \tag{D.31}$$

By applying Equation 3.24 and 3.25 in MAPLE software, two equations with two unknowns are obtained:

$$\begin{aligned} &\frac{\pi}{\omega_{1n}}\left(\hat{f}_s\omega_{1n}\left(b_{11} + \overline{b_1}\right) - \hat{f}_c\omega_{1n}^2(m + a_{11})\right) + \frac{\pi\hat{f}_c}{4\omega_{1n}}\left(4k_1 + 3k_3\left(\hat{f}_c^2 + \hat{f}_s^2\right)\right) = \frac{1}{N}\int_0^{N\cdot T_{1n}} F_{1e}(t)\cdot\cos(\omega_{1n} t)dt \\ &\frac{\pi}{\omega_{1n}}\left(\hat{f}_c\omega_{1n}\left(b_{11} + \overline{b_1}\right) - \hat{f}_s\omega_{1n}^2(m + a_{11})\right) + \frac{\pi\hat{f}_s}{4\omega_{1n}}\left(4k_1 + 3k_3\left(\hat{f}_s^2 + \hat{f}_c^2\right)\right) = \frac{1}{N}\int_0^{N\cdot T_{1n}} F_{1e}(t)\cdot\sin(\omega_{1n} t)dt \end{aligned} \tag{D.32}$$

Now, the time dependency is disappeared, and the equations can be solved for $\hat{f}_c$ and $\hat{f}_s$. Eventually the maximum amplitude is calculated using $x_{max} = \sqrt{\hat{f}_c^2 + \hat{f}_s^2}$.

Note that this section only includes the estimation of the maximum amplitude for the first harmonic. More harmonics till desired order can be added using Equation 3.21. Applying the second harmonic will result in four equation with four unknown Fourier coefficients and the third harmonic in six equations with six unknown Fourier coefficients. Adding harmonics till harmonic index k, the number of equations and unknown Fourier coefficients will increase with $2k$. Keep in mind that adding more harmonics will increase computational time.

D.3. OrcaFlex model

This section describes the calculation procedure to calculate the MPM, or 37-percentile, value of surge response maxima obtained from OrcaFlex using a Gumbel distribution fit.
The 37-percentile from a Gumbel fit is obtained by fitting a Gumbel CDF to the surge response (x) CDF. The CDF of a Gumbel distribution is defined by:

$$F(x) = e^{-e^{\left(\frac{\alpha - x}{\beta}\right)}} \tag{D.33}$$

The scale parameter β for a Gumbel distribution can be defined by the standard deviation of the maxima σ:

$$\beta = \frac{\sqrt{6}}{\pi}\sigma \tag{D.34}$$

The location parameter α for a Gumbel distribution can be defined by the mean of the maxima μ, the Euler-Mascheroni constant γ and the scale parameter:

$$\alpha = \mu - \gamma\beta = \mu - 0.5772\beta \tag{D.35}$$

Based on the scale and shape parameters, the value corresponding to a certain probability of exceedance can be obtained. For 0.63 probability of exceedance, or the 37-percentile case, the MPM value can be calculated using:

$$x_{MPM} = \alpha - \Big(\beta \ln\big(-\ln 0.37\big)\Big) \tag{D.36}$$

E

Additional design tool & OrcaFlex results

This chapter shows the additional results of the design tool and are compared with results of OrcaFlex. In the same way Figure 4.10, either the pendulum length or hang-off height is kept constant while modifying the other one. Results will be presented for fully loaded and ballast conditions separately for the original analyses environmental condition 1 (EC1) and two additional moderate environments (EC2 & EC3). The results show three bars per set of mooring design parameters, corresponding to three ballast weights. The thickest bar represents the largest ballast weight and the thinnest bar the lowest. Note that the results shown here are calculated with deep water wave drift damping estimation.

E.1. Ballast results (EC1)

The ballast results are given for the design parameters given in Table E.1.

Mooring design parameter	Symbol	Unit	Ballast
Pendulum length	L_C	[m]	25 - 28.3 - 31.6 - 35
Hang-off height	HC	[m]	14 - 19 - 24
Ballast weight	BW	[te]	1600 - 1800 - 2000

Table E.1: Modelled ballast conditions

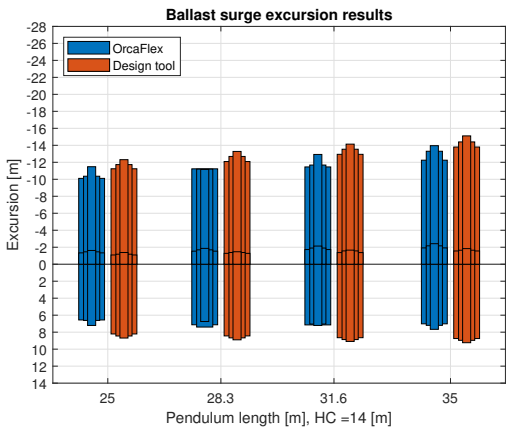

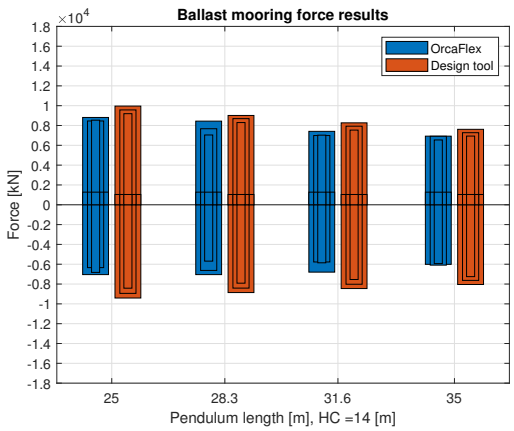

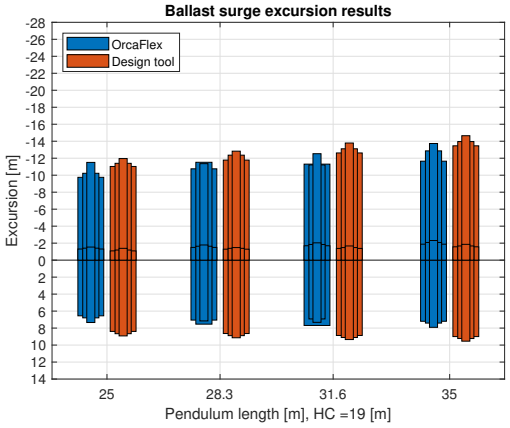
Ballast surge excursion results
OrcaFlex
Design tool
Excursion [m]
-28 -26 -24 -22 -20 -18 -16 -14 -12 -10 -8 -6 -4 -2 0 2 4 6 8 10 12 14
25 28.3 31.6 35
Pendulum length [m], HC =19 [m]

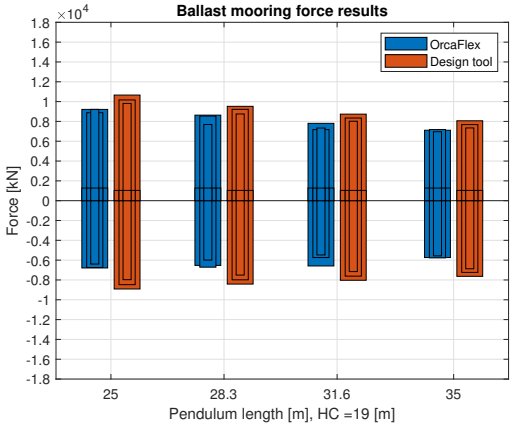
Ballast mooring force results
×10^4
OrcaFlex
Design tool
Force [kN]
1.8 1.6 1.4 1.2 1 0.8 0.6 0.4 0.2 0 -0.2 -0.4 -0.6 -0.8 -1 -1.2 -1.4 -1.6 -1.8
25 28.3 31.6 35
Pendulum length [m], HC =19 [m]

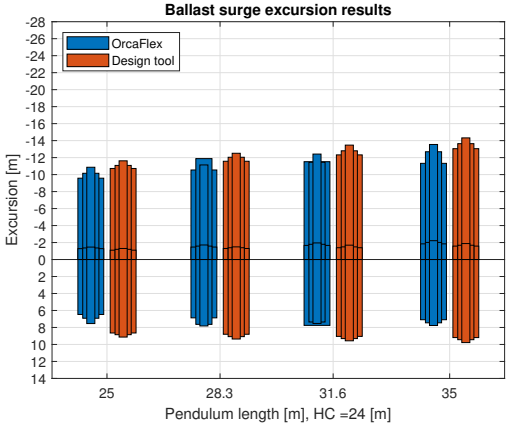
Ballast surge excursion results
OrcaFlex
Design tool
Excursion [m]
-28 -26 -24 -22 -20 -18 -16 -14 -12 -10 -8 -6 -4 -2 0 2 4 6 8 10 12 14
25 28.3 31.6 35
Pendulum length [m], HC =24 [m]

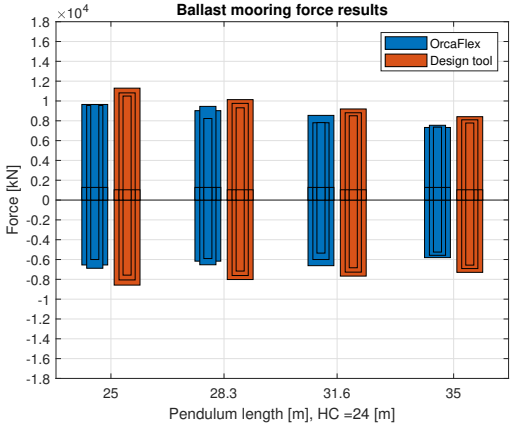
Ballast mooring force results
×10^4
OrcaFlex
Design tool
Force [kN]
1.8 1.6 1.4 1.2 1 0.8 0.6 0.4 0.2 0 -0.2 -0.4 -0.6 -0.8 -1 -1.2 -1.4 -1.6 -1.8
25 28.3 31.6 35
Pendulum length [m], HC =24 [m]

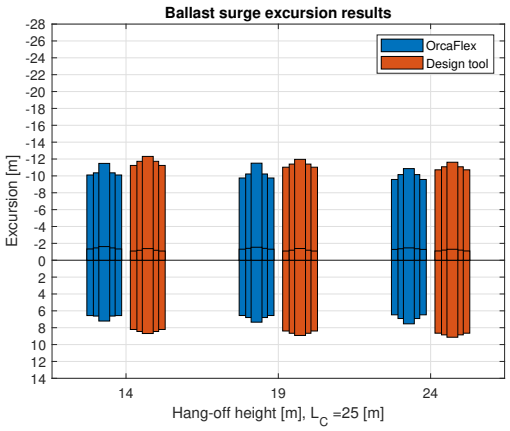
Ballast surge excursion results
OrcaFlex
Design tool
Excursion [m]
-28 -26 -24 -22 -20 -18 -16 -14 -12 -10 -8 -6 -4 -2 0 2 4 6 8 10 12 14
14 19 24
Hang-off height [m], L_C =25 [m]

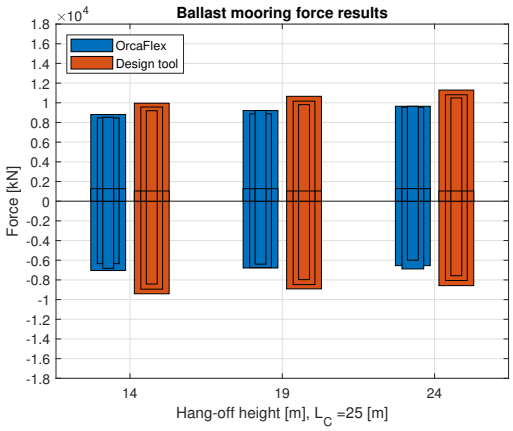
Ballast mooring force results
×10^4
OrcaFlex
Design tool
Force [kN]
1.8 1.6 1.4 1.2 1 0.8 0.6 0.4 0.2 0 -0.2 -0.4 -0.6 -0.8 -1 -1.2 -1.4 -1.6 -1.8
14 19 24
Hang-off height [m], L_C =25 [m]

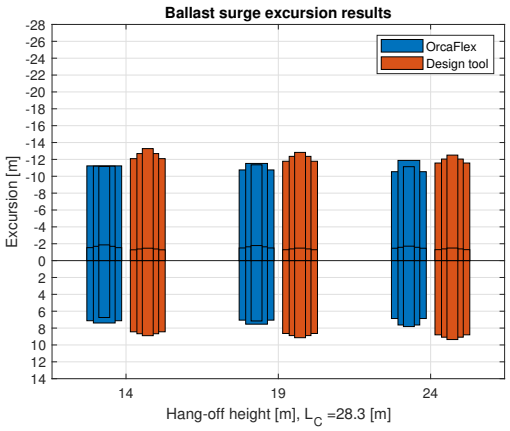
Ballast surge excursion results
OrcaFlex
Design tool
Excursion [m]
-28 -26 -24 -22 -20 -18 -16 -14 -12 -10 -8 -6 -4 -2 0 2 4 6 8 10 12 14
14 19 24
Hang-off height [m], L_C =28.3 [m]

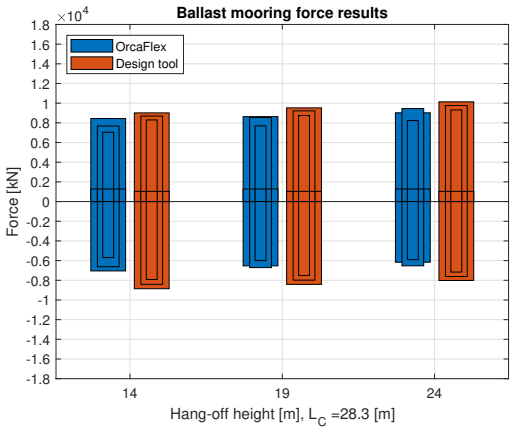
Ballast mooring force results
×10^4
OrcaFlex
Design tool
Force [kN]
1.8 1.6 1.4 1.2 1 0.8 0.6 0.4 0.2 0 -0.2 -0.4 -0.6 -0.8 -1 -1.2 -1.4 -1.6 -1.8
14 19 24
Hang-off height [m], L_C =28.3 [m]

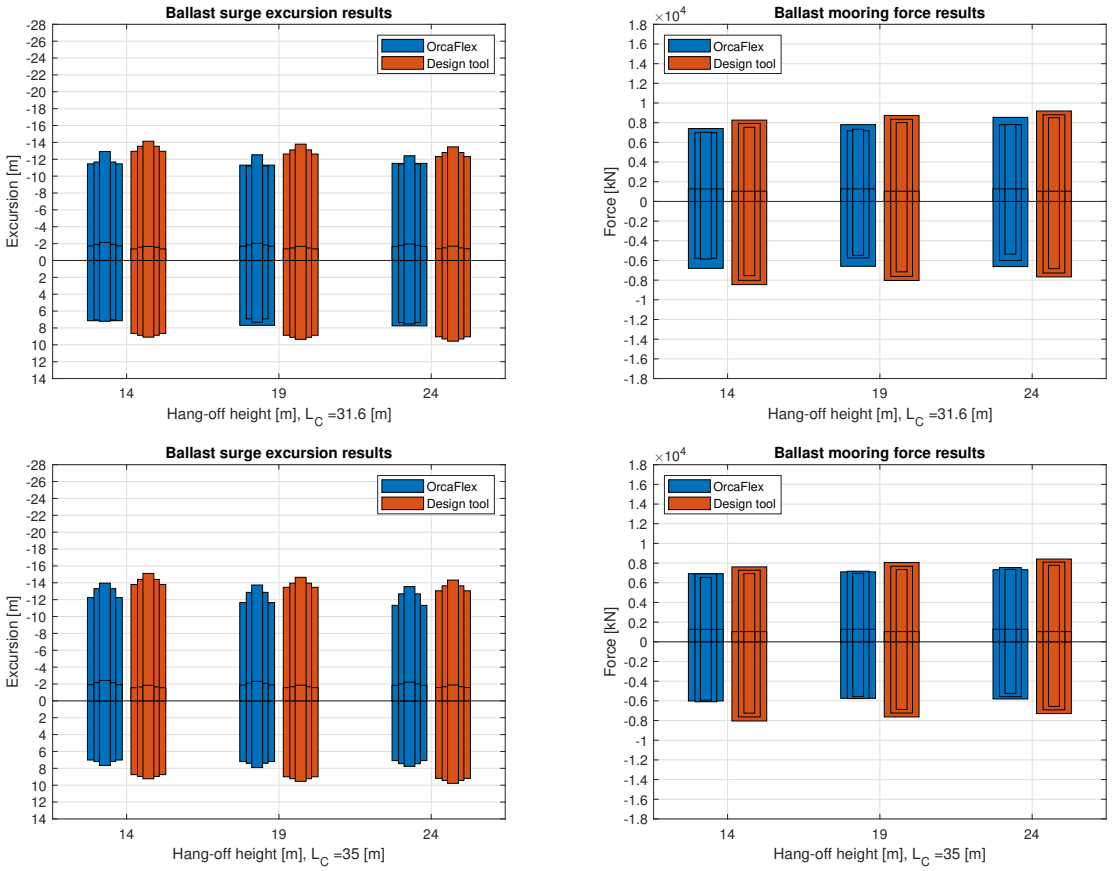

Figure E.1: Sensitivity of mooring design parameter variation for FPSO in ballast condition (EC1)

E.2. Fully loaded results (EC1)

The additional fully loaded results are given for the design parameters given in Table E.2. The optimized set of mooring design parameters for the design tool is indicated in the red rectangle. The optimized set according to OrcaFlex is indicated in the blue rectangle. Note that the absolute maximum mooring force, obtained from OrcaFlex, between the two proposed mooring parameter sets are within a 2% difference from each other.

Mooring design parameter	Symbol	Unit	Fully loaded
Pendulum length	L_C	[m]	25 - 28.3 - 31.6 - 35
Hang-off height	HC	[m]	7 - 12 - 17
Ballast weight	BW	[te]	1600 - 1800 - 2000

Table E.2: Modelled fully loaded conditions

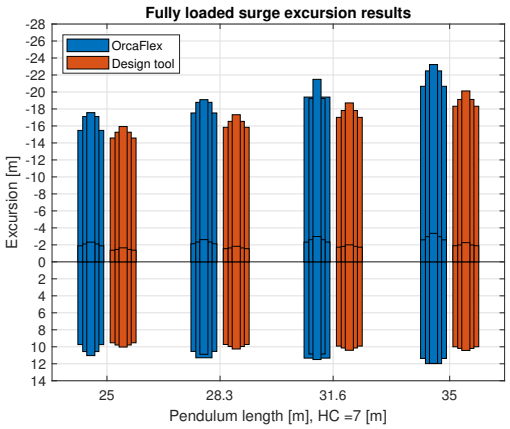

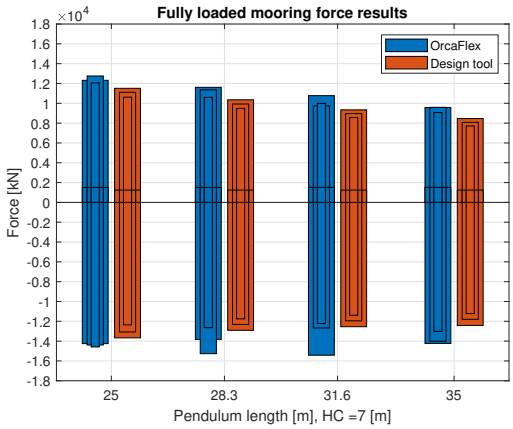

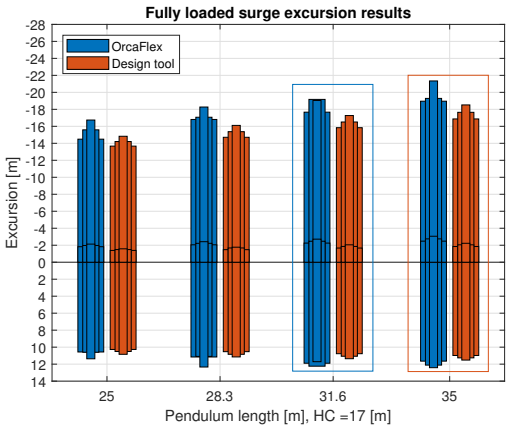

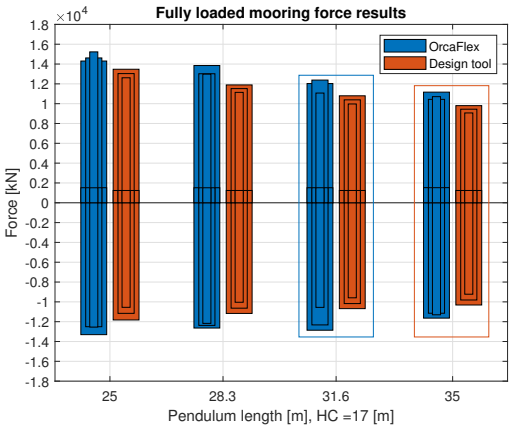

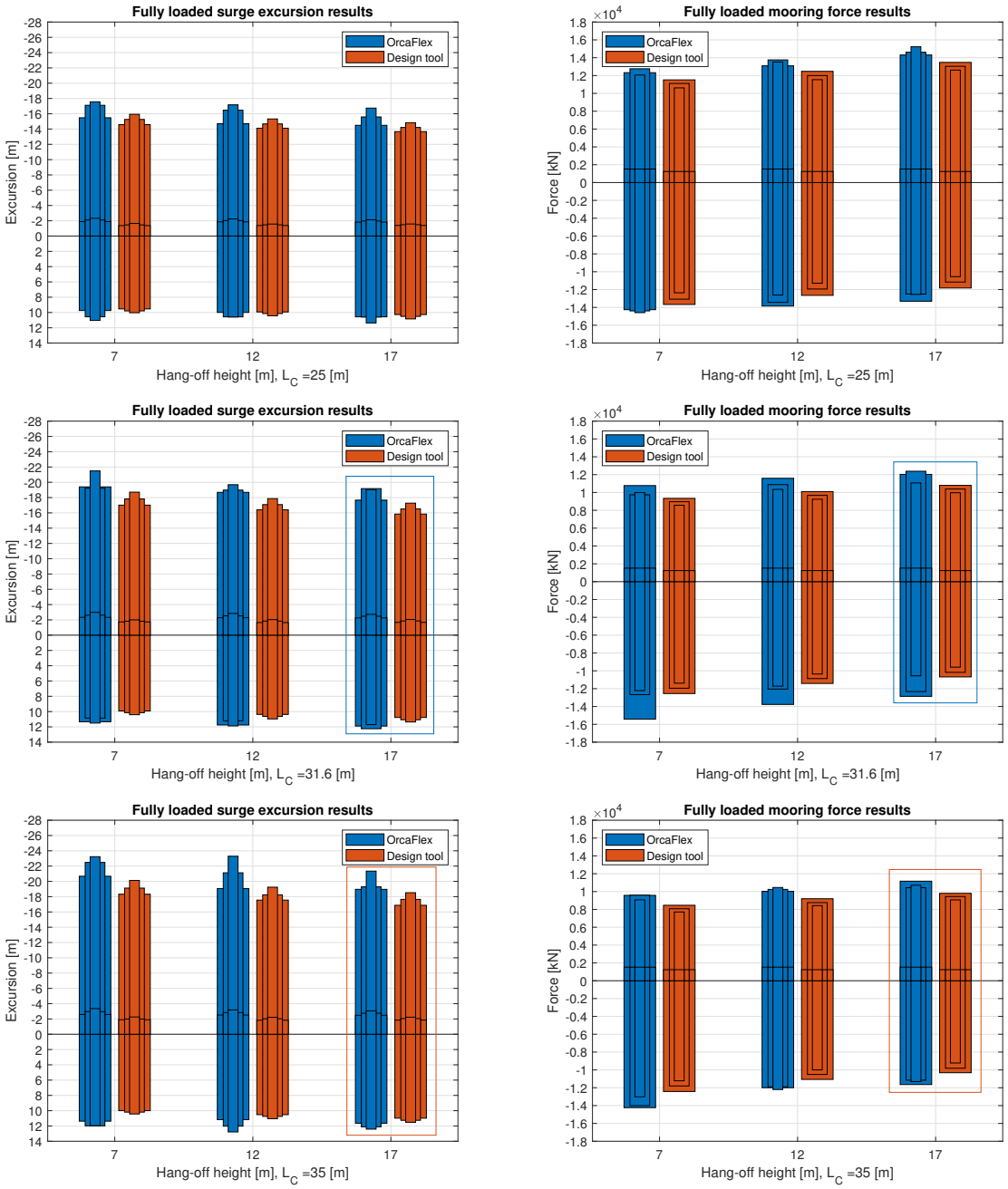

Figure E.2: Sensitivity of mooring design parameter variation for FPSO in fully loaded condition (EC1)

E.3. Ballast results (EC2)

The ballast results of the environmental case 2 analyses are shown below.

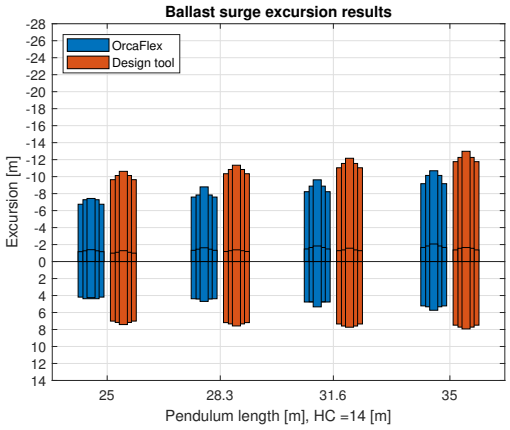

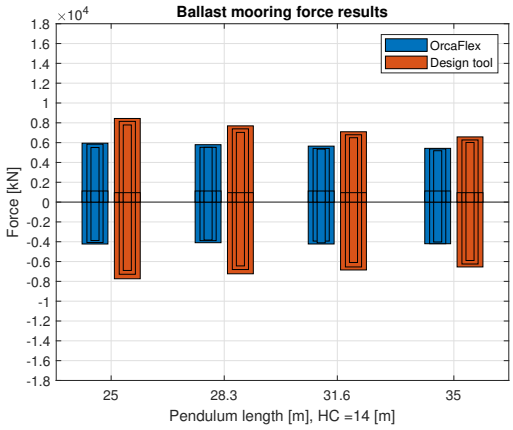

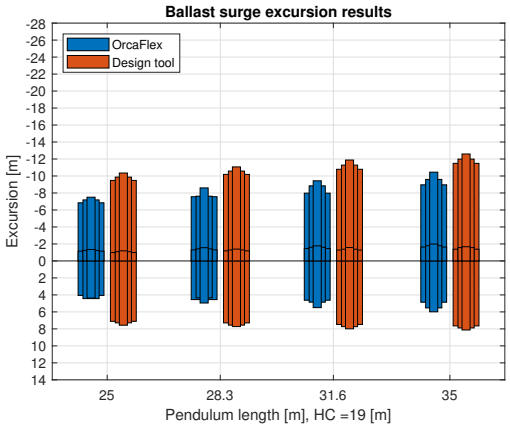

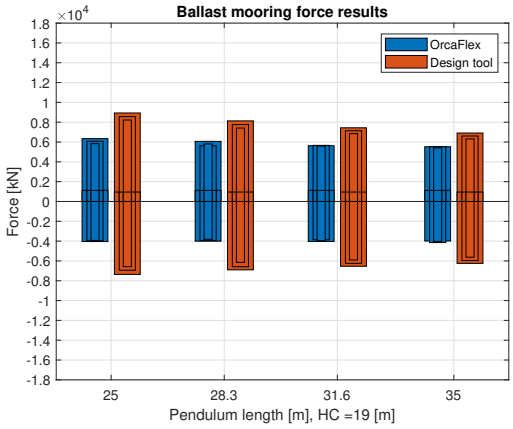

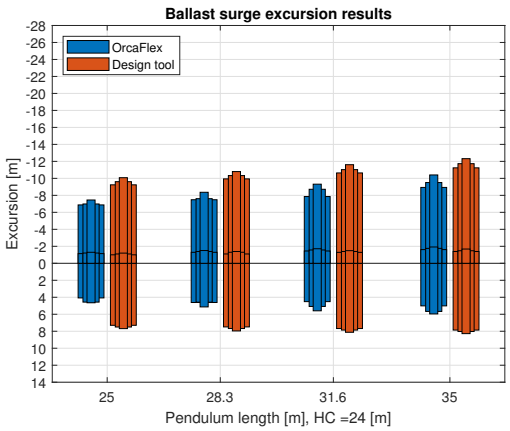

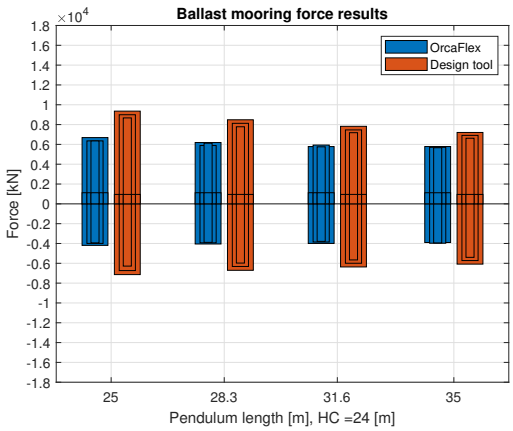

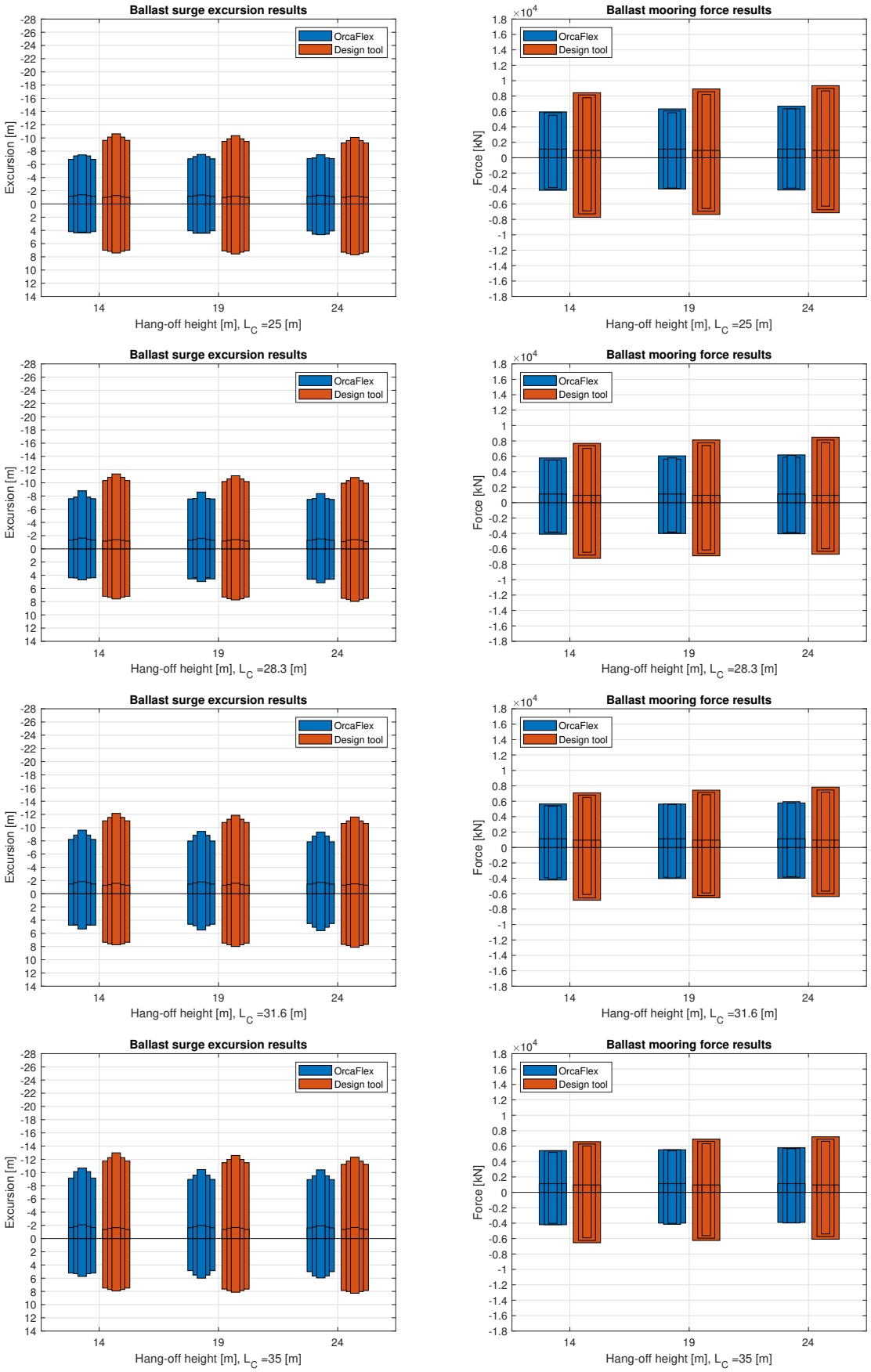

Figure E.3: Sensitivity of mooring design parameter variation for FPSO in ballast condition (EC2)

E.4. Fully loaded results (EC2)

The fully loaded results of the environmental case 2 analyses are shown below. The optimized set of mooring design parameters for the design tool is indicated in the red rectangle. The optimized set according to OrcaFlex is indicated in the blue rectangle. Note that the absolute maximum mooring force, obtained from OrcaFlex, between the two proposed mooring parameter sets are within a 10% difference from each other.

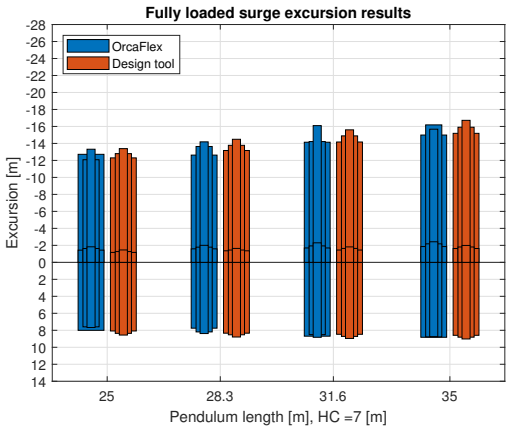

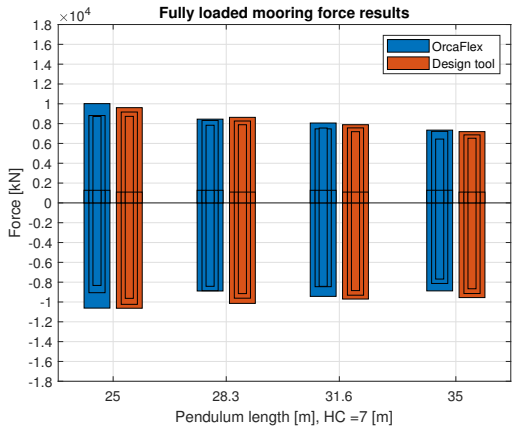

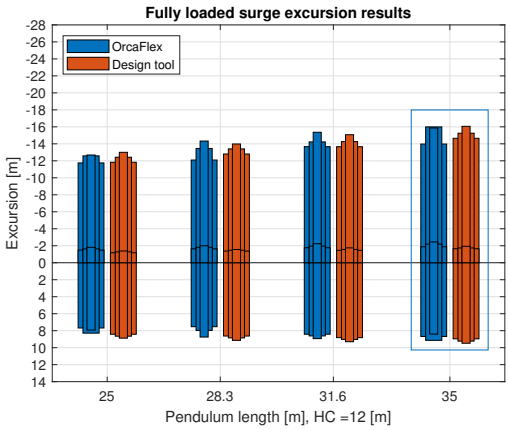

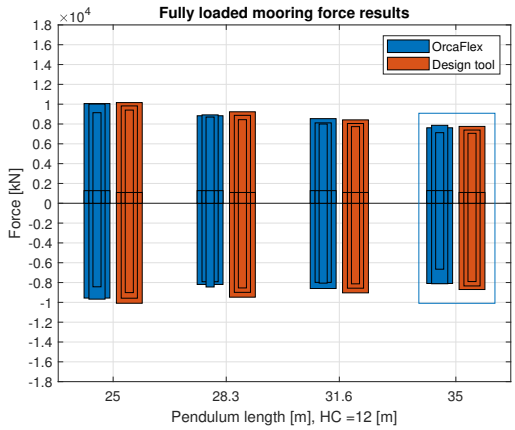

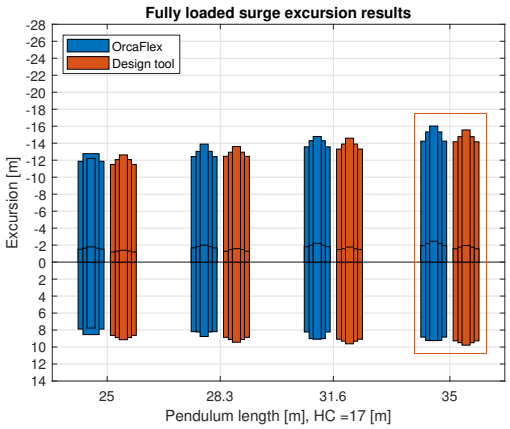

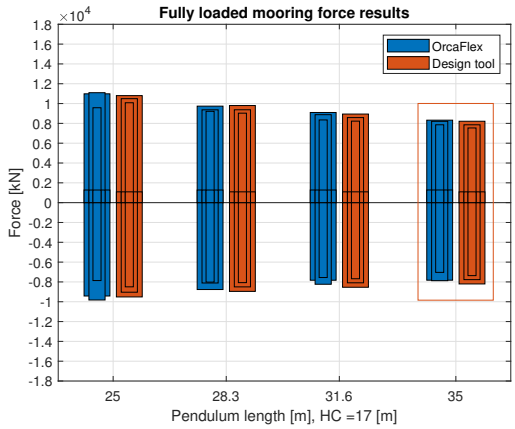

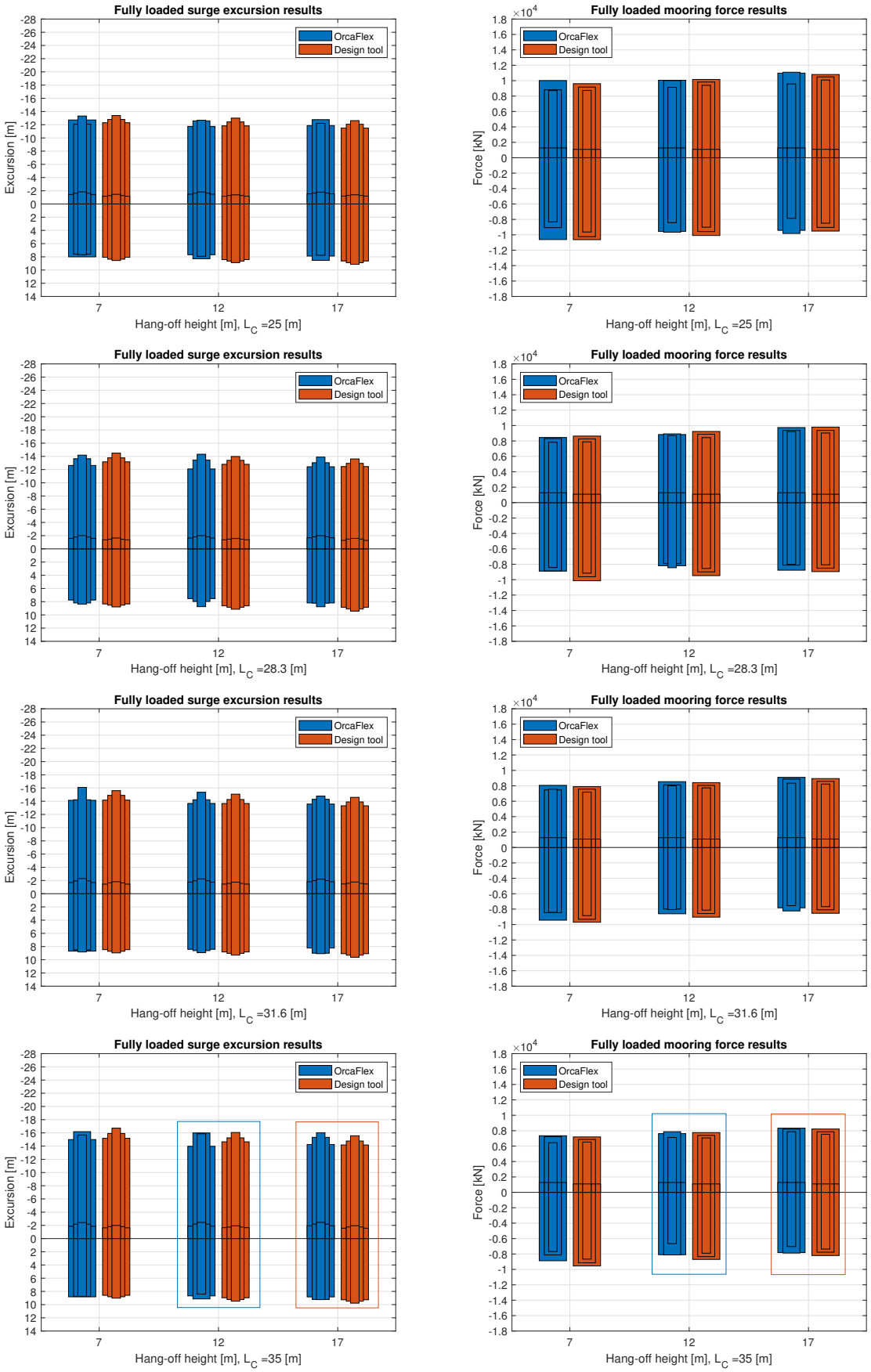

Figure E.4: Sensitivity of mooring design parameter variation for FPSO in fully loaded condition (EC2)

E.5. Ballast results (EC3)

The ballast results of the environmental case 3 analyses are shown below.

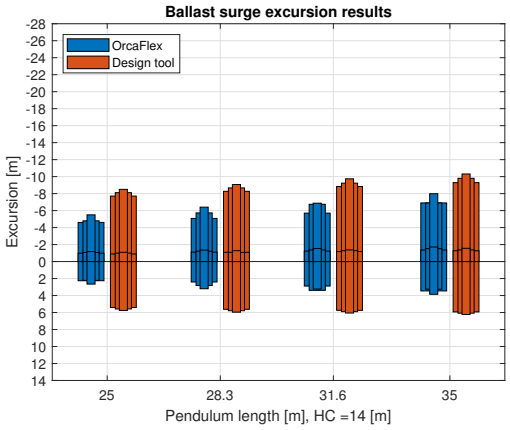

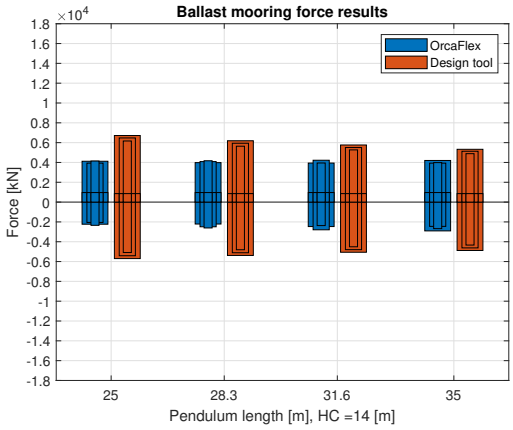

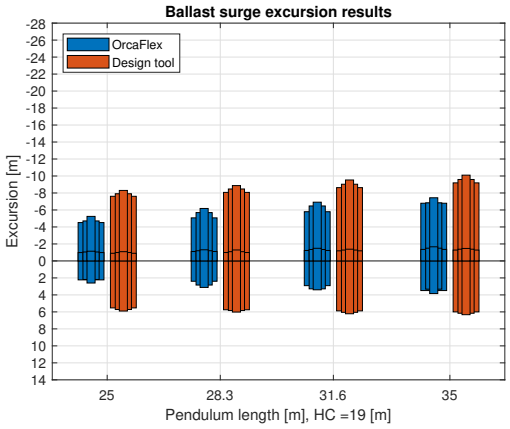

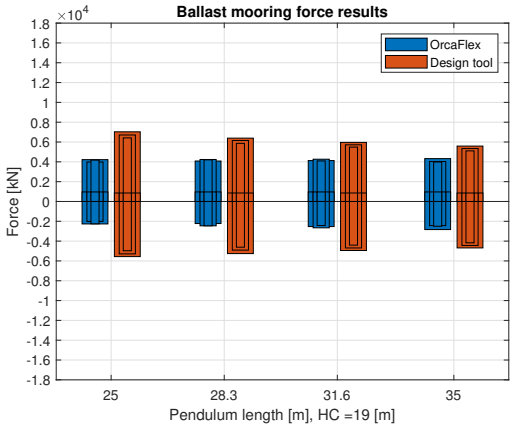

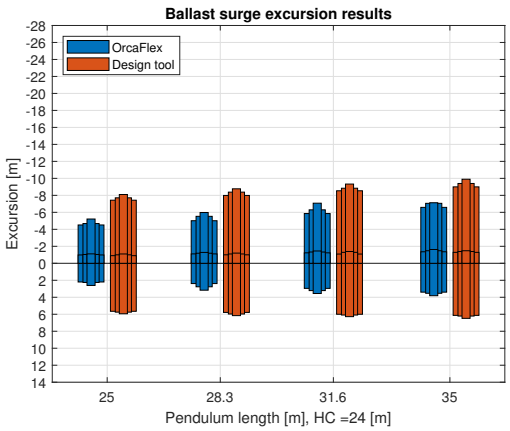

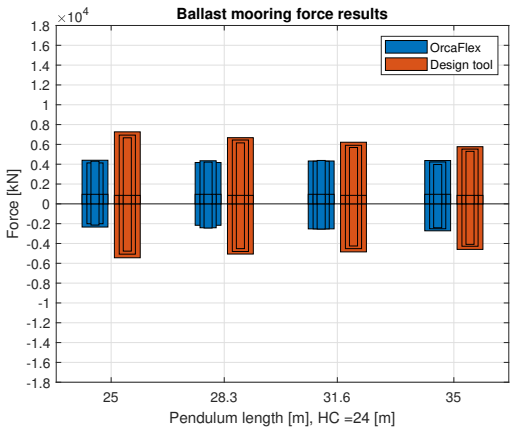

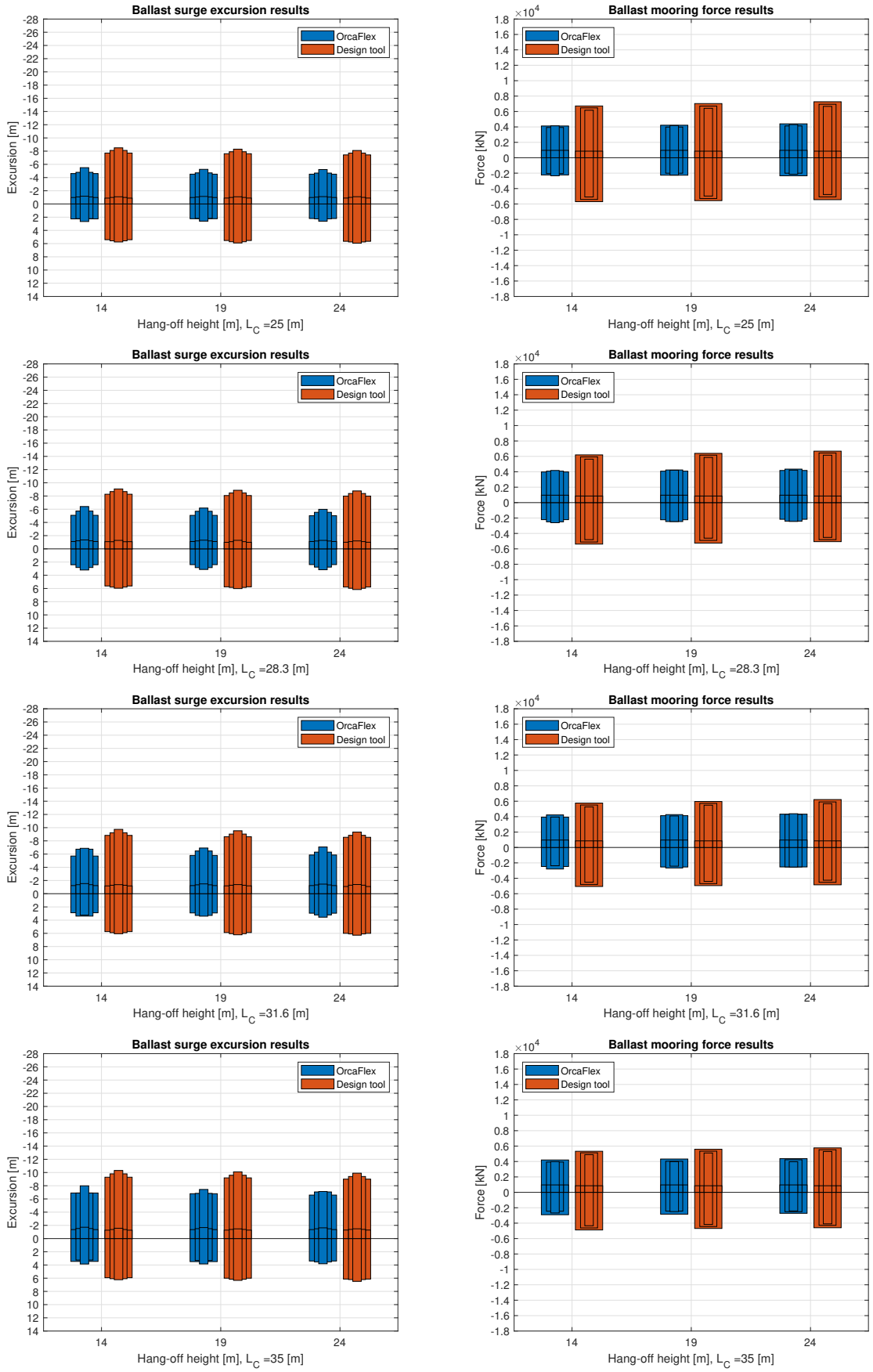

Figure E.5: Sensitivity of mooring design parameter variation for FPSO in ballast condition (EC3)

E.6. Fully loaded results (EC3)

The fully loaded results of the environmental case 3 analyses are shown below. The optimized set of mooring design parameters for the design tool is indicated in the red rectangle. The optimized set according to OrcaFlex is indicated in the blue rectangle. Note that the absolute maximum mooring force, obtained from OrcaFlex, between the two proposed mooring parameter sets are within a 2% difference from each other.

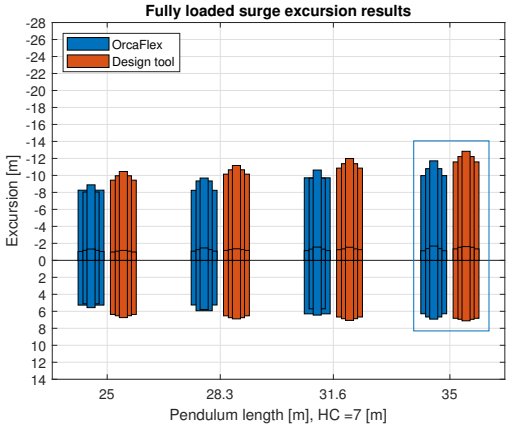

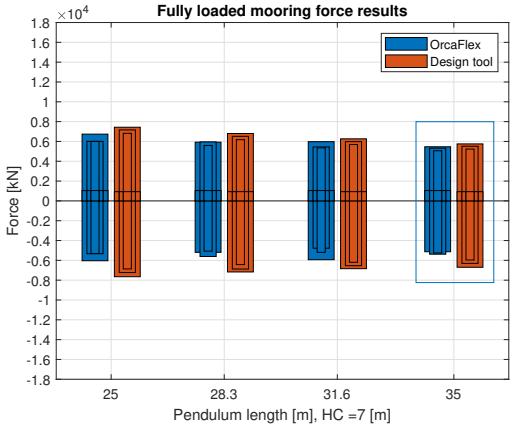

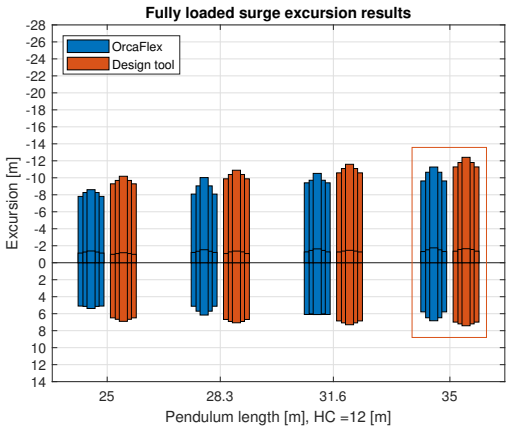

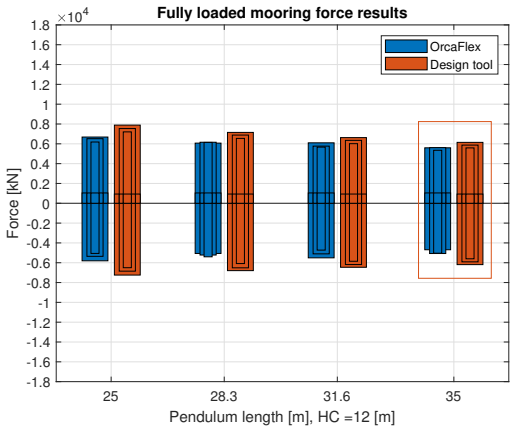

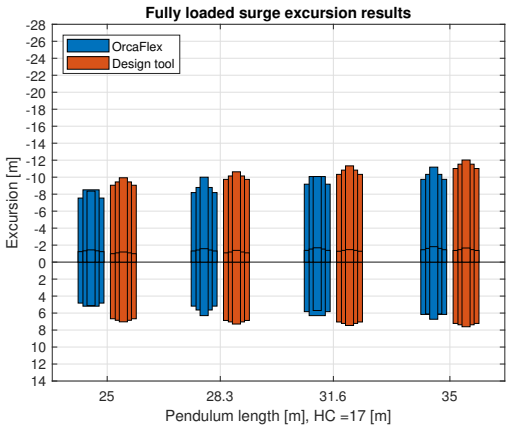

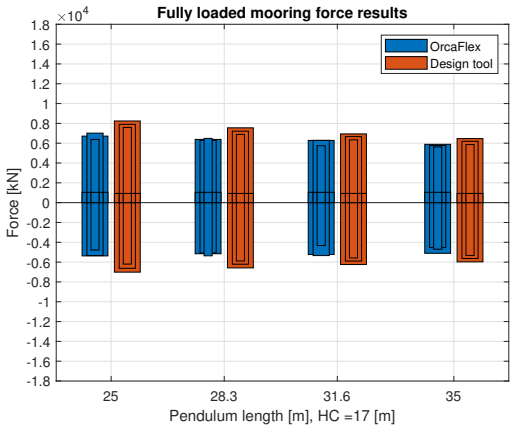

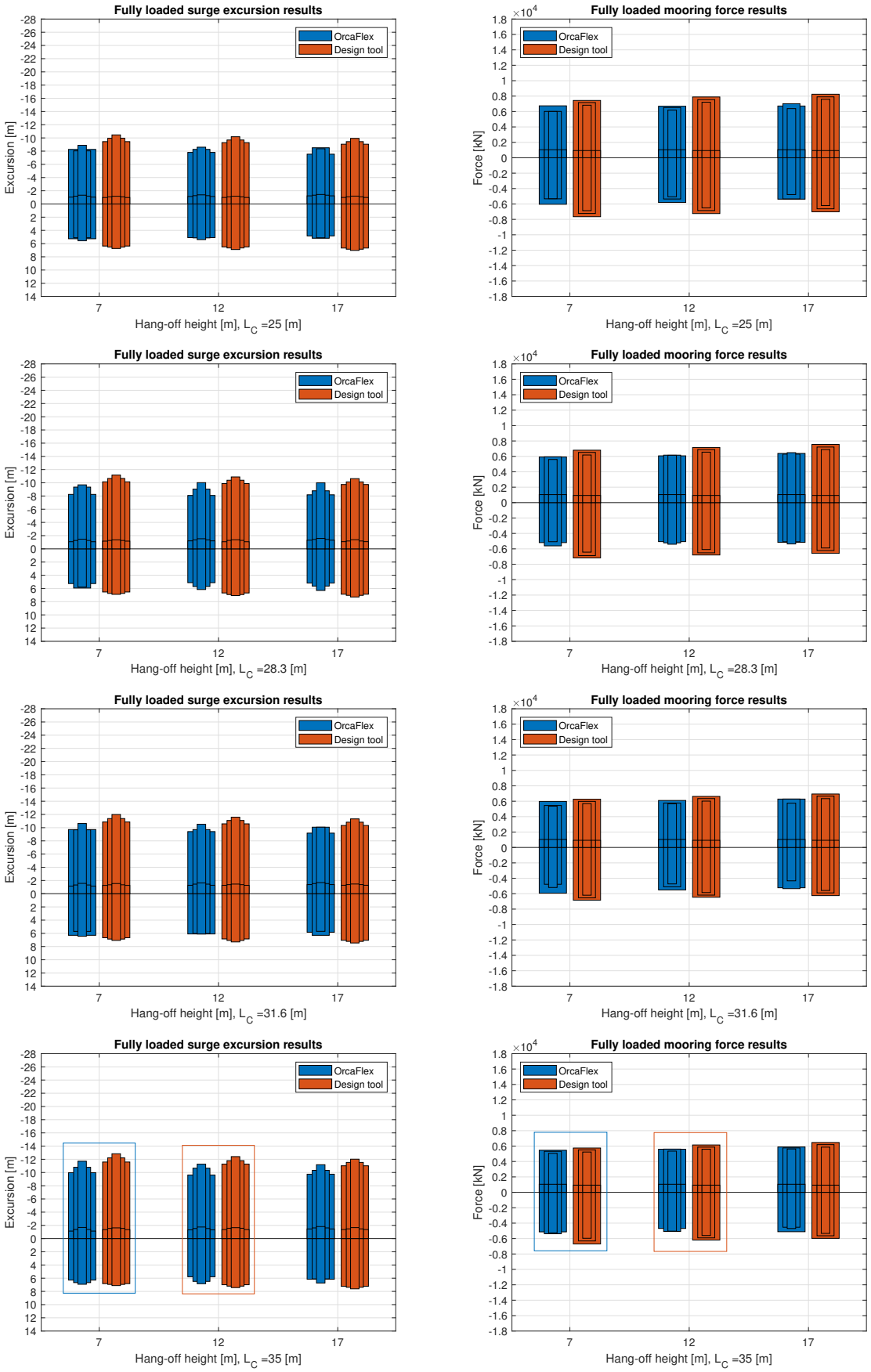

Figure E.6: Sensitivity of mooring design parameter variation for FPSO in fully loaded condition (EC3)

F

Graphical User Interface (GUI)

The developed GUI consists of two tabs, where the user can change design parameters of the mooring system. The first tab is shown in Figure F.1

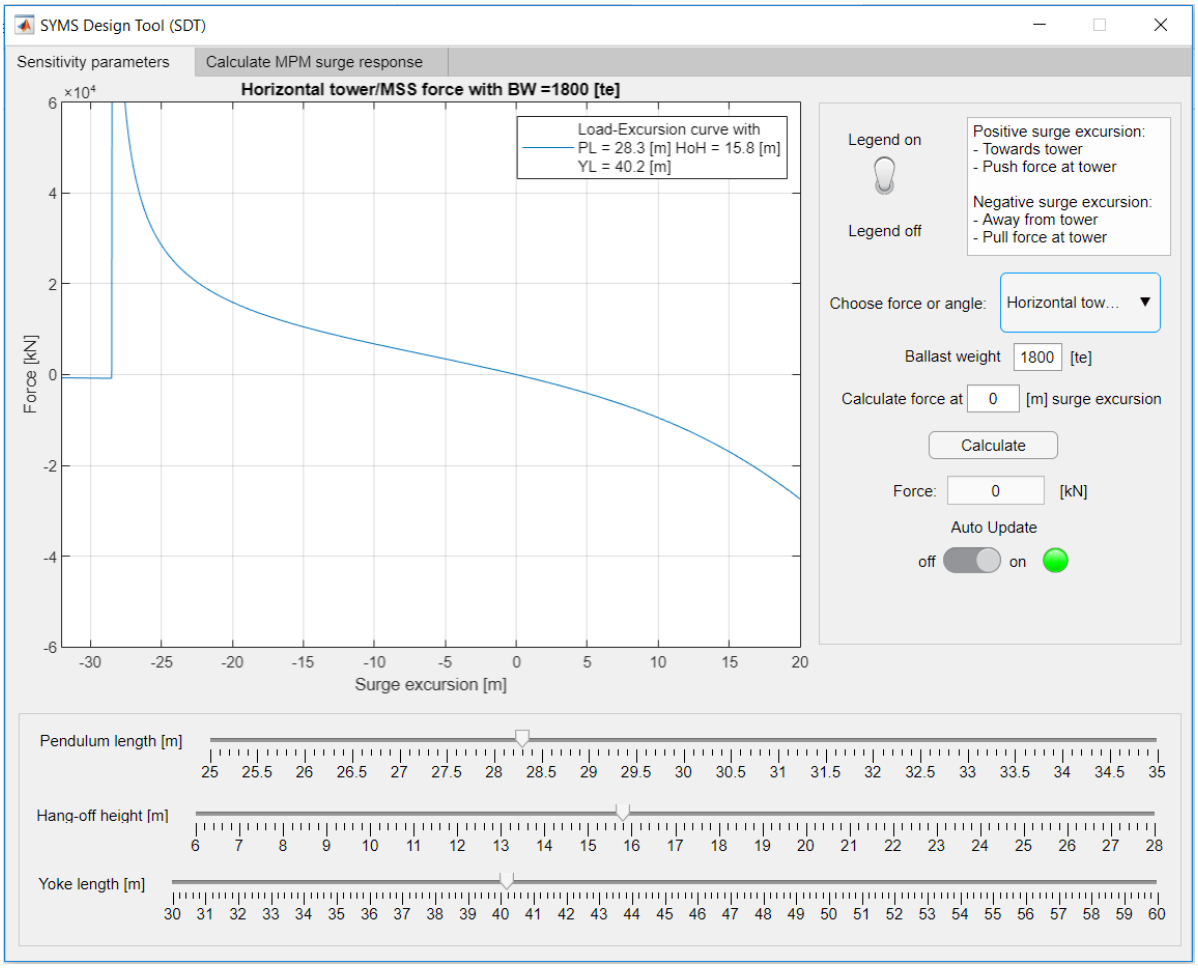

Figure F.1: GUI of the final design tool, tab 1

The user is able to choose between the static forces given in Equation 2.4 and the pendulum and yoke angle to be plotted. In addition, the force at an user defined location away or towards the tower can be calculated using the 'Calculate' button. If the slider 'Auto Update' is on, the plot automatically refreshes when varying mooring design parameters. When 'Auto Update' is off, a plot button appears below. The goal of this tab is to define limits of design parameters, since the asymptotes will be shown.

The second tab is shown in Figure F.2. Here, an user defined environment and vessel properties can be inserted. After ticking 'Select user files', new vessel properties can be entered. When completed, the vessel properties have to be saved by the 'Save vessel properties' button that appears. In addition RAO, QTF, current and wind coefficients (CC & WC) .txt files can be inserted using the browse button that appears. Note that these files have to be equally composed as the original .txt files already implemented. Note that new vessel properties have to be entered twice for ballast and fully loaded condition of the vessel. To switch from loading condition, the switch in the top left corner can be clicked. The raw code that builds the GUI, can be adjusted to own will and fine-tuned in the MATLAB App Designer environment.
By varying mooring design parameters using the sliding bars, the resulting surge excursion, mooring force and load-excursion curve will be updated automatically. The user is able to tick and tick-off the 'Stiffness adjustment method' shown in the load-excursion plot. The goal of this tab is to give the user insight in what range of parameters results in low excursions and mooring forces.

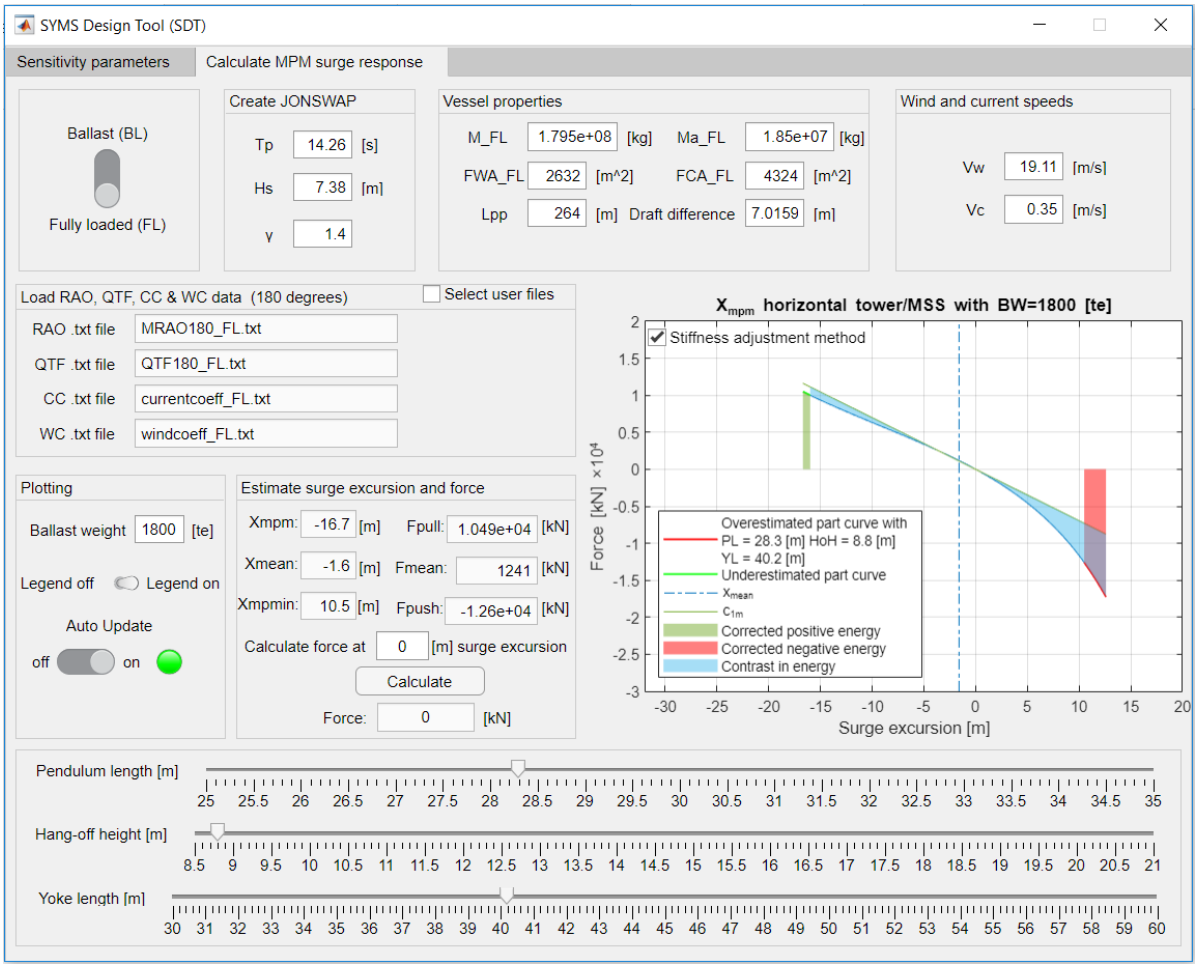

Figure F.2: GUI of the final design tool, tab 2

List of Figures

List of Tables

Acronyms

BES Bluewater Energy Services

BL Ballast

BV Bureau Veritas

CDF Cumulative Distribution Function

CoG Centre of Gravity

DoF Degrees of Freedom

DTYMS Disconnectable Tower Yoke Mooring System

EC Environmental Case

EoM Equation of Motion

FBD Free Body Diagram

FEED Front End Engineering Design

FFT Fast Fourier Transform

FL Fully Loaded

FPSO Floating Production Storage and Offloading

GoM Gulf of Mexico

GUI Graphical User Interface

HBM Harmonic Balance Method

LF Low Frequent

MPM Most Probable Maximum

MSL Mean Sea Level

MSS Mooring Support Structure

ODE Ordinary Differential Equation

PDF Probability Density Function

QTF Quadratic Transfer Function

RAO Response Amplitude Operator

SPM Single Point Mooring

SYMS Soft Yoke Mooring System

WF Wave Frequent

Bibliography

[1] Orcina, *Orcaflex Technical Specification Version 10.3,* Leaflet (2018).

[2] J. E. Wichers, *A simulation model for a single point moored tanker.* PhD Thesis, Delft University of Technology (1990).

[3] L. Xiao, J. Yang, and Z. Hu, *Low frequency wave forces and wave induced motions of a fpso in shallow water,* in *ASME 2007 26th International Conference on Offshore Mechanics and Arctic Engineering* (American Society of Mechanical Engineers, 2007) pp. 37–43.

[4] J. Pinkster, *Mean and low frequency wave drifting forces on floating structures,* Ocean Engineering **6**, 593 (1979).

[5] J. M J Journée and W. W Massie, *Offshore Hydromechanics* (Delft University of Technology, 2001).

[6] J. Pinkster, J. Wichers, *et al.*, *The statistical properties of low-frequency motions of nonlinearly moored tankers,* in *Offshore Technology Conference* (Offshore Technology Conference, 1987).

[7] B. Lyu, W. wu, W. Yao, Y. Wang, Y. Zhang, D. Tang, and Q. Yue, *Multibody dynamical modeling of the fpso soft yoke mooring system and prototype validation,* Applied Ocean Research **84**, 179 (2019).

[8] M. Krack and J. Gross, *Harmonic Balance for Nonlinear Vibration Problems* (2019).

[9] M. M. Bernitsas, J. P. J. Matsuura, and T. Andersen, *Mooring Dynamics Phenomena Due to Slowly-Varying Wave Drift ,* Journal of Offshore Mechanics and Arctic Engineering **126**, 280 (2005).

[10] X. Li, J. Yang, L. Xiao, *et al.*, *Research on motion response of soft yoke mooring fpso system,* in *The Sixteenth International Offshore and Polar Engineering Conference* (International Society of Offshore and Polar Engineers, 2006).

[11] Z. Fan, Q. Yue, X. Qi, and Y. Wang, *Study on the dynamic characteristics of a soft yoke mooring system for floating production storage and offloading based on field measurements,* Advances in mechanical engineering **7**, 1687814015572459 (2015).

[12] W. Wu, Y. Wang, D. Tang, Q. Yue, Y. Du, Z. Fan, Y. Lin, and Y. Zhang, *Design, implementation and analysis of full coupled monitoring system of fpso with soft yoke mooring system,* Ocean engineering **113**, 255 (2016).

[13] Z. Hussain and N. Z. Azlan, *Kane's method for dynamic modeling,* in *2016 IEEE International Conference on Automatic Control and Intelligent Systems (I2CACIS)* (2016) pp. 174–179.

[14] C. G. Källström, *Guidance and control of ocean vehicles : By thor i. fossen. wiley, chichester (1996). isbn 0-471-94113-1,* Automatica **32**, 1235 (1996).

[15] J. Wichers *et al.*, *On the low-frequency surge motions of vessels moored in high seas,* in *Offshore Technology Conference* (Offshore Technology Conference, 1982).

[16] R. Torhaug, *Extreme response of nonlinear ocean structures: Identification of minimal stochastic wave input for time-domain simulation* (Stanford University, 1996).

[17] J. N. Newman, *Second-order, slowly-varying forces on vessels in irregular waves,* (1974).

[18] P. Clark, Š. Malenica, and B. Molin, *An heuristic approach to wave drift damping,* Applied Ocean Research **15**, 53 (1993).

[19] J. Aranha, *A formula for 'wave damping' in the drift of a floating body,* Journal of Fluid Mechanics **275**, 147 (1994).

[20] D. Trassoudaine and M. Naciri, *A comparison of a heuristic wave drift damping formula with experimental results,* Applied Ocean Research - APPL OCEAN RES **21**, 93 (1999).

[21] J. Guo, *Simple and explicit solution of wave dispersion equation,* Coastal Engineering **45**, 71 (2002).

[22] L. H. Holthuijsen, *Waves in Oceanic and Coastal Waters* (Cambridge University Press, 2007).

[23] BV, *Classifications of Mooring Systems for Permanent and Mobile Offshore Units* (Bureau Veritas (BV), 2015) p. 62.

[24] C. Eckart, *The propagation of gravity waves from deep to shallow water,* in *Gravity waves* (1952) p. 165.